Journal of Visualized Experiments

Investigating the Relationship between Sea Surface Chlorophyll and Major Features of the South China Sea with Satellite Information

--Manuscript Draft--

Article Type:	Invited Methods Article - JoVE Produced Video
Manuscript Number:	JoVE61172R4
Full Title:	Investigating the Relationship between Sea Surface Chlorophyll and Major Features of the South China Sea with Satellite Information
Section/Category:	JoVE Environment
Keywords:	Chlorophyll; sea surface temperature; sea surface height; satellite; front; South China Sea; seasonal cycle
Corresponding Author:	Yuntao Wang Second Institute of Oceanography MNR Hangzhou, Zhejiang CHINA
Corresponding Author's Institution:	Second Institute of Oceanography MNR
Corresponding Author E-Mail:	yuntao.wang@sio.org.cn
Order of Authors:	Huan-Huan Chen
	Rui Tang
	Hao-Ran Zhang
	Yi Yu
	Yuntao Wang
Additional Information:	
Question	**Response**
Please indicate whether this article will be Standard Access or Open Access.	Open Access (US$4,200)
Please indicate the **city, state/province, and country** where this article will be **filmed**. Please do not use abbreviations.	Hangzhou, Zhejiang, China

TITLE:

Investigating the Relationship between Sea Surface Chlorophyll and Major Features of the South China Sea with Satellite Information

AUTHORS AND AFFILIATIONS:

Huan-Huan Chen[1,2,*], Rui Tang[2,*], Hao-Ran Zhang[1,2,*], Yi Yu[2], Yuntao Wang[2]

[1]College of Oceanography, Hohai University, Nanjing, China

[2]State Key Laboratory of Satellite Ocean Environment Dynamics, Second Institute of Oceanography, Ministry of Natural Resources, Hangzhou, China

*These authors contributed equally.

Corresponding Author:

Yuntao Wang (yuntao.wang@sio.org.cn)

Email Addresses of Co-Authors:

Huan-Huan Chen (chenhhmirai@163.com)
Rui Tang (362106798@qq.com)
Hao-Ran Zhang (zhanghaoran22@163.com)
Yi Yu (yiyu@sio.org.cn)

KEYWORDS:

chlorophyll, sea surface temperature, sea surface height, South China Sea, seasonal cycle, satellite observations

SUMMARY:

Sea surface chlorophyll, temperature, sea level height, wind, and front data obtained or derived from satellite observations offer an effective way to characterize the ocean. Presented is a method for the comprehensive study of these data, including overall average, seasonal cycle, and intercorrelation analyses, to fully understand regional dynamics and the ecosystem.

ABSTRACT:

Satellite observations offer a great approach to investigate the features of major marine parameters, including include sea surface chlorophyll (CHL), sea surface temperature (SST), sea surface height (SSH), and the factors derived from these parameters (e.g., fronts) which are calculated from the SST gradient. This study shows a step-by-step procedure to use satellite observations to describe major parameters and their relationships in seasonal and anomalous fields. This method is illustrated using satellite datasets from 2002–2017 that were used to describe the surface features of the South China Sea (SCS). Due to cloud coverage, monthly averaged data are used in this study. The empirical orthogonal function (EOF) was applied to describe the spatial distribution and temporal variabilities in different factors. The monsoon wind dominates the variability in the basin. Thus, wind from the reanalysis dataset was used to investigate its driving force on different parameters. The seasonal variability in CHL was

prominent and significantly correlated with other factors in a majority of the SCS. In winter, a strong northeast monsoon induced a deep mixed layer and high level of chlorophyll throughout the basin. Significant correlation coefficients were found among factors during the seasonal cycle. In summer, high CHL levels were mostly found in the western SCS. Instead of seasonal dependence, the region was highly dynamic, and factors correlated significantly in anomalous fields so that unusually high CHL levels were associated with abnormally strong wind and intense frontal activities. The study shows a step-by-step procedure to use satellite observations to describe major parameters and their relationships in seasonal and anomalous fields. The method can be applied to other global oceans and will be helpful for understanding marine dynamics.

INTRODUCTION:

Remote sensing technology offers great datasets with large spatial scales and long periods for describing marine environments. With the increasing spatial resolution of satellites, detailed features are now resolved from the regional scale to a few hundred meters[1,2]. An improved understanding of marine dynamics can be achieved with most updated satellite observations[3].

By incorporating multiple sensors on a remote sensing platform, a comprehensive description of different parameters is available. Sea surface temperature (SST) is the basic parameter that has been observed for more than half a century[4]. Recently, observations for sea surface chlorophyll-a (CHL) have become available and can be used to describe marine productivity[5]. Altimetry satellites are used for measuring sea surface height[6,7], which is strongly related to mesoscale eddy activities in the global ocean[8,9]. In addition to eddies, frontal activities are also important for impacting regional dynamics and primary production[10].

The major focus of the current study is to find a standard procedure to describe the spatial distribution and temporal variabilities of different ocean factors. In this method, the SST, CHL, SSH, and front datasets, which are derived from SST, are analyzed to determine patterns. In particular, the CHL is used to represent the productivity of the ocean, and a method is introduced to investigate the relationship between CHL and other ocean parameters. To validate the method, the time period between October 2002 and September 2017 in the South China Sea was used to examine all parameters. The method can be easily used for other regions around the globe to capture major ocean patterns and explore how marine dynamics impact the ecosystem.

The South China Sea (SCS) was designated as the study region because of its relatively high coverage rate of satellite observations. The SCS is abundant in solar radiation; thus, the CHL is mainly determined by the availability of nutrients[11,12]. With more nutrients being transported into the euphotic layer, CHL levels can increase[13]. Mixing, induced by wind, can introduce nutrients into the ocean surface and enhance CHL[14]. The SCS is uniquely dominated by a monsoon wind system, which determines the dynamics and ecosystem in the region. The monsoon wind is strongest during winter[15]. In summer, the winds change direction and the wind speeds are much weaker than those in winter[16,17]. The wind intensity can determine the strength of vertical mixing, such that the mixed layer depth (MLD) deepens as the wind increases in winter and becomes shallower as the wind decreases in summer[18]. Thus, more nutrients are transported into the euphotic layer during winter when the wind is strong[19] and CHL reaches its highest point of the

year[20,21].

In addition to the wind, MLD can also be determined using other factors, such as SST and sea level anomaly (SLA), which ultimately impact nutrient content and CHL[22]. During winter, the weak vertical gradient is associated with low temperatures at the surface[20]. The corresponding MLD is deep and more nutrients can be transported upward; thus, the CHL in the surface layer is high[17]. An increasing variation in CHL levels can be attributed to mesoscale eddies, which induce vertical transport and mixing[23]. Upwelling is usually found in cyclonic eddies associated with depressed SLA[8,9] and elevated CHL[24]. Downwelling is usually found in anticyclonic eddies associated with elevated SLA[8,9] and depressed CHL[24]. For other seasons, MLD becomes shallow, and mixing becomes weak; thus, low CHL can be observed over the majority of the basin[25]. The seasonal cycles of CHL levels are subsequently predominant for the region[26].

In addition to mixing, fronts and their associated coastal upwelling can further modulate the CHL. The front, which is defined as a boundary of different water masses, is important to determine the regional circulation and ecosystem responses[27]. Frontogenesis is usually associated with coastal upwelling and convergence[28,29], which can induce nutrients and elevate the growth of phytoplankton[30]. Different algorithms have been developed to automatically identify fronts from satellite observations, including histogram and SST gradient methods. The latter approach is adopted in this study[28].

The correlation of time series between CHL and different factors offers great insights for quantifying their relationship. The current study offers a comprehensive description of how to use satellite observations to reveal regional marine dynamics related to productivity. This description can be used as a guide for investigating the surface processes in any part of the ocean. The structure of this article includes a step-by-step protocol, followed by descriptive results in the text and figures. The applicability in addition to the pros and cons of the method are subsequently discussed.

PROTOCOL:

1. Dataset acquisition

1.1. SST and CHL

1.1.1. Download a dataset of satellite observations for SST and CHL from MODIS-Aqua (podaac-tools.jpl.nasa.gov/), where the spatial resolution of both datasets is roughly 4.5 km at daily intervals.

NOTE: Structure the directory of folders and data following the example scripts folder available in the **Supplemental Files**. Store the .nc files of the satellite data in the 'Data' folder. Add the path of the toolbox for NetCDF file in the analysis software (i.e., MATLAB). Select **Add with subfolders** to enclose the paths of the 'UTILITIES' folder and its subfolders.

1.1.2. Determine the time span. To maintain consistency among different datasets, use the same time span for all parameters. Adjust the time span based on the temporal coverage and use the longest observation period among different datasets. For this protocol, download 15 years of data from October 2002 to September 2017.

1.1.3. Determine the spatial coverage.

NOTE: The designed study region is between 105°E and 123°E and between 0° and 25°N.

1.1.4. Check preprocessing instructions. Read instructions in the .nc files regarding the preprocessing requirements of SST and CHL data (e.g., whether scaling is needed).

NOTE: The downloaded dataset already removed the data over land and within 5 km of the coastline, as well as those contaminated by clouds.

1.1.5. Load SST and CHL data into the analysis software. Type **Read_MODIS_SST** in the command window to read the data for SST. Similarly, type **Read_MODIS_CHL** in the command window to read the data for CHL. Transform the CHL data logarithmically because they have a log-normal distribution[31].

NOTE: Loaded variables include SST and CHL in three dimensions, representing meridional location, zonal location, and time in days, respectively. The range of SSTs is between -2 and 44, and the range of CHL is between 0.01 and 20.

1.2. Sea level anomaly (SLA)

1.2.1. Download daily SLA data with a 25 km spatial resolution from 2002–2017[32].

NOTE: SLA describes the difference between the observed sea surface height and the mean sea surface height over 20 years (1993−2012) for the corresponding pixels. The SLA data are processed by SSALTO/DUACS and distributed by Archiving, Validation, and Interpretation of Satellite Oceanographic Data (AVISO, https://www.aviso.altimetry.fr).

1.2.2. Load data into the analysis software. Load single-day SLA data by typing **Read_SLA** in the command window.

NOTE: The 'Data' folder in the **Supplemental Files** only includes one sample datum in the script for illustration.

1.3. Wind speed

1.3.1. Obtain the wind information from an ERA-Interim reanalysis product, which is a global atmospheric reanalysis dataset developed by the European Center for Medium-Range Weather Forecasts (ECMWF)[33]. Download wind data for the same period (October 2002–September 2017)

to maintain consistency with the CHL and SST data.

NOTE: The wind dataset has a spatial resolution of approximately 25 km and was interpolated from the original dataset with a spatial resolution of approximately 0.7°.

1.3.2. Load data into the analysis software. Type **Read_WindVector** in the command window to read the one-month wind data. Calculate the monthly mean by averaging the original data, which is at 6 h intervals.

1.4. Topography

1.4.1. Download the high-resolution topography data from the National Centers for Environmental Information website (NCEI, https://maps.ngdc.noaa.gov/viewers/wcs-client/). The spatial resolution is ~2 km. Obtain the ETOPO1 data for bedrock in XYZ format for the selected study region.

1.4.2. Load data into the analysis software. Type **Read_topography** in the command window to load the topography data into the analysis software.

2. Data preprocessing

2.1. Temporal average

2.1.1. Due to the large cloud coverage in the SST and CHL data, replace the original data with 3-day average data. To do this, after running the **Read_MODIS_SST.m** and **Read_MODIS_CHL.m** scripts (step 1.1.7), type **Temporal_average** in command window to run the script.

2.2. Interpolation into the same grid

2.2.1. Because the spatial resolution is not consistent for different datasets, interpolate the SST and CHL data into a spatial grid that is the same as the wind and SLA spatial grid before making comparisons. After running the **Temporal_average.m** and **Read_WindVector.m** scripts, type **Interpolation_grid** in the command window to run the script.

2.3. Wind stress and wind stress curl

2.3.1. Type **Wind_stress_curl** in the command window to calculate the wind stress (WS) and wind stress curl (WSC) using the following equations:

$$\vec{\tau} = \rho C \vec{u} \cdot |\vec{u}| \quad (1)$$

$$\nabla \times \vec{\tau} = \frac{\partial \tau_y}{\partial x} - \frac{\partial \tau_x}{\partial y} \quad (2)$$

where $\vec{u}$ is the wind speed vector; $\vec{\tau}$ is the WS in the same direction as the wind vector; τ_x and τ_y are the WS in the east and north directions, respectively; ρ is the air density (equal to 1.2 kg/m^3); and C is the drag coefficient (a value of 0.0015 is used) under neutral stability conditions[34].

2.4. Monthly averages

2.4.1. Calculate the monthly SST, wind, and SLA time series as 30-day averages in each pixel by typing **Monthly_average** to run the script. Due to the high cloud coverage rate, use a 60-day average as the monthly time series for CHL, including 30 days before to 30 days after the 15th day of the month.

3. SST front detection

3.1. Spatial smoothing

3.1.1. Type **Spatial_smoothing** to run the script to average the three-day SST data in each pixel.

NOTE: A large amount of noise was identified in the SST data. Thus, data was smoothened with a 3 x 3 spatial average. When no data were available in the original 3-day averaged data, the spatial averaged data were set as unavailable.

3.2. SST gradient

3.2.1. Type **SST_gradient** to run the script to calculate the zonal and meridional SST gradients (i.e., G_x and G_y, respectively) as the SST difference between the nearest two pixels divided by the corresponding distance via equation (3). Use the obtained gradient vector to calculate the total gradient, *G,* as a scalar following equation (4).

$$G_x = \frac{\partial SST_x}{\partial x},\ G_y = \frac{\partial SST_y}{\partial y} \quad (3)$$

$$G = ({G_x}^2 + {G_y}^2)^{0.5} \quad (4)$$

3.3. Local maximum

3.3.1. Identify a front by testing the value of SST gradient: label the pixel as a potential frontal pixel if the value is larger than a designated threshold. Only maintain the local maximum pixel in the same direction perpendicular to the gradient direction if there are connected pixels with values larger than the threshold. Here, define the threshold as 0.035 °C/km following former studies[10,28].

NOTE: The corresponding script '**Local_maximum.m**' is available in **Supplemental Files**.

3.4. Monthly frontal probability (FP)

NOTE: The frontal probability (FP) describes the probability of observing a front take place.

3.4.1. Calculate FP for a certain time span (in this case, the monthly interval), by typing **Monthly_FP** to run the script. Divide the occurrence of fronts at each pixel during a time window by the day number that is free of clouds.

4. Spatial and temporal variability

4.1. Seasonal cycle

4.1.1. Calculate the seasonal cycles of different factors as the averages of different seasons. Define the seasons as follows: winter is from December to February, spring is from March to May, summer is from June to August, and fall is from September to November.

NOTE: The seasonal cycle is not shown in this study; the following method (EOF) is used to explain the spatial and temporal variability instead.

4.2. Empirical orthogonal function (EOF)

4.2.1. Remove the temporal average and unavailable pixels. Before conducting the EOF, subtract the overall mean at each pixel and exclude the locations where missing observations exceed 20% because of cloud coverage. Load data by typing **load('Monthly_data_for_EOF.mat')** in the command window.

4.2.2. Apply an EOF to describe the spatial and temporal variabilities in different parameters. Type **Empirical_orthogonal_function.m** to run the script to calculate the magnitude (Mag), eigenvalues (Eig), and amplitude (Amp) of the EOFs for the dataset (i.e., time series of monthly averaged SST, wind stress, wind stress curl, CHL, and FP).

NOTE: The function decomposes the monthly time series into different modes, which are composed of spatial and temporal patterns and the variance explained by each mode decreases with increasing mode number.

5. Intercorrelation

5.1. Correlation at the seasonal scale

5.1.1. Calculate the correlations between two factors using their time series at each pixel by typing **Seasonal_correlation** to run the script. Because the seasonal cycle is not removed, check the significance of the correlation for all correlations.

5.2. Correlation of an anomalous field

5.2.1. Calculate the correlations between the monthly anomalies of the CHL and other factors, such as SST, WS, fronts, and SLA. Obtain the monthly anomalies (i.e., the deviation from the mean status) by subtracting the overall average for the corresponding month from the monthly time series. Type **Anomalous_correlation** to run the script and obtain the correlations.

6. Displaying information and calculating relationships

6.1. Display satellite information.

6.1.1. Type **Sat_SCS_Fig3457** to run the script to generate a showcase of satellite information, including SST, CHL, and frontal distribution. Set the current folder as 'scripts' where the data 'Sat_SCS_data.mat' are located.

NOTE: **Figure 1**, **Figure 2**, **Figure 3**, and **Figure 4** show SST, CHL, fronts, wind, and topography for the selected date as an example.

6.2. Display EOF result by typing **Sat_SCS_Fig890.m** to run the script.

NOTE: **Figure 5**, **Figure 6**, and **Figure 7** describe the spatial magnitude, monthly average, and time series of first two modes for CHL, SST, and fronts, respectively.

6.3. Calculate the relationship between chlorophyll and other factors at seasonal and anomalous fields by typing **Sat_SCS_Fig1112.m** to run the script. Obtain the correlation map for seasonal variability (**Figure 8**) and anomalous field (**Figure 9**).

REPRESENTATIVE RESULTS:

The spatial and temporal pattern of sea surface CHL in the SCS was described using satellite observations. Satellite information for CHL (**Figure 1A**) and SST (**Figure 1B**) can be contaminated by cloud coverage, which resulted in a large portion of data not being available. The reanalyzed data for wind (**Figure 1C**) and SLA (**Figure 1D**) was not impacted by daily clouds. The topography (**Figure 1E**) had a prominent impact on the spatial distribution of CHL. High CHL was mainly distributed along the coast, where the topography is shallow. Wind was also influenced by orography, and the lee side of mountains was characterized by weak wind; thus, a prominent WSC was identified southwest of the SCS. In contrast, the SLA did not depend much on topography, and an unusually high SLA was found in the basin of the SCS.

[Place Figure 1 here]

Because of the severe cloud impact on satellite observations, a lot of data were either not available or spatially inconsistent. An effective and efficient method was applied to fill some data gaps and smooth the field. The data were first replaced with a 3-day average at each pixel, which can effectively fill some gaps, because clouds vary daily (**Figure 2B**). A spatial average was further applied at each pixel so that the data were replaced by the mean of surrounding values (3 x 3

pixels). Thus, the spatial inconsistency was greatly reduced (**Figure 2C**).

[Place Figure 2 here]

The daily distribution of the SST front was derived from the SST gradient (**Figure 3A**). The thresholds applied here effectively captured the location of the front (**Figure 3B**) and ensured the depiction of the boundaries of entire water masses (**Figure 3C**). The gradient and front were nearly identical because the front was mainly obtained from the gradient.

[Place Figure 3 here]

Due to cloud coverage in the CHL, SST, and front data, the monthly average time series were calculated and applied in this study. A random example is shown in **Figure 4** for the month of April 2015. There was no existing gap for any of the parameters. The general patterns for different parameters were highly consistent regarding their spatial variance. For example, CHL was high near the coast and low in the central basin, while SST was low near the coast and high in the central basin. The monthly average offered comprehensive information to depict regional features. Fronts were mainly distributed along the coast, where the dynamics are complex. A large portion of the basin was free of fronts; thus, the center of the SCS was characterized by a value close to zero (**Figure 4E**).

[Place Figure 4 here]

Most surface features were characterized by prominent seasonal variability, which was clearly observed using EOFs. The EOF is a useful mathematic method that is widely used in atmospheric and marine sciences. The method can delineate spatial patterns and temporal signals from time series over spatial domains[28]. After spatiotemporal decomposition for sea surface features in SCS, the first two modes are generally needed for describing the spatial and temporal variabilities. The first two EOFs for CHL described 44% and 12% of the total variance, respectively. EOF1 captured a large variance in the northern section of the SCS (**Figure 5A**). The corresponding monthly average of the time series (**Figure 5C**) showed that the CHL was elevated during the winter and depressed during the summer. The region next to the southwest coast was characterized by weak magnitude, and the corresponding variability was mainly captured by EOF2 (**Figure 5B**). CHL values were high in the summer and low in the winter. This was mainly out of phase compared with the northern section. The monthly time series for EOFs showed clear seasonal variability, and EOF2 led EOF1 by approximately 4 months (**Figure 5E**).

[Place Figure 5 here]

The explained variance in the first two EOFs for SST was prominently high, equaling 91% and 5% for EOF1 and EOF2, respectively. It is important to emphasize that the overall average must be removed before conducting EOF; thus, the mean field was excluded. EOF1 dominated the total variance, and its magnitude was largest in the northern SCS and decreased southward (**Figure 6A**). The corresponding monthly average of the time series (**Figure 6C**) showed that the SST was

elevated during summer and depressed during winter. The southern SCS was characterized by a weak magnitude, attributed to persistent high temperatures at low latitudes. The variability in the southern section was mainly captured by EOF2 (**Figure 6B**). The corresponding SST was enhanced between March and June, while low values persistently occurred in the remaining months. Prominent warming occurred in 2010 and 2016, where the SST off the coast southwest of the SCS was much higher than that in the other years (**Figure 6E**). This interannual variability is mainly attributed to El Niño events that reduce the southwest summer monsoon and result in weak upwelling[12]. Because seasonal variability is the major focus of the current study, this feature is not discussed further.

[Place Figure 6 here]

Because of the noisy nature of the gradient, the derived front explained much less of the variance. Indeed, EOF1 and EOF2 of FP only explained 19% and 9% of the total variance, respectively. EOF1 captured the variances in the north and northeast SCS (**Figure 7A**). The corresponding monthly average of the time series (**Figure 7C**) showed that in those regions, more FP occurred during winter and less during summer. The phase off the coast southwest of the SCS was the opposite, although the corresponding variability was much less prominent. EOF2 captured the spring enhancement of FP (**Figure 7D**) in the western SCS (**Figure 7B**). The monthly time series of EOF1 and EOF2 were characterized by weak interannual variability.

[Place Figure 7 here]

Different factors were investigated for their relationships with CHL (**Figure 8**). For example, SST described the fundamental features of the ocean that can influence the growth rate of phytoplankton and subsequently impact CHL. For the majority of the SCS, there were high correlations between SST and CHL (**Figure 8A**), and most of the correlations reached more than -0.8. It is important to point out that high correlation does not indicate causation between these two factors. As SST reached its annual maximum in summer, the MLD became shallowest[21]. Nutrients supplied to the euphotic layer were low because vertical mixing was blocked by intensive stratification[13]. As a result, low nutrients limited the growth rate of phytoplankton and resulted in low CHL. In contrast, high CHL occurred in winter when the MLD was deeper, and low SST induced weak stratification[35].

[Place Figure 8 here]

Wind-driven mixing can be approximately gauged by WS and was used to describe vertical mixing[18]. Large correlation coefficients, with values of approximately 0.8, were identified between the WS and CHL levels north of the SCS (**Figure 8B**), particularly in the regions with the strongest winter wind located on the northern shelf of the SCS. Weak but significant correlations were found to the south. Correlations between WSC and CHL were significant in the majority of the SCS (**Figure 8C**), although they showed opposing trends in the north and south. The positive correlation coefficient between CHL and WSC was to the south, and the negative values were in the north. The correlation in the region between them was not significant. The WS and CHL were

found to be strongly correlated in the corresponding region where the winter WS was largest.

The front can induce CHL variability. A large correlation was found in the northeast and southwest of the SCS (**Figure 8D**). CHL increased as frontal activities became more active[36]. The SLA showed a significant negative correlation with CHL from the northeast SCS towards the southwest and a positive correlation along the west coast of the SCS (**Figure 8E**). It is interesting to note that the positive correlations were limited in the region with shallow topography.

To the northeast of the SCS, all the correlations were large (**Figure 8**). Thus, the correlations of monthly time series between CHL and other parameters were calculated using the spatial average in a designated box (**Figure 8A**). The results show that most of the factors were intercorrelated with significant correlations (top right section of **Table 1**). Because the seasonal cycle dominated the time series, the correlation was no longer valid after removing the monthly average (bottom left section of **Table 1**).

[Place Table 1 here]

The correlations in the seasonal cycle were not significant for some regions, such as the southwest of the SCS (**Figure 8**). The region was dominated by dynamic processes (e.g., upwelling and wind-induced offshore transport) that determine the variability in CHL[17]. A significant correlation between CHL and other factors (e.g., SST, WS, fronts, and WSC) was identified in anomalous fields (**Figure 9**). The anomalies were calculated for the monthly time series by removing the corresponding monthly average. The effective number of degrees of freedom could be increased, but it did not impact the underlying relationships among their time series[28, 37].

[Place Figure 9 here]

In anomalous fields, CHL and SST were significantly correlated in the majority of the SCS (**Figure 9A**). When SSTs were unusually high, CHL became unusually low, and vice versa. Similarly, an unusually high WSC and fronts to the southwest of the SCS can induce a large CHL, and vice versa (**Figure 9C, 9D**). In addition, a negative correlation was found between the anomalous SLA and CHL levels (**Figure 9E**). Different lags were tested, and the correlation only became significant if no lag was deployed. Thus, CHL was simultaneously impacted by anomalies in SST, WSC, fronts, and SLA. Their relationship was further investigated using the spatially averaged monthly time series southwest of the SCS, designated as a green box in **Figure 9A**. The results show that most of the factors were intercorrelated with significant correlations in the anomalous field (bottom left section of **Table 2**).

[Place Table 2 here]

FIGURE AND TABLE LEGENDS:

Figure 1: Original observations for major parameters on April 15, 2015. (**A**) Sea surface chlorophyll (CHL), (**B**) sea surface temperature (SST), (**C**) wind stress curl (WSC, shading) with wind stress (WS, vector), (**D**) sea surface anomaly, and (**E**) topography for the ocean basin.

Figure 2: SST for a single day on April 15, 2015. (**A**) Original SST from MODIS, (**B**) Three-day averaged SST, and (**C**) SST after spatial smoothing.

Figure 3: Procedure for front detection derived from SST. (**A**) Magnitude of SST gradient, (**B**) the distribution of the SST front in thin black color, and (**C**) front distribution with the corresponding SST.

Figure 4: Monthly average for major parameters in April 2015. (**A**) CHL (in logarithm scale), (**B**) SST, (**C**) WSC (shading) with WS (vector), (**D**) sea surface anomaly, and (**E**) frontal probability (FP).

Figure 5: The EOF for CHL. (**A**) Magnitude of EOF1, (**B**) magnitude of EOF2, (**C**) monthly averaged time series for EOF1, (**D**) monthly average time series for EOF2, and (**E**) monthly time series of EOF1 (black) and EOF2 (blue).

Figure 6: The EOF for SST. (**A**) Magnitude of EOF1, (**B**) magnitude of EOF2, (**C**) monthly averaged time series for EOF1, (**D**) monthly averaged time series for EOF2, and (**E**) monthly time series of EOF1 (black) and EOF2 (blue).

Figure 7: The EOF for FP. (**A**) Magnitude of EOF1, (**B**) magnitude of EOF2, (**C**) monthly averaged time series for EOF1, (**D**) monthly averaged time series for EOF2, and (**E**) monthly time series of EOF1 (black) and EOF2 (blue).

Figure 8: Correlations between CHL and other factors in the seasonal scale. (**A**) SST, (**B**) WS, (**C**) WSC, (**D**) FP, and (**E**) SLA. The gray color indicates that the correlation is nonsignificant. Spatially averaged variables are calculated based on the green box in panel **A**. Their time series are used to obtain the correlation coefficients in **Table 1**. This figure has been modified from Yu et al.[17].

Figure 9: Correlation between CHL and other factors in the anomalous field. (**A**) SST, (**B**) WS, (**C**) WSC, (**D**) FP, and (**E**) SLA. The gray color indicates that the correlation is nonsignificant. Spatially averaged variables are calculated based on the green box in panel **A** Their time series are used to obtain the correlation coefficients shown in **Table 2**. This figure has been modified from Yu et al.[17].

Table 1: Correlation coefficients of the time series among factors, located northeast of the SCS, e.g., SST (sea surface temperature), FP (frontal probability), WSC (wind stress curl) and WS (wind stress), using the box shown in Figure 8A. The monthly average and anomaly are shown in the top right section and left bottom section, respectively. Numbers in bold and italics indicate that the correlation cannot fulfill the 95% confidence level. The table has been modified from Yu et al.[17].

Table 2: Correlation coefficients of the time series among factors, located southwest of the SCS, e.g., SST (sea surface temperature), FP (frontal probability), WSC (wind stress curl) and WS (wind stress), using the box shown in Figure 9A. The monthly average and anomaly are shown

in the top right section and left bottom section, respectively. Numbers in bold and italics indicate that the correlation cannot fulfill the 95% confidence level. The table has been modified from Yu et al.[17].

DISCUSSION:

In this study, the major features of marine systems are described using satellite observations. The CHL, which can be used to represent ocean production, is selected as an indicator factor. Factors related to CHL variability were investigated using monthly averaged time series, e.g., SST, WS, WSC, FP and SLA. Three critical steps are described in this study: acquiring satellite data for different parameters, describing their spatial and temporal variabilities via EOF, and determining interrelationships among different factors by calculating correlation coefficients. A detailed procedure showing the identification for daily frontal distribution, which is derived from the SST observations, is included. Two major approaches have been developed for SST front detection: the gradient method[10,38] and the histogram method[39,40]. The histogram method is based on a similar range of values for SST, which can be used to divide the water masses into different groups. The Pixels with values between different groups representing the pixel in a transitional band are defined as fronts. On the other hand, the gradient method separates several relatively uniform water bodies as pixels with large gradient values. A comparison study was conducted, and they found lower false rates using the histogram method and fewer missed fronts using the gradient method[41]. In this study, the gradient-based method[38] was adopted following former studies[10,28]. The algorithm can avoid front break-up into multiple edge fragments by allowing the magnitude to decrease to a level below a smaller threshold. In addition to the dataset included here, other satellite observations, such as the aerosol index, can also be used with a similar approach.

Most of the procedures can be directly applied in other regions or datasets. Modification may take place to change the threshold of front detection. Because the SST gradient in the SCS is comparable with the Eastern Boundary Current System[28], the same thresholds were implemented for the current study. A previous study revealed that the SST gradient from different datasets can vary as much as three times[42], which makes the method somehow less objective. Substantial studies have investigated frontal activities around the global oceans[28,43]. The best approach to validate fronts is to compare them with in situ observations. Yao[44] described the monthly frontal distribution for the SCS. Their results agreed well with the in situ measurements. The overall gradient should be checked and adjusted since its value may vary depending on the spatial resolution and instruments. In particular, the threshold should be updated when another SST dataset is used. A basic understanding of the regional dynamics is fundamental to understanding frontogenesis[45,46,47]. The front detection script can be developed by individual authors based on the description in this paper.

Satellite information offers a comprehensive understanding of surface features, and a results comparison with in situ observations can aid in evaluating credibility. However, satellite observations are limited to the ocean surface, which limits the application for understanding the vertical structure of the water column. In a recent study, satellite observations revealed that the surface CHL increased by 15 times, but the vertical integrated value only increased by 2.5 times[48].

This difference was because the surface value was impacted by the coeffects of phytoplankton growth and shoaling of MLD, resulting in an unrealizable value at the surface. Thus, the surface feature may not offer an accurate description for the entire water column. Additionally, the influence of cloud coverage limits the continuous observations of satellites. Thus, monthly time series are calculated for different factors over the same region and same period. This will guarantee the credibility of calculating the correlations among different factors. However, the short-period events, e.g., typhoons that last for a few days to a week, will not be resolved.

Compared with former studies, the proposed method can offer spatial information at the pixel level, which can help to evaluate the dynamics in a more detailed manner. Some former studies averaged the entire SCS as a single number and obtained a time series. They found that an unusually strong WS and high SST can induce anomalously high CHL[16], which is consistent with current result. However, the spatial variation in the relationships was not resolved. In this study, the basin-scale correlation between WS and CHL was weak in the anomalous field. A large significant correlation was only identified for certain areas, e.g., in the center of the SCS (**Figure 9B**). Thus, the current method offers a comprehensive description for investigating spatial variations. Similarly, observations from two Bio-Argo floats were used and revealed that WSC did not correlate with CHL variability[20]. However, the trajectories of the two floats are only located in certain regions. In this case, it was exactly within the band where the correlation between the CHL level and the WSC was not significant (**Figure 8D**). The proposed method is very helpful for resolving the spatial dependence among factors, which is a fundamental characteristic of the global ocean.

In summary, the method used here can accurately describe the spatial distribution and temporal variability in ocean surface features using satellite observations. With the increasing resolution of satellite datasets, more detailed features can be identified and investigated, which enables a general understanding of regional features, including CHL, SST, and SSH. The correlation of monthly time series among different factors can aid in understanding their dynamic relationships and potential impact on an ecosystem[49]. Because the correlation can largely vary at different spatial locations, the proposed method offers a detailed and comprehensive description. A similar approach can be applied to any ocean basin worldwide, which will be greatly helpful to improve the understanding of marine dynamics and ecosystems.

ACKNOWLEDGMENTS:
The support from the National Key Research and Development Program of China (No. 2016YFC1401601), the Postgraduate Research & Practice Innovation Program of Jiangsu Province (No. SJKY19_0415) supported by the Fundamental Research Funds for the Central Universities (No. 2019B62814), the National Natural Science Foundation of China (Nos. 41890805, 41806026 and 41730536) and Joint Advanced Marine and Ecological Studies in the Bay of Bengal and the eastern equatorial Indian Ocean were greatly acknowledged. The authors appreciate the provision of data from sources including the National Aeronautics and Space Administration (NASA), the European Centre for Medium-Range Weather Forecasts (ECMWF), the Copernicus Marine and Environment Monitoring Service (CMEMS) and the National Oceanic and Atmospheric Administration (NOAA).

DISCLOSURES:

The authors have nothing to disclose.

REFERENCES:

1. Behrenfeld, M. J., Falkowski, P. G. Photosynthetic rates derived from satellite-based chlorophyll concentration. *Limnology and Oceanography.* **42** (1), 1-20 (1997).

2. Loisel, H. et al. Assessment and analysis of the chlorophyll-a concentration variability over the Vietnamese coastal waters from the MERIS ocean color sensor (2002–2012). *Remote Sensing of Environment.* **190**, 217-232 (2017).

3. Gohin, F. et al. Towards a better assessment of the ecological status of coastal waters using satellite-derived chlorophyll-a concentrations. *Remote Sensing of Environment.* **112** (8), 3329-3340 (2008).

4. Bates, J. J., Smith, W. L. Sea surface temperature: Observations from geostationary satellites. *Journal of Geophysical Research.* **90**, 11609-11618 (1985).

5. Antoine, D., Andre, J., Morel, A. Oceanic primary production: 2. Estimation at global scale from satellite (Coastal Zone Color Scanner) chlorophyll. *Global Biogeochemical Cycles.* **10** (1), 57-69 (1996).

6. Mason, E., Pascual, A., McWilliams, J. C. A new sea surface height-based code for oceanic mesoscale eddy tracking. *Journal of Atmospheric and Oceanic Technology.* **31** (5), 1181-1188 (2014).

7. Sterlini, P., De Vries, H., Katsman, C. A. Sea surface height variability in the North East Atlantic from satellite altimetry. *Climate Dynamics.* **47**, 1285-1302 (2016).

8. Chelton, D. B., Schlax, M. G., Samelson, R. M., De Szoeke, R. A. Global observations of large oceanic eddies. *Geophysical Research Letters.* **34**, L15606 (2007).

9. Chelton, D. B., Schlax, M. G., Samelson, R. M. Global observations of nonlinear mesoscale eddies. *Progress in Oceanography.* **91** (2), 167-216 (2011).

10. Castelao, R. M., Wang, Y. Wind-driven variability in sea surface temperature front distribution in the California Current System. *Journal of Geophysical Research: Oceans.* **119** (3), 1861-1875 (2014).

11. Pauly, D., Christensen, V. Stratified model of large marine ecosystems: A general approach and an application to the South China Sea, in Large Marine Ecosystems: Stress, Mitigation, and Sustainability. Sherman, K., Alexander, L. M., Gold, B. D., eds. *Washington, DC: AAAS Press.* pp. 148–174 (1993).

12. Gao, S., Wang, H., Liu, G., Li, H. Spatio-temporal variability of chlorophyll a and its responses to sea surface temperature, winds and height anomaly in the western South China Sea. *Acta Oceanologica Sinica.* **32** (1), 48-58 (2013).

13. Chen, Y.-L. Spatial and seasonal variations of nitrate-based new production and primary production in the South China Sea. *Deep-sea Research Part I.* **52** (2), 319-340 (2005).

14. Kahru, M. et al. Global correlations between winds and ocean chlorophyll. *Journal of Geophysical Research.* **115**, C12040 (2010).

15. Wu, C.-R., Shaw, P.-T., Chao, S.-Y. Seasonal and Interannual Variations in the Velocity Field of the South China Sea. *Journal of Oceanography.* **54**, 361-372 (1998).

16. Liu, K. K. et al. Inter-annual variation of chlorophyll in the northern South China Sea observed

at the SEATS Station and its asymmetric responses to climate oscillation. *Biogeosciences.* **10**, 7449-7462 (2013).

17. Yu, Y. et al. The variability of chlorophyll-a and its relationship with dynamic factors in the basin of the South China Sea. *Journal of Marine Systems.* **200**, 103230 (2019).

18. Qu, T., Du, Y., Gan, J., Wang, D. Mean seasonal cycle of isothermal depth in the South China Sea. *Journal of Geophysical Research.* **112**, C02020 (2007).

19. Chen, C.-C., Shiah, F.-K., Chung, S.-W., Liu, K.-K. Winter phytoplankton blooms in the shallow mixed layer of the South China Sea enhanced by upwelling. *Journal of Marine Systems.* **59**, 97-110 (2006).

20. Zhang, W.-Z., Wang, H. Chai, F. Qiu, G. Physical drivers of chlorophyll variability in the open South China Sea. *Journal of Geophysical Research: Oceans.* **121**, 7123–7140 (2016).

21. Zeng, L., Wang, D., Chen, J. Wang, W. Chen, R. SCSPOD14, a South China Sea physical oceanographic dataset derived from in situ measurements during 1919-2014. *Scientific Data.* **3**, 160029 (2016).

22. Greer, A. T., Cowen, R. K., Guigand, C. M., Hare, J. A. Fine-scale planktonic habitat partitioning at a shelf-slope front revealed by a high-resolution imaging system. *Journal of Marine Systems.* **142**, 111-125 (2015).

23. Piontkovski, S. A., Nezlin, N. P., Alazri, A., Alhashmi, K. Mesoscale eddies and variability of chlorophyll-a in the Sea of Oman. *Journal of Remote Sensing.* **33** (17), 5341-5346 (2012).

24. Kahru, M., Fiedler, P. C., Gille, S. T., Manzano, M., Mitchell, B. G. Sea level anomalies control phytoplankton biomass in the Costa Rica Dome area. *Geophysical Research Letters*. **34**, L22601 (2007).

25. Palacz, A. P., Xue, H., Armbrecht, C., Zhang, C., Chai, F. Seasonal and inter-annual changes in the surface chlorophyll of the South China Sea. *Journal of Geophysical Research.* **116**, C09015 (2011).

26. Tang, S., Liu, F., Chen, C. Seasonal and intraseasonal variability of surface chlorophyll a concentration in the South China Sea. *Aquatic Ecosystem Health and Management*. **17**, 242-251 (2014).

27. Fedorov, K. N. The physical nature and structure of oceanic fronts. *Springer-Verlag, Berlin.* viii+333 (1986).

28. Wang, Y., Castelao, R. M., Yuan, Y. Seasonal variability of alongshore winds and sea surface temperature fronts in Eastern Boundary Current Systems. *Journal of Geophysical Research: Oceans.* **120** (3), 2385-2400 (2015).

29. Chen, H.-H., Qi, Y., Wang, Y. Chai, F. Seasonal variability of SST fronts and winds on the southeastern continental shelf of Brazil. *Ocean Dynamics.* **69** (11), 1387-1399 (2019).

30. Woodson, C. B., Litvin, S. Y. Ocean fronts drive marine fishery production and biogeochemical cycling. *Proceedings of the National Academy of Sciences of the United States of America.* **112** (6), 1710-1715 (2015).

31. Siegel, D. A. et al. Regional to global assessments of phytoplankton dynamics from the SeaWiFS mission. *Remote Sensing of Environment.* **135**, 77-91 (2013).

32. Ducet, N., Traon, P. Y. L., Reverdin, G. Global high-resolution mapping of ocean circulation from Topex/Poseidon and ERS-1/2. *Journal of Geophysical Research-Atmospheres.* **105** (C8), 19477-19498 (2000).

33. Dee, D. P. et al. The ERA Interim reanalysis: Configuration and performance of the data

assimilation system. *Quarterly Journal of the Royal Meteorological Society.* **137** (656), 553-597 (2011).
34. Hellerman, S. Computations of wind stress fields over the Atlantic Ocean. *Monthly Weather Review.* **93** (4), 239-244 (1965).
35. Xian, T., Sun, L., Yang, Y.-J., Fu, Y. F. Monsoon and eddy forcing of chlorophyll-a variation in the northeast South China Sea. *International Journal of Remote Sensing.* **33** (23), 7431-7443 (2012).
36. Hu, J. Y., Kawamura, H., Tang, D. Tidal front around the Hainan Island, northwest of the South China Sea. *Journal of Geophysical Research.* **108** (C11), 3342 (2003).
37. Chelton, D. B. Large-scale response of the California Current to forcing by the wind stress curl. *CalCOFI Reports.* **23**, 130-148 (1982).
38. Canny, J. A computational approach to edge-detection. *IEEE Transactions on Pattern Analysis and Machine Intelligence.* **6**, 679–698 (1986).
39. Cayula, J. F., Cornillon, P., Holyer, R., Peckinpaugh, S. Comparative study of two recent edge-detection algorithms designed to process sea-surface temperature fields. *IEEE Geoscience and Remote Sensing Letters.* **29** (1), 175–177 (1991).
40. Cayula J. F., Cornillon P. Cloud detection from a sequence of SST images. *Remote Sensing of Environment.* **55** (1), 80-88 (1996).
41. Ullman, D. S., Cornillon, P. Evaluation of Front Detection Methods for Satellite-Derived SST Data Using in Situ Observations. *Journal of Atmospheric and Oceanic Technology.* **17** (12), 1667-1675 (2000).
42. Oey, L., Chang, M. C., Huang, S., Lin, Y. C., Lee, M. The influence of shelf-sea fronts on winter monsoon over East China Sea. *Climate Dynamics.* **45**, 2047-2068 (2015).
43. Legeckis, R. A survey of worldwide sea surface temperature fronts detected by environmental satellites. *Journal of Geophysical Research.* **83** (C9), 4501–4522 (1978).
44. Yao, J., Belkin, I. M., Chen, J., Wang, D. Thermal fronts of the southern South China Sea from satellite and in situ data. *International Journal of Remote Sensing.* **33** (23), 7458-7468 (2012).
45. Chen, G. et al. Eddy heat and salt transports in the South China Sea and their seasonal modulations. *Journal of Geophysical Research.* **117**, C05021 (2012).
46. Wang, G., Li, J., Wang, C., Yan, Y. Interactions among the winter monsoon, ocean eddy and ocean thermal front in the South China Sea. *Journal of Geophysical Research.* **117**, C08002 (2012).
47. Guo, L. et al. Enhanced chlorophyll concentrations induced by Kuroshio Intrusion Fronts in the Northern South China Sea. *Geophysical Research Letter.* **44** (22), 565-572 (2017).
48. Xing, X. G., Qiu, G. Q., Boss, E., Wang, H. L. Temporal and Vertical Variations of Particulate and Dissolved Optical Properties in the South China Sea. *Journal of Geophysical Research-Oceans.* **124** (6), 3779-3795 (2019).
49. Belkin, I. M., Cornillon, P., Sherman, K. Fronts in Large Marine Ecosystems. *Progress in Oceanography.* **81**, 223-236 (2009).

Figure 1

Click here to access/download;Figure;Figure 1.psd

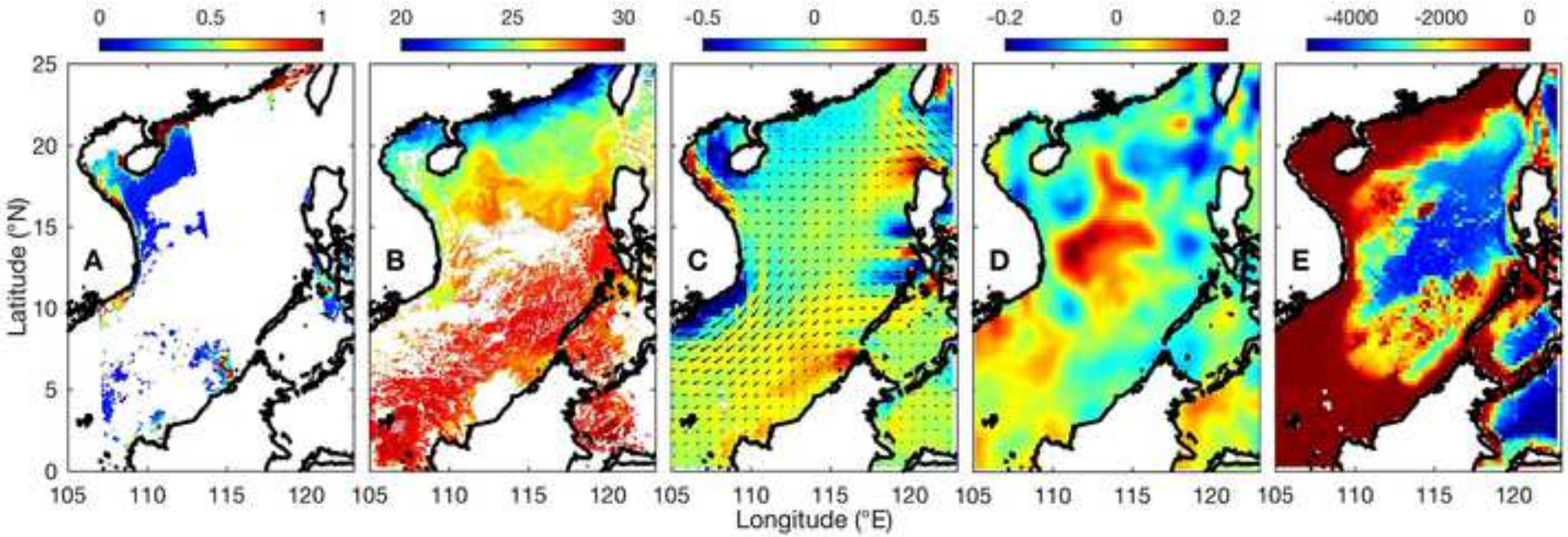

Figure 2

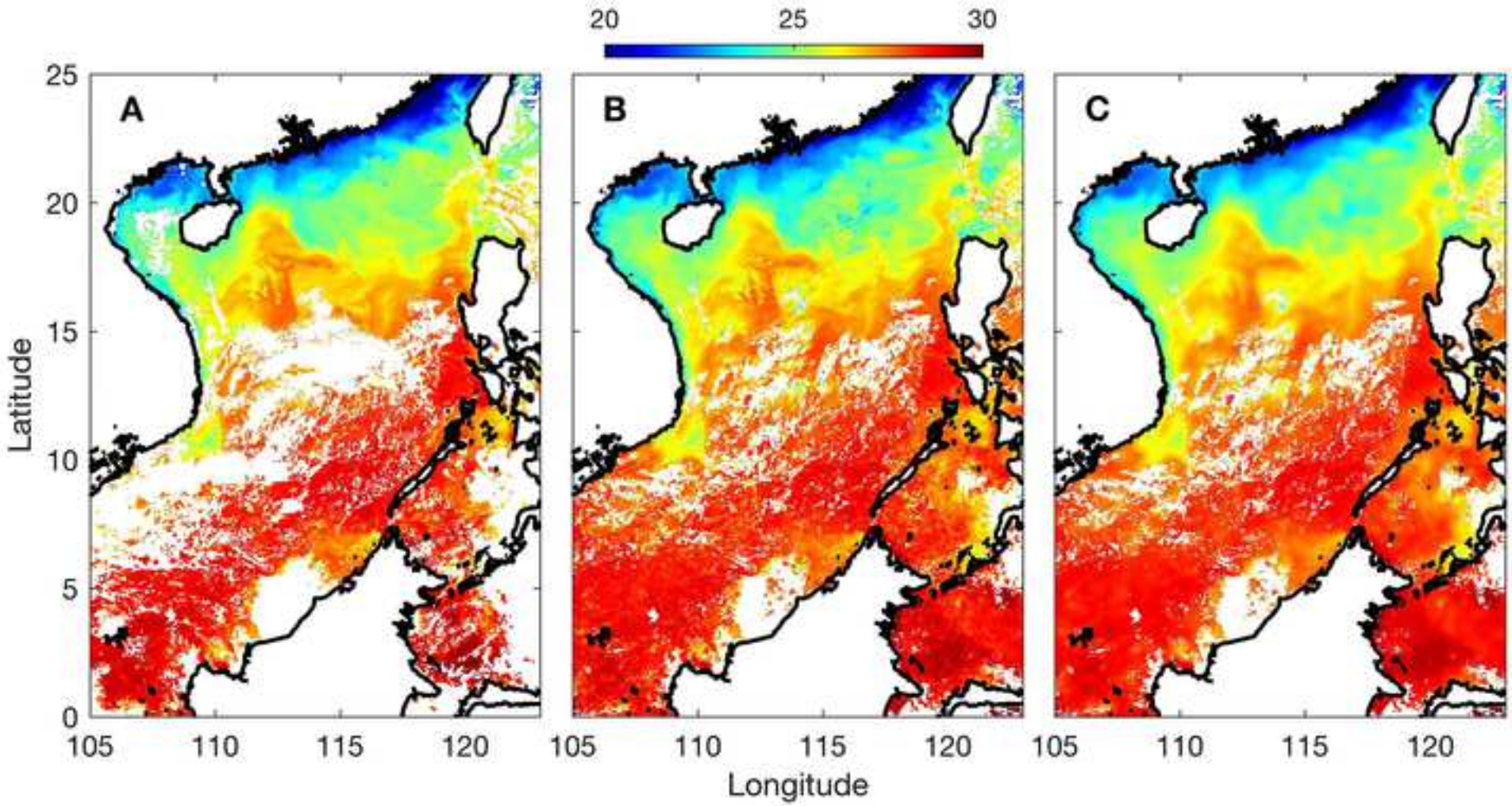

Figure 3

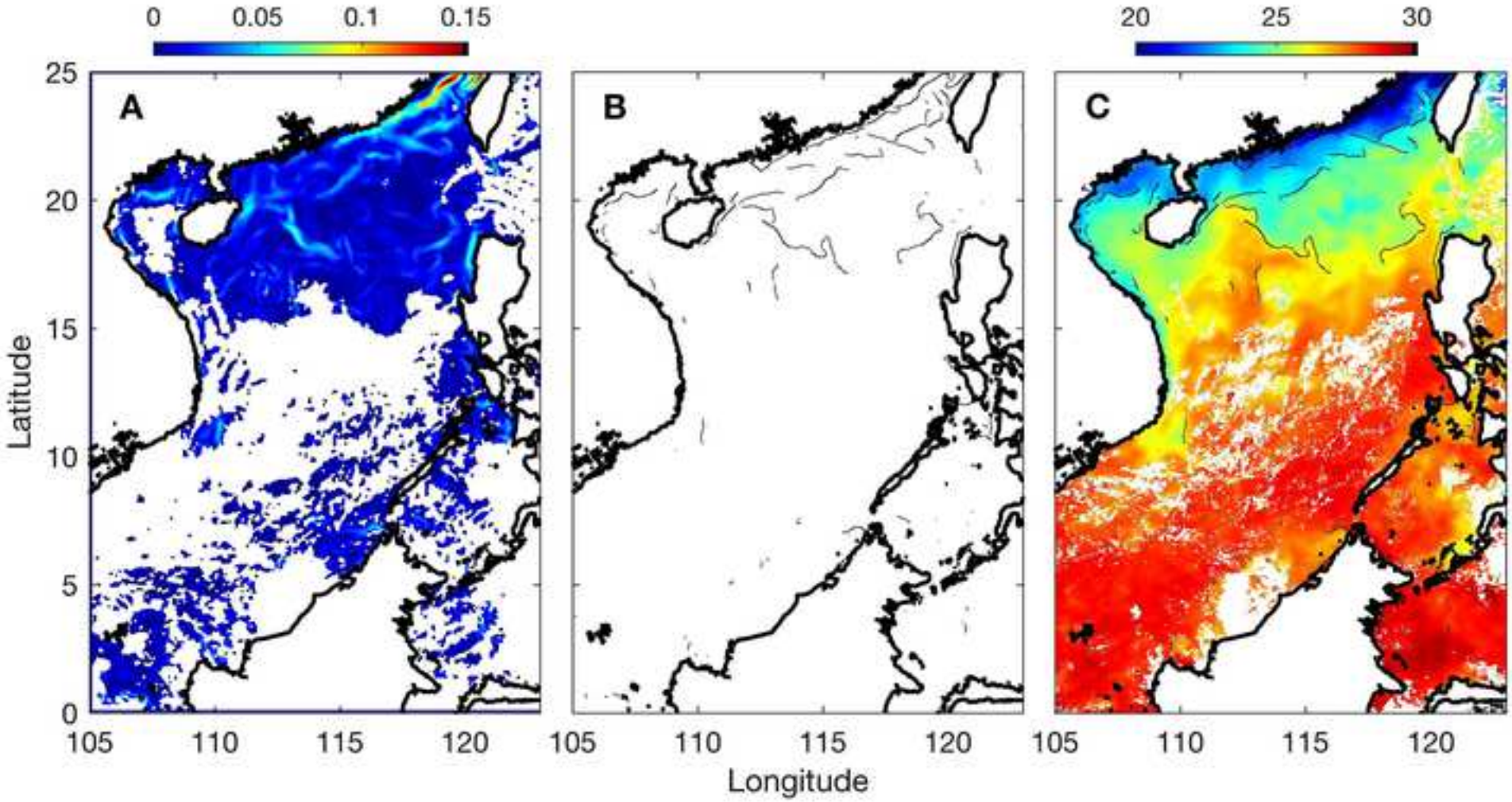

Figure 4

Click here to access/download;Figure;Figure 4.psd

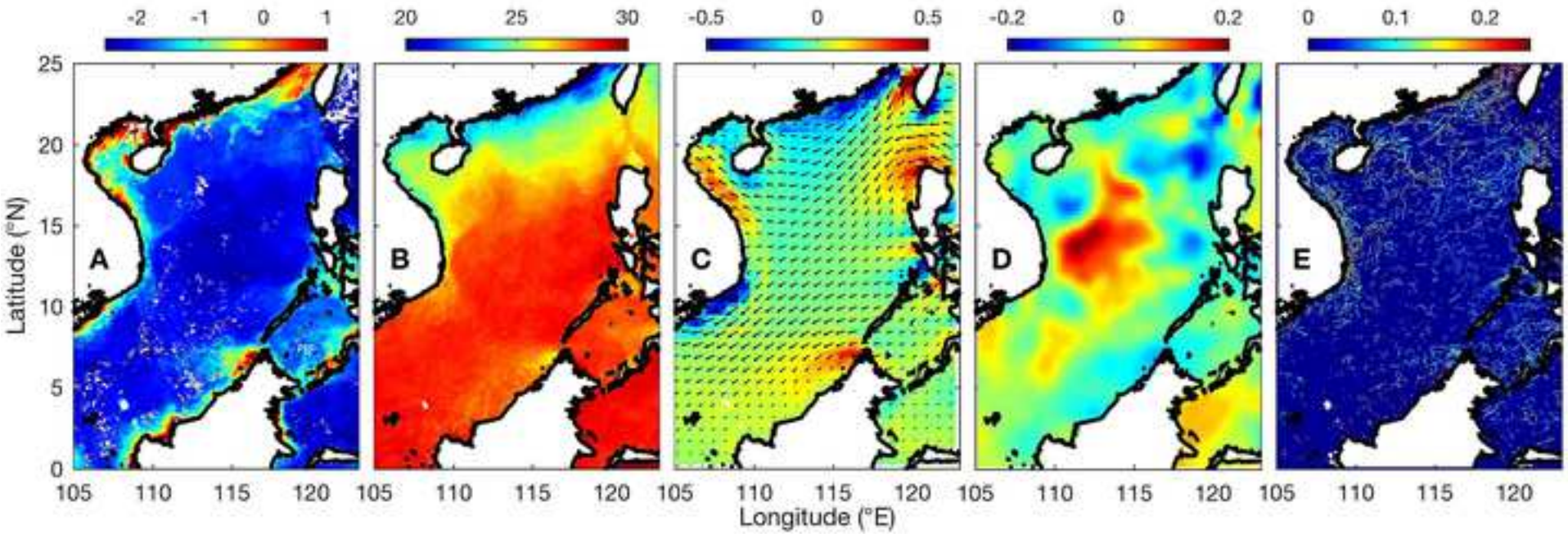

Figure 5

Click here to access/download;Figure;Figure 5.psd

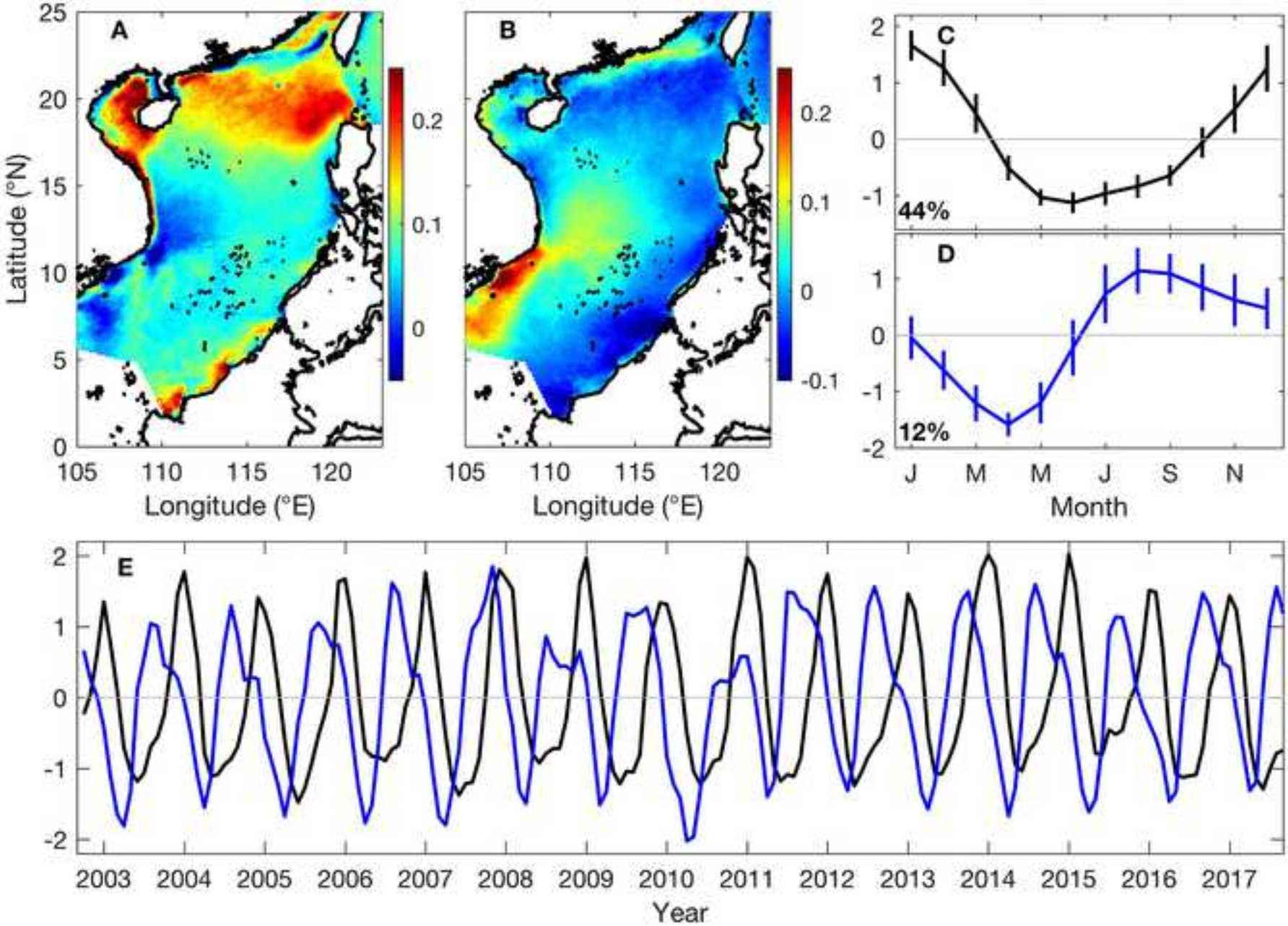

Figure 6

Click here to access/download;Figure;Figure 6.psd

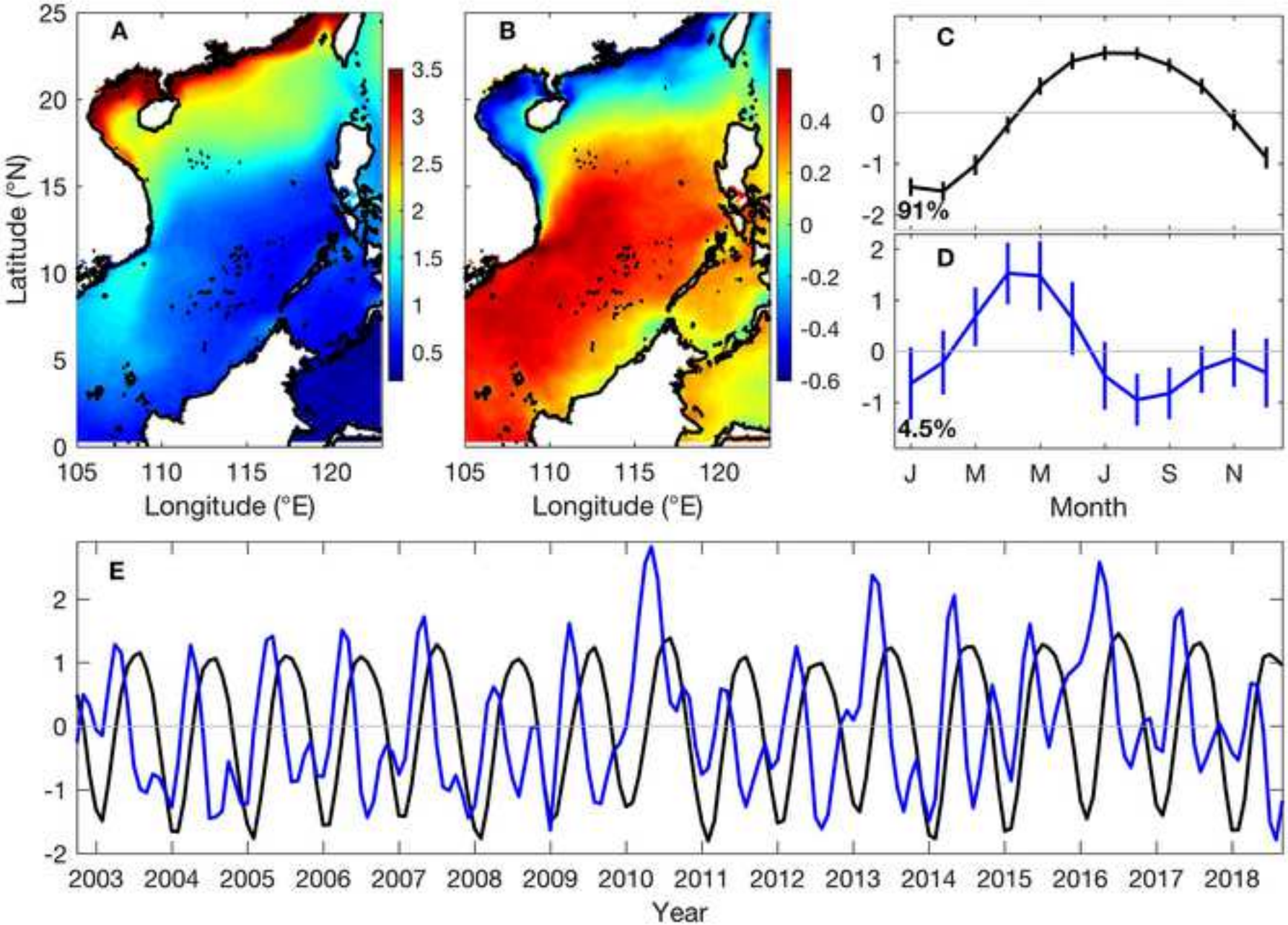

Figure 7

Click here to access/download;Figure;Figure 7.psd

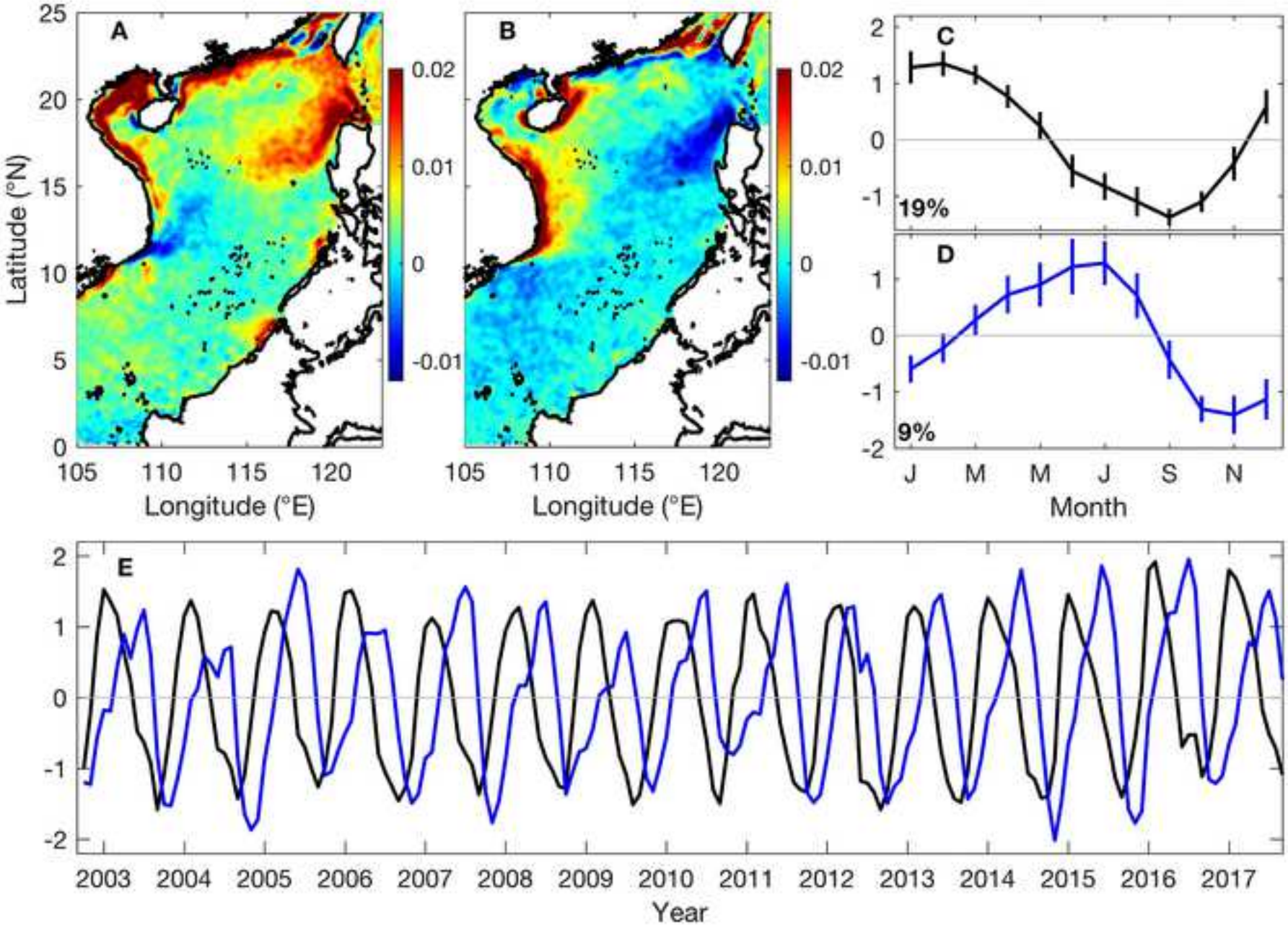

Figure 8

Click here to access/download;Figure;Figure 8.psd

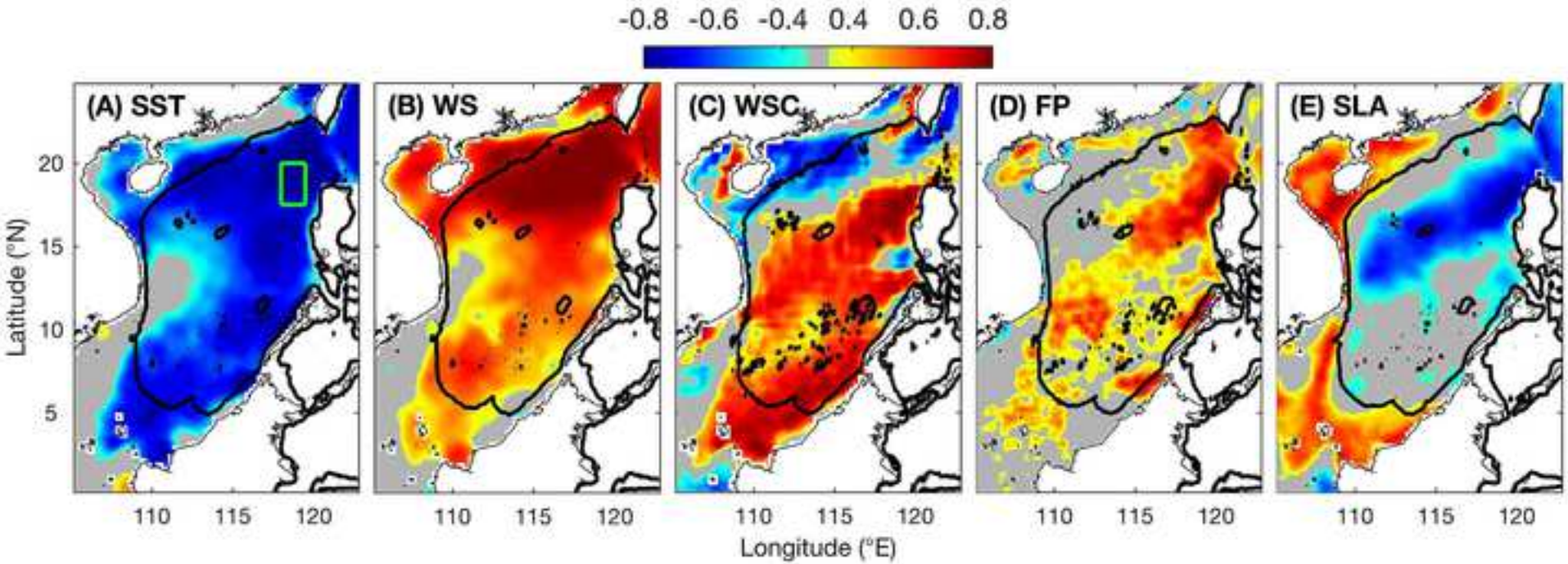

Figure 9

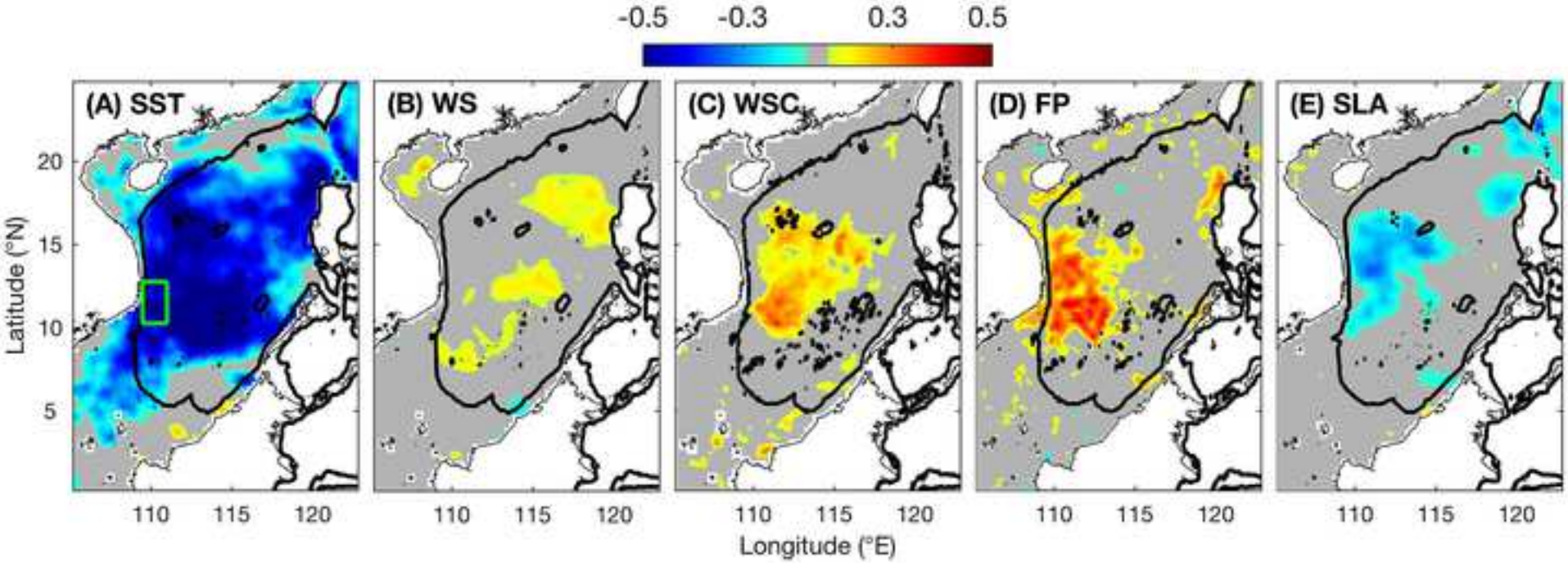

Table1 Click here to access/download;Table;Table_1.xlsx

	Chl-a	SST	WS	WSC	FP	SLA
Chl-a		-0.8	0.78	0.67	0.74	-0.71
SST	-0.41		-0.47	-0.51	-0.79	0.86
WS	0.32	***0.04***		0.63	0.51	***-0.38***
WSC	***0***	***0.08***	***-0.02***		0.52	***-0.37***
FP	0.21	***-0.09***	***0.03***	***0.15***		-0.74
SLA	-0.25	0.42	***0.07***	***0.13***	***-0.08***	

Table2 Click here to access/download;Table;Table_2.xlsx

	Chl-a	SST	WS	WSC	FP	SLA
Chl-a		***-0.15***	***0.36***	***0.35***	***0.26***	***-0.15***
SST	-0.59		-0.48	0.61	***0.07***	***0.17***
WS	0.25	-0.24		-0.14	***-0.02***	***0.1***
WSC	0.29	***-0.1***	0.41		0.53	***-0.21***
FP	0.57	-0.42	0.24	0.29		-0.42
SLA	-0.3	0.54	-0.23	-0.29	-0.47	

Name of Material/Software	Agent/Company	Dateset/Catalog N	Comments/Description
Matlab	MathWorks	Matlab R2016	https://www.mathworks.com/products/matlab.html; referred to analysis soft
Sea surface chlorophyll	NASA	MODIS	mg/mg^3 (podaac-tools.jpl.nasa.gov)
Sea surface height	AVISO	AVISO	meter (www.aviso.altimetry.fr)
Sea surface temperature	NASA	MODIS	°C (podaac-tools.jpl.nasa.gov)
Topography	NOAA	NGDC	meter (maps.ngdc.noaa.gov/viewers/wcs-client/)
Wind	ECMWF	ERA-interim	m/s (www.ecmwf.int/en/forecasts/datasets)

tware in the protocol

TITLE:

Using Satellite Information to Investigate Sea Surface Chlorophyll and its Relationship with Major Features in the South China Sea

AUTHORS AND AFFILIATIONS:

Huan-Huan Chen[1,2,*], Rui Tang[2,*], Hao-Ran Zhang[1,2,*], Yi Yu[2], Yuntao Wang[2]

[1]College of Oceanography, Hohai University, Nanjing, China

[2]State Key Laboratory of Satellite Ocean Environment Dynamics, Second Institute of Oceanography, Ministry of Natural Resources, Hangzhou, China

*These authors contributed equally.

Corresponding Author:

Yuntao Wang (yuntao.wang@sio.org.cn)

Email Addresses of Co-Authors:

Huan-Huan Chen (chenhhmirai@163.com)
Rui Tang (362106798@qq.com)
Hao-Ran Zhang (zhanghaoran22@163.com)
Yi Yu (yiyu@sio.org.cn)

KEYWORDS:

chlorophyll, sea surface temperature, sea surface height, South China Sea, seasonal cycle, satellite observations

SUMMARY:

The sea surface chlorophyll, temperature, sea level height, wind and front data obtained or derived from satellite observations offer an effective way to characterize the ocean. A comprehensive analysis of these data is conducted, including overall average, seasonal cycle, and intercorrelation analyses, to fully understand its regional dynamics and ecosystem.

ABSTRACT:

Satellite observations offer a great approach to investigate the features of major marine parameters. In this study, satellite datasets from 2002 to 2017 were used to describe the surface features in the South China Sea (SCS). Major parameters include sea surface chlorophyll (CHL); sea surface temperature (SST); sea surface height (SSH); and factors derived from these parameters, e.g., fronts, which were calculated from the SST gradient. Due to cloud coverage, monthly averaged data are used in this study. The empirical orthogonal function (EOF) is applied to describe the spatial distribution and temporal variabilities in different factors. The monsoon wind dominates the majority of the variability in the basin; thus, wind from the reanalysis dataset is used to investigate its driving force on different parameters. The seasonal variability in CHL was indeed prominent and significantly correlated with other factors in a majority of the SCS. In winter, a strong northeast monsoon induces a deep mixed layer and high level of chlorophyll

throughout the basin. Significant correlation coefficients are found among factors during the seasonal cycle. In summer, high CHL levels were mostly found in the western SCS. Instead of seasonal dependence, the region is highly dynamic, and factors are significantly correlated in anomalous fields such that anomalously high CHL levels are associated with abnormally strong wind and intense frontal activities. The study showed a step-by-step procedure regarding how to use satellite observations to describe major parameters and their relationships in seasonal and anomalous fields. The method can be applied in other global oceans and will be helpful for understanding marine dynamics.

INTRODUCTION:

The development of remote sensing technology offers a great dataset for describing marine environments with large spatial scales and long periods. With the increasing spatial resolution of satellites, detailed features are now resolved from the regional scale to a few hundred meters[1,2]. An improved understanding of marine dynamics can be achieved with most updated satellite observations[3].

By incorporating multiple sensors on the remote sensing platform, a comprehensive description is available for different parameters. Sea surface temperature (SST) is the basic parameter that has been observed for more than half century[4]. Recently, observations for sea surface chlorophyll-a (CHL) have become available and can be used to describe marine productivity[5]. Altimetry satellites are used for measuring sea surface height[6,7], which is highly related to mesoscale eddy activities in the global ocean[8,9]. In addition to eddies, frontal activities are also important for impacting regional dynamics and primary production[10]. In this study, the SST, CHL, SSH and front datasets, which are derived from SST, are used to analyze their patterns. The time period between October 2002 and September 2017 is used for all parameters.

A major focus of the current study is to find a standard procedure to describe the spatial distribution and temporal variabilities in different factors. In particular, the CHL is used to represent the productivity of the ocean, and a method can be widely used is introduced to investigate the relationship between CHL and other ocean parameters. The method can be used in the future for other regions around the globe to capture major ocean patterns and explore how marine dynamics impact the ecosystem.

The South China Sea (SCS) is designated as the study region because of its relatively high coverage rate of satellite observations. The SCS is abundant in solar radiation; thus, the CHL is mainly determined by the availability of nutrients[11,12]. With more nutrients being transported into the euphotic layer, the CHL levels can increase[13]. Mixing, induced by wind, can introduce nutrients into the ocean surface and enhance CHL[14]. The SCS is uniquely dominated by a monsoon wind system, which subsequently determines the dynamics and ecosystem in the region. The monsoon wind is strongest during winters each year[15]. In summer, the winds change direction and the wind speeds are much weaker than those in winter[16,17]. The wind intensity can determine the strength of vertical mixing such that the mixed layer depth (MLD) deepens (shoal) as the wind increases (decreases)[18]. More nutrients will be transported into the euphotic layer during winter when the wind is strong[19] and CHL reaches its highest point over the year[20,21].

In addition to the wind, MLD can also be determined by other factors, e.g., SST and sea level anomaly (SLA), which ultimately impact nutrient content and CHL[22]. During winter, the weak vertical gradient is associated with low temperatures at the surface[20]. The corresponding MLD is deep, and more nutrients can be transported upward; thus, the CHL in the surface layer is high[17]. An increasing variation in CHL levels can be attributed to mesoscale eddies, which induce vertical transport and mixing[23]. Upwelling (downwelling) is usually found in cyclonic (anticyclonic) eddies associated with depressed (elevated) SLA[8,9] and elevated (depressed) CHL[24]. For other seasons, MLD becomes shallow, and mixing becomes weak; thus, low CHL can be observed over the majority of the basin[25]. The seasonal cycles of CHL levels are subsequently predominant for the region[26].

In addition to mixing, fronts and their associated coastal upwelling can further modulate the CHL. The front, which is defined as a boundary of different water masses, is important to determine the regional circulation and ecosystem responses[27]. Frontogenesis is usually associated with coastal upwelling and convergence[28,29], which can induce nutrients and elevate the growth of phytoplankton[30]. Different algorithms have been developed to automatically identify fronts from satellite observations, including histogram and SST gradient methods, and the latter approach is adopted in this study[28].

The correlation of time series between CHL and different factors offers great insights for quantifying their relationship. The current study offers a comprehensive description of how to use satellite observations to reveal regional marine dynamics related to productivity. This description can be used as a guide for investigating the surface processes in any part of the ocean. The structure of the manuscript includes a step-by-step protocol in the next section, followed by descriptive results in the text and figures. The applicable situation and pros/cons of the method are subsequently discussed.

PROTOCOL:

1. Dataset acquisition

1.1. SST and CHL

1.1.1. Download dataset. Obtain a dataset of satellite observations for SST and CHL from MODIS-Aqua (podaac-tools.jpl.nasa.gov/) where the spatial resolutions of both of these data are approximately 4.5 km at daily intervals (Figure S1).

Formatted: Font: Not Bold

~~[Place Figure 1 here]~~

1.1.2. Determine time span. To maintain consistency among different datasets, use the same time span for all parameters. Adjust the time span based on their temporal coverage and use the longest observing period among different datasets. In this study, download 15 years of data from October 2002 to September 2017.

1.1.3. Perform spatial configuration. ~~Remove the data over land and within 5 km of the coastline, as well as those contaminated by clouds.~~ Transform the CHL data logarithmically because they have a log-normal distribution[31].

NOTE: The designed study region is between 105°E and 123°E and between 0° and 25°N. Downloaded dataset already removed the data over land and within 5 km of the coastline, as well as those contaminated by clouds.

1.1.4. Check preprocessing instruction. Read instructions in the .nc files regarding the preprocessing of SST and CHL data, e.g., scaling is not needed for the SST and CHL data.

NOTE: The range of SSTs is between -2 and 44, and the range of CHL is between 0.01 and 20.

1.1.5. Add the path of the toolbox for NetCDF file in Matlab ~~(**Figure 2**)~~. Use the option 'Add with subfolers' to enclose the paths of the folder 'UTILITIES' and its subfolders (Figure S2).

~~NOTE: All required functions are enclosed in the supplementary folder.~~

~~[Place Figure 2 here]~~

1.1.6. Load and store data into Matlab. Type 'Read_MODIS_SST.m' in the command window to ~~Read~~ read the data for SST. Similarly, type 'Read_MODIS_CHL.m' in the command window to read the data for ~~and~~ CHL ~~by running 'Read_MODIS_SST.m' and 'Read_MODIS_CHL.m', respectively, via clicking the 'RUN' button~~ (Figure S3). Store the .nc files of the satellite data in the folder 'Data'. Structure directory of folders and data following supplementary file.

NOTE: The output variables include SST and CHL in three dimensions, representing meridional location, zonal location and time in days, respectively.

~~[Place Figure 3 here]~~

1.2. Sea level anomaly (SLA)

1.2.1. Download daily SLA data with a 25 km spatial resolution from 2002 to 2017[32]. The SLA data are processed by SSALTO/DUACS and distributed by Archiving, Validation and Interpretation of Satellite Oceanographic Data (AVISO, https://www.aviso.altimetry.fr).

NOTE: SLA describes the difference between the observed sea surface height and the mean sea surface height over 20 years (1993-2012) for the corresponding pixels. ~~The SLA data are processed by SSALTO/DUACS and distributed by Archiving, Validation and Interpretation of Satellite Oceanographic Data (AVISO, https://www.aviso.altimetry.fr).~~

1.2.2. Load and read single-day SLA data by typing 'Read_SLA.m' in the command window ~~and~~

Commented [A1]: How is this done?

Formatted: Highlight

Commented [A2]: It was performed by NASA when producing the satellite dataset.

Commented [A3]: Do you mean "UTILITIES" as Figure 2 shows the screenshot of the procedure to add 'UTILITIES' with subfolders to the Matlab path?

Formatted: Not Highlight

Formatted: Not Highlight

Formatted: Not Highlight

Formatted: Font: Not Bold, Not Highlight

Formatted: Not Highlight

Commented [A4]: All required functions for what?

Commented [A5]: Which supplementary folder?

Commented [A6R5]: The folder I uploaded to 'Dropbox' as you requested. It includes all scripts and the example data.

Formatted: Highlight

Formatted: Not Highlight

Commented [A7]: Considering rephrasing to: Type 'Read_MODIS_SST.m' in the command window and click Run to read the data for SST. Similarly, type 'Read_MODIS_CHL.m' and click Run to read the data for CHL

Formatted: Font: Not Bold

Commented [A8]: How is this done? Do you manually move the .nc files to the "Data" folder?

Commented [A9R8]: Yes. The folders and data should be structured as supplementary file. The information has been added.

Commented [A10]: How is this related to step 1.1.6?

Formatted: Highlight

Commented [A11]: From where? From reference #32 or the link provided in the note? Are these data already processed or do you have to process them after you download the data?

Formatted: Highlight

Formatted: Highlight

Formatted: Highlight

Formatted: Highlight

~~clicking **Run**~~ (Figure S4).

NOTE: Supplementary folder only includes one sample datum in the script for illustration.

~~[Place Figure 4 here]~~

1.3. Wind speed

1.3.1. Obtain the wind information from an ERA-Interim reanalysis product, which was a global atmospheric reanalysis dataset developed by the European Center for Medium-Range Weather Forecasts (ECMWF)[33]. The dataset has a spatial resolution of approximately 25 km and was interpolated from the original dataset with a spatial resolution of approximately 0.7°. Download data for the same period (between October 2002 and September 2017) to maintain consistency with the CHL and SST data.

1.3.2. Load data into Matlab. Type 'Read_WindVector' in the command window ~~and click **Run**~~ to read the one-month wind data (Figure S5). Calculate the monthly mean by averaging the original data, which is at 6-h intervals.

~~[Place Figure 5 here]~~

1.4. Topography

1.4.1. Download the high-resolution topography data from the website of the National Centers for Environmental Information (NCEI, https://maps.ngdc.noaa.gov/viewers/wcs-client/) ~~(Figure 6)~~. The spatial resolution is approximately 2 km. Obtain the ETOPO1 data for bedrock in xyz format for the selected study region (Figure S6).

~~[Place Figure 6 here]~~

1.4.2. Load data into Matlab. ~~Obtain the ETOPO1 data for bedrock in xyz format for the selected study region.~~ Type 'Read_topography.m' in the command window ~~and click Run~~ to read the topography (Figure S7).

~~[Place Figure 7 here]~~

2. Data preprocessing

2.1. Temporal average

2.1.1. Due to the large cloud coverage in the SST and CHL data, replace the original data with 3-day average data. To do this, after running the 'Read_MODIS_SST.m' and 'Read_MODIS_CHL.m' scripts (step 1.1.6), type 'Temporal_average.m' in the command window to ~~and click R~~run the script (Figure S8).

Commented [A12]: I rephrased this sentence. Please review for accuracy.

Commented [A13R12]: Thanks. There are two ways to run a function, either by typing the function name in the command window or clicking 'run' button.

Commented [A14]: Which supplemental folder?

Commented [A15R14]: The folder 'Data' I uploaded to Dropbox.

Formatted: Not Highlight

Formatted: Highlight

Formatted: Font: Not Bold

Commented [A16]: How?

Formatted: Highlight

Commented [A17]: How?

Formatted: Font: Not Bold

Commented [A18]: Please review for accuracy.

Formatted: Highlight

Formatted: Highlight

NOTE: The data are handled at each pixel for each time step. ~~(Note that the script is run)~~

~~[Place Figure 8 here]~~

2.2. Interpolation into the same grid

2.2.1. Because the spatial resolution is not consistent for different datasets, interpolate the SST and CHL data into a spatial grid that is the same as the wind and SLA spatial grid before making comparisons. ~~Use the script 'Interpolation_grid.m' after~~ After running the 'Temporal_average.m' and 'Read_ WindVector.m' scripts, type 'Interpolation_grid.m' in the command window to run the script (Figure S9).

~~[Place Figure 9 here]~~

2.3. Wind stress (curl)

2.3.1. Run the script "Wind_stress_curl.m" (Figure S10) to calculate the wind stress (WS) and wind stress curl (WSC) using the following equations:

$$\vec{\tau} = \rho C \vec{u} \cdot |\vec{u}| \quad (1)$$

$$\nabla \times \vec{\tau} = \frac{\partial \tau_y}{\partial x} - \frac{\partial \tau_x}{\partial y} \quad (2)$$

where $\vec{u}$ is the wind speed vector; $\vec{\tau}$ is the WS in the same direction as the wind vector; τ_x and τ_y are the WS in the east and north directions, respectively; ρ is the air density (equal to 1.2 kg/m^3); and C is the drag coefficient (a value of 0.0015 is used) under neutral stability conditions[34].

~~[Place Figure 10 here]~~

2.4. Monthly average

2.4.1. Calculate the monthly SST, wind and SLA time series as 30-day averages in each pixel by running 'Monthly_average.m' (Figure S11). Due to the high cloud coverage rate, use a 60-day average as the monthly time series for CHL, including 30 days before to 30 days after the 15th day of the month.

~~[Place Figure 11 here]~~

3. SST front detection

3.1. Spatial smoothing

Formatted: Highlight

Formatted: Tab stops: 0.13", Left

3.1.1. ~~Use~~ Run the 'Spatial_smoothing.m' script to average the three-day SST data in each pixel (Figure S12).

NOTE: Large noise was identified in the SST data; thus, smooth data with a 3*3 spatial average were used. When no data were available in the 3-day averaged data, these data were set as unavailable.

~~[Place Figure 12 here]~~

3.2. SST gradient

3.2.1. Run 'SST_gradient.m' to calculate the zonal and meridional SST gradients (G_x and G_y, respectively) as the SST difference between the nearest two pixels divided by the corresponding distance via (Figure S13) following equations (3). Use the obtained gradient vector to calculate the total gradient, G, as a scalar following equation (4).

$$G_x = \frac{\partial SST_x}{\partial x},\ G_y = \frac{\partial SST_y}{\partial y}\ (3)$$

$$G = ({G_x}^2 + {G_y}^2)^{0.5}\ (4)$$

~~[Place Figure 13 here]~~

3.3. Local maximum

3.3.1. Identify a front by testing the value of SST gradient, e.g., label the pixel as a potential frontal pixel if the value is larger than a designated threshold. Only maintain the local maximum pixel in the same direction perpendicular with the gradient direction if there are connected pixels with values larger than the threshold (Figure S14). Here, define the threshold equal to 0.035 °C/km following former studies[10,28].

NOTE: Find corresponding scripts in the supplementary document as 'Local_maximum.m'.

~~[Place Figure 14 here]~~

3.4. Monthly frontal probability (FP)

NOTE: The frontal probability (FP) describes the probability when the front takes place.

3.4.1. Calculate FP for a certain time span, which in this case is the monthly interval by running 'Monthly_FP.m' (Figure S15). Divide the occurrence of fronts at each pixel during a time window by the day number that is free of clouds.

~~[Place Figure 15 here]~~

Formatted: Not Highlight

Formatted: Highlight

Formatted: Not Highlight

Formatted: Not Highlight

Formatted: Not Highlight

Commented [A19]: Please specify the software actions.

Formatted: Highlight

4. Spatial and temporal variability

4.1. Seasonal cycle

4.1.1. Calculate the seasonal cycles of different factors as the averages of different seasons. Here, define the seasons as follows: winter is from Dec. to Feb., spring is from March to May, summer is from Jun. to Aug., and fall is from Sep. to Nov.

~~4.1.1.~~ NOTE: The seasonal cycle is not shown in this study, the following method (EOF) is used to explain the spatial and temporal variability instead.

4.2. Empirical orthogonal function (EOF)

~~4.2.1.~~ Remove temporal average and unavailable pixels. ~~Load data by typing 'load('Monthly_data_for_EOF.mat')' in the command window. Apply an empirical orthogonal function (EOF) to describe the spatial and temporal variabilities in different parameters.~~ Before conducting the EOF, subtract the overall mean at each pixel and exclude the locations where missing observations exceed 20% because of cloud coverage.

~~1.1.1.~~

~~NOTE: The function decomposes the monthly time series into different modes, which are composed of spatial and temporal patterns and the variance explained by each mode decreases with increasing mode number.~~

4.2.1. Load data by typing 'load('Monthly_data_for_EOF.mat')' in the command window.

4.2.2. Apply an empirical orthogonal function (EOF) to describe the spatial and temporal variabilities in different parameters. Run the script 'Empirical_orthogonal_function.m' to calculate the magnitude (Mag), eigenvalues (Eig) and amplitude (Amp) of the EOFs for dataset ~~D~~ (i.e., time series of monthly averaged SST, wind stress, wind stress curl, CHL and FP; Figure S16).

NOTE: The function decomposes the monthly time series into different modes, which are composed of spatial and temporal patterns and the variance explained by each mode decreases with increasing mode number.

~~[Place Figure 16 here]~~

5. Intercorrelation

5.1. Correlation at the seasonal scale

5.1.1. Calculate the correlations between two factors using their time series at each pixel via 'Seasonal_correlation.m' (Figure S17). Because the seasonal cycle is not removed, check the significance of the correlation for all correlations.

Commented [A20]: Is this done manually or using a code?

Formatted: Highlight

Formatted: Normal, No bullets or numbering

Formatted: Font: +Body (Calibri), Font color: Auto, Highlight

Commented [A21]: How are these actually done? Please specify software actions.

Formatted: Font: (Default) +Body (Calibri), Font color: Auto

Formatted: Outline numbered + Level: 3 + Numbering Style: 1, 2, 3, … + Start at: 1 + Alignment: Left + Aligned at: 0" + Indent at: 0"

Formatted: Indent: Left: 0.5", Tab stops: Not at 0.13"

Formatted: List Paragraph

Formatted: Highlight

Formatted: Highlight

Formatted: Font: Not Bold

~~[Place Figure 17 here]~~

5.2. Correlation of an anomalous field

5.2.1. Calculate the correlations between the monthly anomalies of the CHL and other factors, such as SST, WS, fronts and SLA. Obtain the monthly anomalies (the deviation from the mean status) by subtracting the overall average for the corresponding month from the monthly time series. Use the script 'Anomalous_correlation.m' to obtain the correlations (Figure S18).

~~[Place Figure 18 here]~~

6. Display information and calculate relationship~~REPRESENTATIVE RESULTS:~~

6.1. ~~6.1~~ Display satellite information

6.1.1
~~Satellite observations for CHL and SST can be contaminated by cloud coverage, which results in a large portion of data that is not available.~~ Run 'Sat_SCS_Fig3457.m' ~~(Figure 19) is run~~ to produce Figures ~~22~~1 to Figure~~, 23, 24 and 28~~4 about satellite information. ~~The~~ Set current folder ~~is ensured to be set to~~as 'scripts' where the data 'Sat_SCS_data.mat' are located (Figure S19).

6.2. ~~6.2~~ Display EOF result

6.2.1 Run 'Sat_SCS_Fig890.m' to ~~produce Figure 5 to Figure 7 about~~ display EOF results (Figure S20). Figure 5 to Figure 7 describe the spatial magnitude, monthly average and time series of first two modes for CHL, SST and fronts, respectively.

6.3. ~~6.3~~ Calculate relationship between chlorophyll and others

6.3.1 Run 'Sat_SCS_Fig1112.m' to calculate the relationship between chlorophyll and other factors at seasonal and anomalous field (Figure S21). Obtain the correlation map shown as Figure 8 and Figure 9.

REPRESENTATIVE RESULTS:

~~[Place Figure 19 here]~~

Satellite observations for CHL (Figure 1A) and SST (Figure 1B) can be contaminated by cloud coverage, which results in a large portion of data that is not available. The reanalyzed data for wind (Figure 1C) and SLA (Figure 1D) ~~are~~is not impacted by daily clouds. The topography (Figure 1E) has a prominent impact on the spatial distribution of CHL ~~(Figure 20)~~. High CHL is mainly distributed along the coast where the topography is shallow ~~(Figure 20E)~~. Wind is also influenced by orography, and the lee side of mountains is characterized by weak wind; thus, a prominent WSC can be identified, e.g., southwest of the SCS. In contrast, the SLA does not depend much on

Formatted: Not Highlight

Formatted: Font: (Default) +Body (Calibri), Bold, Font color: Auto

Formatted: Font: Not Bold

Formatted: Outline numbered + Level: 2 + Numbering Style: 1, 2, 3, … + Start at: 1 + Alignment: Left + Aligned at: 0" + Indent at: 0", Tab stops: 0.13", Left

Formatted: Font: (Default) +Body (Calibri), Bold, Font color: Auto

Formatted: List Paragraph

Formatted: Highlight

Formatted: Font: Not Bold

Formatted: List Paragraph, Outline numbered + Level: 2 + Numbering Style: 1, 2, 3, … + Start at: 1 + Alignment: Left + Aligned at: 0" + Indent at: 0", Tab stops: 0.13", Left

Formatted: Font: Not Bold

Formatted: Font: Not Bold, Highlight

Formatted: Highlight

Formatted: Font: Not Bold, Highlight

Formatted: Highlight

Formatted: Font: Not Bold, Highlight

Formatted: Font: Not Bold

Formatted: Highlight

Formatted: Font: Not Bold

Formatted: Font: Not Bold

Formatted: List Paragraph, Outline numbered + Level: 2 + Numbering Style: 1, 2, 3, … + Start at: 1 + Alignment: Left + Aligned at: 0" + Indent at: 0", Tab stops: 0.13", Left

Formatted: Font: Not Bold

Formatted: Highlight

Formatted: Highlight

Commented [A22]: Please move this to the protocol.

topography, and an anomalously high SLA can be found in the basin of the SCS.

[Place Figure ~~20~~ 1 here]

Because of the severe cloud impact on satellite observations, many data are not available or spatially inconsistent. An effective and efficient method is applied to fill some data gaps and smooth the field. The data are first replaced with a 3-day average at each pixel, which can effectively fill some gaps as the cloud varies on a daily basis (Figure 2~~1~~B). A spatial average is further applied at each pixel such that the data are replaced by the mean of surrounding values (3*3 pixels). Thus, the spatial inconsistency can be greatly reduced (Figure 2~~1~~C). The locations where satellite data are unavailable after a 3-day average remain unavailable (the blank regions are the same for Figure 2~~1~~B and Figure 2~~1~~C).

[Place Figure 2~~1~~ here]

The daily distribution of the SST front is derived from the SST gradient (Figure 3~~22~~A). The thresholds applied here can effectively capture the location of the front (Figure 3~~22~~B) and ensure depiction of the boundaries of entire water masses (Figure 3~~22~~C). In comparing the gradient and front, they are highly identical because the front is mainly obtained from the gradient.

[Place Figure 3~~22~~ here]

Due to cloud coverage in the CHL, SST and front data, the monthly average time series are calculated and applied in this study. A random example is shown in Figure ~~23~~ 4 for the month of April 2015. There is no existing gap for any of the parameters. The general patterns for different parameters are highly consistent regarding their spatial variance. For example, CHL (SST) is high (low) near the coast and low (high) in the central basin. The monthly average can offer comprehensive information for depicting the regional features. Fronts are mainly distributed along the coast where the dynamics are complex. A large portion of the basin is free of fronts; thus, the center of the SCS is characterized by a value close to zero (Figure 4~~23~~E).

[Place Figure ~~23~~ 4 here]

Most of the surface features are characterized by prominent seasonal variability, which can be clearly observed by EOFs ~~(Figure 24)~~. EOF is a useful mathematic method, which has been widely used in atmospheric and marine sciences. The method can delineate spatial patterns and temporal signals from time series over spatial domains[28]. After spatiotemporal decomposition for sea surface feature in SCS, the first two modes are generally needed for describing the spatial and temporal variabilities. The first two EOFs for CHL describe 44% and 12% of the total variance, respectively. EOF1 captured a large variance in the northern section of the SCS (Figure ~~2~~5A). The corresponding monthly average of the time series (Figure ~~2~~5C) shows that the CHL is elevated (depressed) during winter (summer). The region next to the southwest coast is characterized by a weak magnitude, and the corresponding variability is mainly captured by EOF2 (Figure ~~2~~5B). High (low) CHL values occur during summer (winter), which is mainly out of phase compared with

the northern section. The monthly time series for EOFs show clear seasonal variability, and EOF2 leads EOF1 by approximately 4 months (Figure ~~2~~5E).

~~[Place Figure 24 here]~~

[Place Figure ~~2~~5 here]

The explained variance in the first two EOFs for SST is prominently high, equaling 91% and 5% for EOF1 and EOF2, respectively. It is important to emphasize that the overall average be removed before conducting EOF; thus, the mean field is excluded. EOF1 dominates the total variance, and its magnitude is largest in the northern SCS and decreases southward (Figure ~~2~~6A). The corresponding monthly average of the time series (Figure ~~2~~6C) shows that the SST is elevated (depressed) during summer (winter). The southern SCS is characterized by a weak magnitude, which is attributed to persistent high temperatures at low latitudes. The variability in the southern section is mainly captured by EOF2 (Figure ~~2~~6B). The corresponding SST is enhanced between March and June, while low values persistently occur in the remaining months. Prominent warming occurred in 2010 and 2016, where the SST off the coast southwest of the SCS was much higher than that in the other years (Figure ~~2~~6E). This interannual variability is mainly attributed to El Niño events that reduce the southwest summer monsoon and result in weak upwelling[12]. Because seasonal variability is the major focus of the current study, this feature will not be further discussed.

[Place Figure ~~2~~6 here]

Because of the noisy nature of the gradient, the derived front explained much less of the variance. Indeed, EOF1 and EOF2 of FP only explained 19% and 9% of the total variance, respectively. EOF1 captured the variances in the north and northeast SCS (Figure ~~2~~7A). The corresponding monthly average of the time series (Figure ~~2~~7C) shows that more (less) FP occurs during winter (summer) in those regions. The phase off the coast southwest of the SCS is the opposite, although the corresponding variability is much less prominent. EOF2 captures the spring enhancement of FP (Figure ~~2~~7D) in the western SCS (Figure ~~2~~7B). The monthly time series of EOF1 and EOF2 are characterized by weak interannual variability.

[Place Figure ~~2~~7 here]

Different factors are investigated for their relationships with CHL (Figure ~~2~~8). For example, SST describes the fundamental features of the ocean that can influence the growth rate of phytoplankton and subsequently impact CHL. For the majority of the SCS, there are high correlations between SST and CHL (Figure 8~~29~~A), and most of the correlations can reach more than -0.8. It is important to point out that high correlation does not indicate causation between these two factors. As SST reached its annual maximum in summer, the MLD became shallowest[21]. Nutrients supplied to the euphotic layer were low because vertical mixing was blocked by intensive stratification[13]. As a result, low nutrients limited the growth rate of phytoplankton and resulted in low CHL. In contrast, high CHL occurred in winter when the MLD was deeper, and low

SST induced weak stratification[35].

[Place Figure ~~2~~8 here]

Wind-driven mixing can be approximately gauged by WS and was used to describe vertical mixing[18]. Large correlation coefficients, with values of approximately 0.8, are identified between the WS and CHL levels north of the SCS (Figure 8~~29~~B), particularly in the regions with the strongest winter wind located on the northern shelf of the SCS. Weak but significant correlations can be found to the south. Correlations between WSC and CHL were significant in the majority of the SCS (Figure 8~~29~~C), although they showed opposing signs in the north and south. The positive correlation coefficient between CHL and WSC is to the south, and the negative values are in the north. The region between them is characterized by a nonsignificant correlation. The WS and CHL were found to be strongly correlated in the corresponding region where the winter WS was largest.

The front can induce CHL variability, which was investigated here. A large correlation was found in the northeast and southwest of the SCS (Figure 8~~29~~D). CHL increased as frontal activities became more active[36]. The SLA showed a significant negative correlation with CHL from the northeast SCS towards the southwest and a positive correlation along the west coast of the SCS (Figure 8~~29~~E). It is interesting to note that the positive correlations are limited in the region with shallow topography.

~~[Place Figure 29 here]~~

To the northeast of the SCS, all the correlations are prominent (Figure ~~29~~8). Thus, the correlations of monthly time series between CHL and other parameters are calculated using the spatial average in a designated box (Figure 8~~29~~A). The results show that most of the factors are intercorrelated with significant correlations (top right section of Table 1). Because the seasonal cycle dominates the time series, the correlation is no longer valid after removing the monthly average (bottom left section of Table 1).

[Place Table 1 here]

~~[Place Table 1 here]~~

The correlations in the seasonal cycle are not significant for some regions, e.g., southwest of the SCS (Figure ~~2~~8~~9~~). The region is dominated by dynamic processes, e.g., upwelling and wind-induced offshore transport, which determine the variability in CHL[17]. A significant correlation between CHL and other factors, e.g., SST, WS, fronts and WSC, was identified in anomalous fields (Figure ~~30~~9). The anomalies were calculated for the monthly time series by removing the corresponding monthly average. The effective number of degrees of freedom can be increased, but it does not impact the underlying relationships among their time series[28, 37].

[Place Figure ~~30~~ 9 here]

In anomalous fields, CHL and SST were significantly correlated in the majority of the SCS (Figure 9~~30~~A). When SSTs were anomalously high (low), CHL became anomalously low (high). Similarly, an anomalously high (low) WSC and fronts to the southwest of the SCS can induce a large (weak) CHL (Figure 9~~30~~C, 9~~30~~D). In addition, a negative correlation is found between the anomalous SLA and CHL levels (Figure 9~~30~~E). Different lags were tested, and the correlation only became significant if no lag was deployed; thus, CHL is simultaneously impacted by anomalies in SST, WSC, fronts, and SLA. Their relationship was further investigated using the spatially averaged monthly time series southwest of the SCS (designated as a green box in Figure 9~~30~~A). The results show that most of the factors are intercorrelated with significant correlations in the anomalous field (bottom left section of Table 2).

[Place Table 2 here]

FIGURE AND TABLE LEGENDS:

~~**Figure 1: Procedure for downloading SST and CHL data from websites, shown as snapshots. A.** The website of Po.Daac: **B.** access the data drive, **C.** login to the data system, **D.** locate designated data directory **and E.** click to download daily data file in nc format.~~

~~**Figure 2: Screenshot of the procedure to add 'UTILITIES' with subfolders to the Matlab path**~~

~~**Figure 3: Screenshot of the procedure to read the CHL and SST data by running 'Read_MODIS_CHL.m' and 'Read_MODIS_SST.m', respectively.**~~

~~**Figure 4: Screenshot of the procedure to read the SLA data by running 'Read_SLA.m'.**~~

~~**Figure 5: Screenshot of the procedure to read the wind vector data by running 'Read_WindVector.m'.**~~

~~**Figure 6: Screenshot of the procedure to download topography data from websites, which are shown as snapshots. A.** The website of the National Oceanic and Atmospheric Administration (NOAA) National Center for Environmental Information: **B.** select data using the range of longitude and latitude and **C.** download data in xyz format.~~

~~**Figure 7: Screenshot of the procedure to read the topography data by running 'Read_topography.m'.**~~

~~**Figure 8: Screenshot of the procedure to replace the original SST and CHL data with 3-day average data using 'Temporal_average.m'.**~~

~~**Figure 9: Screenshot of the procedure to interpolate 3-day averaged SST and CHL into the same grid as the wind data.**~~

~~**Figure 10: Screenshot of the procedure to calculate the wind stress curl using**~~

~~**'Wind_stress_curl.m'.**~~

~~**Figure 11: Screenshot of the procedure to the calculated time series of monthly averaged SST and CHL using 'Monthly_average.m'.**~~

~~**Figure 12: Screenshot of the procedure to smooth 3-day average SST data spatially using 'Spatial_smoothing.m'.**~~

~~**Figure 13: Screenshot of the procedure to obtain the SST gradient vector using 'SST_gradient.m'.**~~

~~**Figure 14: Screenshot of the procedure to identify the front as the local maximum and suppress pixels with a gradient less than 90% of the maximum using 'Local_maximum.m'.**~~

~~**Figure 15: Screenshot of the procedure to calculate the monthly frontal probability using 'Monthly_FP.m'.**~~

~~**Figure 16: Screenshot of the procedure to decompose monthly time series using 'Empirical_orthogonal_function.m' for different variables to obtain spatial and temporal variability.** 'Amp' is the amplitude, 'Mag' is the magnitude, and 'Eig' is the Eigen values for different modes.~~

~~**Figure 17: Screenshot of the procedure to calculate seasonal correlation using monthly time series of different variables via 'Seasonal_correlation.m'.**~~

~~**Figure 18: Screenshot of the procedure to calculate anomalous correlation using monthly time series of different variables via 'Anomalous_correlation.m'.**~~

~~**Figure 19: Screenshot of the procedure to produce Figures 20, 21, 22 and 25.**~~

Figure 1~~20~~: Original observations for major parameters on April 15, 2015. A. Chlorophyll (CHL), **B.** sea surface temperature (SST), **C.** wind stress curl (WSC) with wind stress (WS) vector, **D.** sea surface anomaly and **E.** topography for the ocean basin.

Figure 2~~1~~: Sea surface temperature (SST) for a single day on April 15, 2015. A. Original SST from MODIS, **B**. three-day averaged SST and **C.** SST after spatial smoothing.

Figure 3~~22~~: Procedure for front detection derived from SST. A. Magnitude of SST gradient, **B**. the distribution of the SST front in thin black color and **C.** front distribution with the corresponding SST.

Figure 4~~23~~: Monthly average for major parameters in April 2015. A. CHL (in logarithm scale), **B.** SST, **C.** wind stress curl (WSC) with wind stress (WS) vector, **D.** sea surface anomaly and **E.** frontal probability (FP).

~~**Figure 24: Screenshot of the procedure to produce Figures 25, 26 and 27.**~~

Figure ~~2~~5: The EOF for CHL. A. Magnitude of EOF1, **B.** magnitude of EOF2, **C.** monthly averaged time series of EOF1, **D.** monthly average for EOF2 and **E.** monthly time series of EOF1 (black) and EOF2 (blue).

Figure ~~2~~6: Same as in Figure 25 but for SST.

Figure ~~2~~7: Same as in Figure 25 but for FP.

~~**Figure 28: Screenshot of the procedure to produce Figures 29 and 30.**~~

Figure ~~29~~8: Correlations between CHL and other factors at the seasonal scale. A. SST, **B.** wind stress (WS), **C.** wind stress curl (WSC), **D.** frontal probability (FP) and **E.** sea level anomaly (SLA). The gray color indicates that the correlation is nonsignificant. Spatially averaged variables are calculated based on the green box in the left panel. Their time series are used to obtain the correlation coefficients in Table 1. This figure has been modified from Yu et al. (2019)[17].

Figure ~~30~~9: Correlation between CHL and other factors in the anomalous field. A. SST, **B.** WS, **C.** WSC, **D.** FP and **E.** SLA. The gray color indicates that the correlation is nonsignificant. Spatially averaged variables are calculated based on the green box in the left panel. Their time series are used to obtain the correlation coefficients shown in Table 2. This figure has been modified from Yu et al. (2019)[17].

Table 1. Correlation coefficients of the time series among factors, located northeast of the SCS, e.g., SST (sea surface temperature), FP (frontal probability), WSC (wind stress curl) and WS (wind stress), using the box shown in Figure 11A. The monthly average and anomaly top are shown in the top right section and left bottom section, respectively. Red fonts indicate that the correlation cannot fulfill the 95% confidence level. The table has been modified from Yu et al. (2019)[17].

Table 2. Similar to Table 1 but for correlation coefficients of anomalous time series in the southwest SCS (see Figure 12A for location). The table has been modified from Yu et al. (2019)[17].

DISCUSSION:

In this study, the major features of marine systems are described using satellite observations. The CHL, which can be used to represent ocean production, is selected as an indicator factor. Factors related to CHL variability were investigated using monthly averaged time series, e.g., SST, WS, WSC, FP and SLA. Three critical steps are described in this study: acquiring satellite data for different parameters, describing their spatial and temporal variabilities via EOF, and determining interrelationships among different factors by calculating correlation coefficients. A detailed procedure showing the identification for daily frontal distribution, which is derived from the SST observations, is included. Two major approaches have been developed for SST front detection: the gradient method[10,38] and the histogram method[39,40]. The histogram method is based on a

similar range of values for SST, which can be used to divide the water masses into different groups. The pixels with values between different groups representing the pixel in a transitional band are defined as fronts. On the other hand, the gradient method separates several relatively uniform water bodies as pixels with large gradient values. A comparison study was conducted, and they found lower false rates using the histogram method and fewer missed fronts using the gradient method[41]. In this study, the gradient-based method[38] was adopted following former studies[10,28]. The algorithm can avoid front break-up into multiple edge fragments by allowing the magnitude to decrease to a level below a smaller threshold. In addition to the dataset included here, other satellite observations, such as the aerosol index, can also be used with a similar approach.

Most of the procedures can be directly applied in other regions or datasets. Modification may take place to change the threshold of front detection. Because the SST gradient in the SCS is comparable with the Eastern Boundary Current System[28], the same thresholds were implemented for the current study. A previous study revealed that the SST gradient from different datasets can vary as much as three times[42], which makes the method somehow less objective. Substantial studies have investigated frontal activities around the global oceans[28,43]. The best approach to validate fronts is to compare them with in situ observations. Yao[44] described the monthly frontal distribution for the SCS. Their results agreed well with the in situ measurements. The overall gradient should be checked and adjusted since its value may vary depending on the spatial resolution and instruments. In particular, the threshold should be updated when another SST dataset is used. A basic understanding of the regional dynamics is fundamental to understanding frontogenesis[45,46,47]. The front detection script can be developed by individual authors based on the description in this paper.

Satellite information offers a comprehensive understanding of surface features, and a results comparison with in situ observations can aid in evaluating credibility. However, satellite observations are limited to the ocean surface, which limits the application for understanding the vertical structure of the water column. In a recent study, satellite observations revealed that the surface CHL increased by 15 times, but the vertical integrated value only increased by 2.5 times[48]. This difference was because the surface value was impacted by the coeffects of phytoplankton growth and shoaling of MLD, resulting in an unrealizable value at the surface. Thus, the surface feature may not offer an accurate description for the entire water column. Additionally, the influence of cloud coverage limits the continuous observations of satellites. Thus, monthly time series are calculated for different factors over the same region and same period. This will guarantee the credibility of calculating the correlations among different factors. However, the short-period events, e.g., typhoons that last for a few days to a week, will not be resolved.

Compared with former studies, the proposed method can offer spatial information at the pixel level, which can help to evaluate the dynamics in a more detailed manner. Some former studies averaged the entire SCS as a single number and obtained a time series. They found that an unusually strong WS and high SST can induce anomalously high CHL[16], which is consistent with current result. However, the spatial variation in the relationships was not resolved. In this study, the basin-scale correlation between WS and CHL was weak in the anomalous field. A large

significant correlation was only identified for certain areas, e.g., in the center of the SCS (Figure 32B). Thus, the current method offers a comprehensive description for investigating spatial variations. Similarly, observations from two Bio-Argo floats were used and revealed that WSC did not correlate with CHL variability[20]. However, the trajectories of the two floats are only located in certain regions. In this case, it was exactly within the band where the correlation between the CHL level and the WSC was not significant (Figure 31D). The proposed method is very helpful for resolving the spatial dependence among factors, which is a fundamental characteristic of the global ocean.

In summary, the method used here can accurately describe the spatial distribution and temporal variability in ocean surface features using satellite observations. With the increasing resolution of satellite datasets, more detailed features can be identified and investigated, which enables a general understanding of regional features, including CHL, SST, and SSH. The correlation of monthly time series among different factors can aid in understanding their dynamic relationships and potential impact on an ecosystem[49]. Because the correlation can largely vary at different spatial locations, the proposed method offers a detailed and comprehensive description. A similar approach can be applied to any ocean basin worldwide, which will be greatly helpful to improve the understanding of marine dynamics and ecosystems.

ACKNOWLEDGMENTS:
The support from the National Key Research and Development Program of China (No. 2016YFC1401601), the Postgraduate Research & Practice Innovation Program of Jiangsu Province (No. SJKY19_0415) supported by the Fundamental Research Funds for the Central Universities (No. 2019B62814), the National Natural Science Foundation of China (Nos. 41890805, 41806026 and 41730536) and Joint Advanced Marine and Ecological Studies in the Bay of Bengal and the eastern equatorial Indian Ocean were greatly acknowledged.
Appreciate the provision of data from sources including the National Aeronautics and Space Administration (NASA), the European Centre for Medium-Range Weather Forecasts (ECMWF), the Copernicus Marine and Environment Monitoring Service (CMEMS) and the National Oceanic and Atmospheric Administration (NOAA).

DISCLOSURES:
The authors have nothing to disclose.

REFERENCES:
1. Behrenfeld, M.J., Falkowski, P.G. Photosynthetic rates derived from satellite-based chlorophyll concentration. *Limnology and Oceanography*, **42** (1), 1-20 (1997).
2. Loisel, H. et al. Assessment and analysis of the chlorophyll-a concentration variability over the Vietnamese coastal waters from the MERIS ocean color sensor (2002–2012). *Remote Sensing of Environment*, **190**, 217-232 (2017).
3. Gohin, F. et al. Towards a better assessment of the ecological status of coastal waters using satellite-derived chlorophyll-a concentrations. *Remote Sensing of Environment*, **112** (8), 3329-3340 (2008).
4. Bates, J.J., Smith, W.L. Sea surface temperature: Observations from geostationary satellites.

Journal of Geophysical Research, **90**, 11609-11618 (1985).
5. Antoine, D., Andre, J., Morel, A. Oceanic primary production: 2. Estimation at global scale from satellite (Coastal Zone Color Scanner) chlorophyll. *Global Biogeochemical Cycles*, **10** (1), 57-69 (1996).
6. Mason, E., Pascual, A., Mcwilliams, J.C. A new sea surface height-based code for oceanic mesoscale eddy tracking. *Journal of Atmospheric and Oceanic Technology*, **31** (5), 1181-1188 (2014).
7. Sterlini, P., De Vries, H., Katsman, C.A. Sea surface height variability in the North East Atlantic from satellite altimetry. *Climate Dynamics*, **47**, 1285-1302 (2016).
8. Chelton, D.B., Schlax, M.G., Samelson, R.M., De Szoeke, R.A. Global observations of large oceanic eddies. *Geophysical Research Letters*, **34**, L15606 (2007).
9. Chelton, D.B., Schlax, M.G., Samelson, R.M. Global observations of nonlinear mesoscale eddies. *Progress in Oceanography*, **91** (2), 167-216 (2011).
10. Castelao, R.M., Wang, Y. Wind-driven variability in sea surface temperature front distribution in the California Current System. *Journal of Geophysical Research: Oceans*, **119** (3), 1861-1875 (2014).
11. Pauly, D., Christensen, V. Stratified model of large marine ecosystems: A general approach and an application to the South China Sea, in Large Marine Ecosystems: Stress, Mitigation, and Sustainability, Sherman, K., Alexander, L. M., Gold, B. D., Eds. *Washington, DC: AAAS Press*, pp. 148–174 (1993).
12. Gao, S., Wang, H., Liu, G., Li, H. Spatio-temporal variability of chlorophyll a and its responses to sea surface temperature, winds and height anomaly in the western South China Sea. *Acta Oceanologica Sinica*, **32**(1), 48-58 (2013).
13. Chen, Y.-L. Spatial and seasonal variations of nitrate-based new production and primary production in the South China Sea. *Deep-sea Research Part I*, **52**(2), 319-340 (2005).
14. Kahru, M. et al. Global correlations between winds and ocean chlorophyll. *Journal of Geophysical Research,* **115,** C12040 (2010).
15. Wu, C.-R., Shaw, P.-T., Chao, S.-Y. Seasonal and Interannual Variations in the Velocity Field of the South China Sea. *Journal of Oceanography*, **54,** 361-372 (1998).
16. Liu, K. K., Wang, L.-W., Dai, M., Tseng, C.-M., Yang, Y., Sui, C.-H. Inter-annual variation of chlorophyll in the northern South China Sea observed at the SEATS Station and its asymmetric responses to climate oscillation. *Biogeosciences*, **10,** 7449-7462 (2013).
17. Yu, Y., Xing, X., Liu, H., Yuan, Y., Wang, Y., Chai, F. The variability of chlorophyll-a and its relationship with dynamic factors in the basin of the South China Sea. *Journal of Marine Systems*, **200**, 103230 (2019).
18. Qu, T., Du, Y., Gan, J., Wang, D. Mean seasonal cycle of isothermal depth in the South China Sea. *Journal of Geophysical Research*, **112,** C02020 (2007).
19. Chen, C.-C., Shiah, F.-K., Chung, S.-W., Liu, K.-K. Winter phytoplankton blooms in the shallow mixed layer of the South China Sea enhanced by upwelling. *Journal of Marine Systems*, **59**, 97-110 (2006).
20. Zhang, W.-Z., Wang, H. Chai, F. Qiu, G. Physical drivers of chlorophyll variability in the open South China Sea. *Journal of Geophysical Research: Oceans*, **121,** 7123–7140 (2016).
21. Zeng, L., Wang, D., Chen, J. Wang, W. Chen, R. SCSPOD14, a South China Sea physical oceanographic dataset derived from in situ measurements during 1919-2014. *Scientific Data*, **3,**

160029 (2016).
22. Greer, A.T., Cowen, R.K., Guigand, C.M., Hare, J.A. Fine-scale planktonic habitat partitioning at a shelf-slope front revealed by a high-resolution imaging system. *Journal of Marine Systems*, **142,** 111-125 (2015).
23. Piontkovski, S.A., Nezlin, N.P., Alazri, A., Alhashmi, K. Mesoscale eddies and variability of chlorophyll-a in the Sea of Oman. *Journal of Remote Sensing*, **33**(17), 5341-5346 (2012).
24. Kahru, M., Fiedler, P.C., Gille, S.T., Manzano, M., Mitchell, B.G. Sea level anomalies control phytoplankton biomass in the Costa Rica Dome area. *Geophysical Research Letter,* **34,** L22601 (2007).
25. Palacz, A. P., Xue, H., Armbrecht, C., Zhang, C., Chai, F. Seasonal and inter-annual changes in the surface chlorophyll of the South China Sea. *Journal of Geophysical Research*, **116,** C09015 (2011).
26. Tang, S., Liu, F., Chen, C. Seasonal and intraseasonal variability of surface chlorophyll a concentration in the South China Sea. *Aquatic Ecosystem Health and Management*, **17,** 242-251 (2014).
27. Fedorov, K.N. The physical nature and structure of oceanic fronts. *Springer-Verlag, Berlin etc.,* **viii+333** (1986).
28. Wang, Y., Castelao, R.M., Yuan, Y. Seasonal variability of alongshore winds and sea surface temperature fronts in Eastern Boundary Current Systems. *Journal of Geophysical Research: Oceans*, **120**(3), 2385-2400 (2015).
29. Chen, H.-H., Qi, Y., Wang, Y. Chai, F. Seasonal variability of SST fronts and winds on the southeastern continental shelf of Brazil. *Ocean Dynamics*, **69** (11), 1387-1399 (2019).
30. Woodson, C.B., Litvin, S.Y. Ocean fronts drive marine fishery production and biogeochemical cycling. *Proceedings of the National Academy of Sciences of the United States of America*, **112** (6), 1710-1715 (2015).
31. Siegel, D.A. et al. Regional to global assessments of phytoplankton dynamics from the SeaWiFS mission. *Remote Sensing of Environment*, **135**, 77-91 (2013).
32. Ducet, N., Traon, P.Y.L., Reverdin, G. Global high-resolution mapping of ocean circulation from Topex/Poseidon and ERS-1/2. *Journal of Geophysical Research-Atmospheres*, **105** (C8), 19477-19498 (2000).
33. Dee, D.P. et al. The ERA Interim reanalysis: Configuration and performance of the data assimilation system. *Quarterly Journal of the royal meteorological society*, **137** (656), 553-597 (2011).
34. Hellerman, S. Computations of wind stress fields over the Atlantic Ocean. *Monthly Weather Review*, **93**(4), 239-244 (1965).
35. Xian, T., Sun, L., Yang, Y.-J., Fu, Y.F. Monsoon and eddy forcing of chlorophyll-a variation in the northeast South China Sea. *International Journal of Remote Sensing*, **33**(23), 7431-7443 (2012).
36. Hu, J.Y., Kawamura, H., Tang, D. Tidal front around the Hainan Island, northwest of the South China Sea. *Journal of Geophysical Research*, **108**(C11), 3342 (2003).
37. Chelton, D.B. Large-scale response of the California Current to forcing by the wind stress curl. *CalCOFI Rep.,* **23**, 130-148 (1982).
38. Canny, J. A computational approach to edge-detection. *IEEE Transactions on Pattern Analysis and Machine Intelligence*, **6**, 679–698 (1986).

39. Cayula, J.F., Cornillon, P., Holyer, R., Peckinpaugh, S. Comparative study of two recent edge-detection algorithms designed to process sea-surface temperature fields. *IEEE Geoscience and Remote Sensing Letters*, **29**(1), 175–177 (1991).
40. Cayula J.F., Cornillon P. Cloud detection from a sequence of SST images. *Remote Sensing of Environment*, **55**(1), 80-88 (1996).
41. Ullman, D.S., Cornillon, P. Evaluation of Front Detection Methods for Satellite-Derived SST Data Using in Situ Observations. *Journal of Atmospheric and Oceanic Technology*, **17**(12), 1667-1675 (2000).
42. Oey, L., Chang, M.C., Huang, S., Lin, Y.C., Lee, M. The influence of shelf-sea fronts on winter monsoon over East China Sea. *Climate Dynamics*, **45**, 2047-2068 (2015).
43. Legeckis, R. A survey of worldwide sea surface temperature fronts detected by environmental satellites. *Journal of Geophysical Research*, **83**(C9), 4501–4522 (1978).
44. Yao, J., Belkin, I.M., Chen, J., Wang, D. Thermal fronts of the southern South China Sea from satellite and in situ data. *International Journal of Remote Sensing*, **33**(23), 7458-7468 (2012).
45. Chen, G., Gan, J., Xie, Q., Chu, X., Wang, D., Hou, Y. Eddy heat and salt transports in the South China Sea and their seasonal modulations. *Journal of Geophysical Research*, **117**, C05021 (2012).
46. Wang, G., Li, J., Wang, C., Yan, Y. Interactions among the winter monsoon, ocean eddy and ocean thermal front in the South China Sea. *Journal of Geophysical Research*, **117**, C08002 (2012).
47. Guo, L., Xiu, P., Chai, F., Xue, H., Wang, D., Sun, J. Enhanced chlorophyll concentrations induced by Kuroshio Intrusion Fronts in the Northern South China Sea. *Geophysical Research Letter*, **44**(22), 565-572 (2017).
48. Xing, X.G., Qiu, G.Q., Boss, E., Wang, H.L. Temporal and Vertical Variations of Particulate and Dissolved Optical Properties in the South China Sea. *Journal of Geophysical Research-Oceans*, **124**(6): 3779-3795 (2019).
49. Belkin, I. M., Cornillon, P., Sherman, K. Fronts in Large Marine Ecosystems. *Progress in Oceanography,* **81**, 223-236 (2009).

Screenfile1

Click here to access/download;Supplemental File (Figures, Permissions, etc.);Figure S1.psd

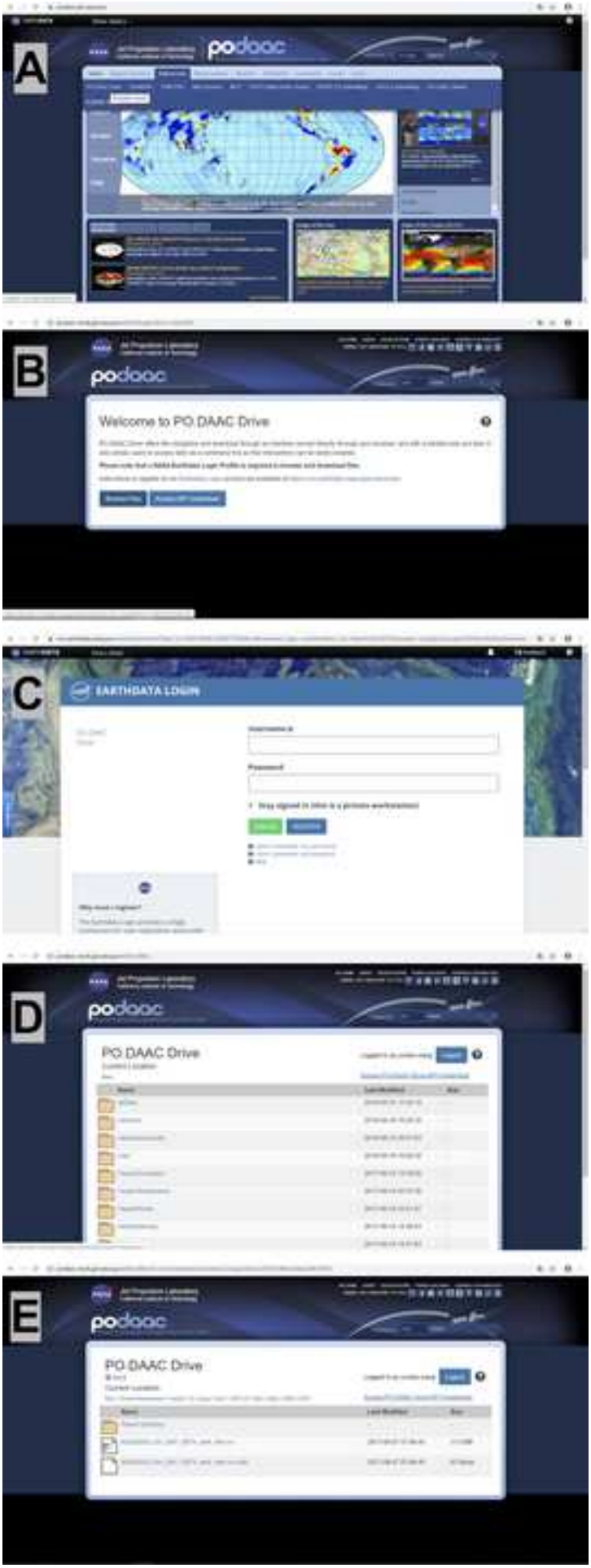

Screenfile2

Click here to access/download;Supplemental File (Figures, Permissions, etc.);Figure S2.psd

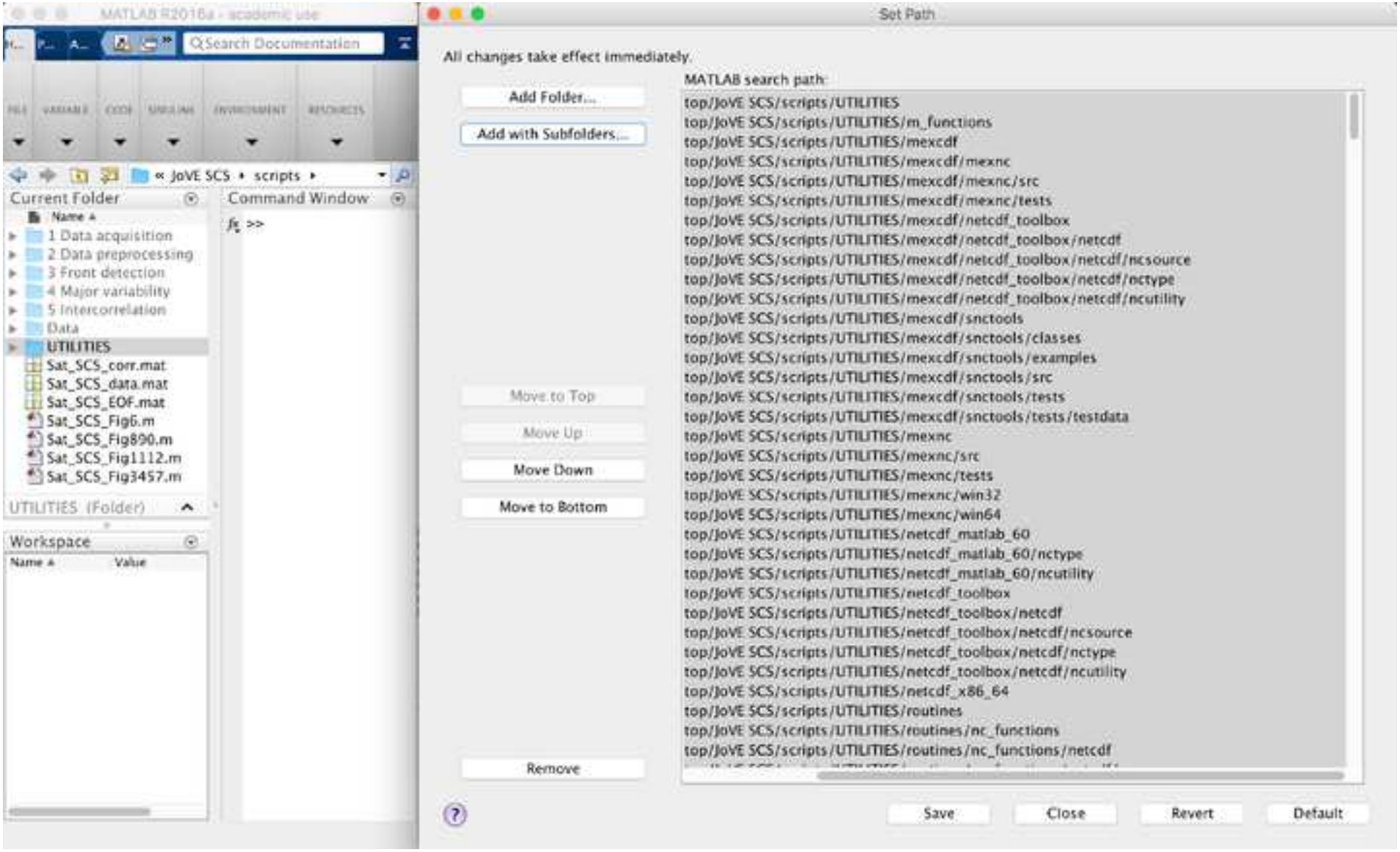

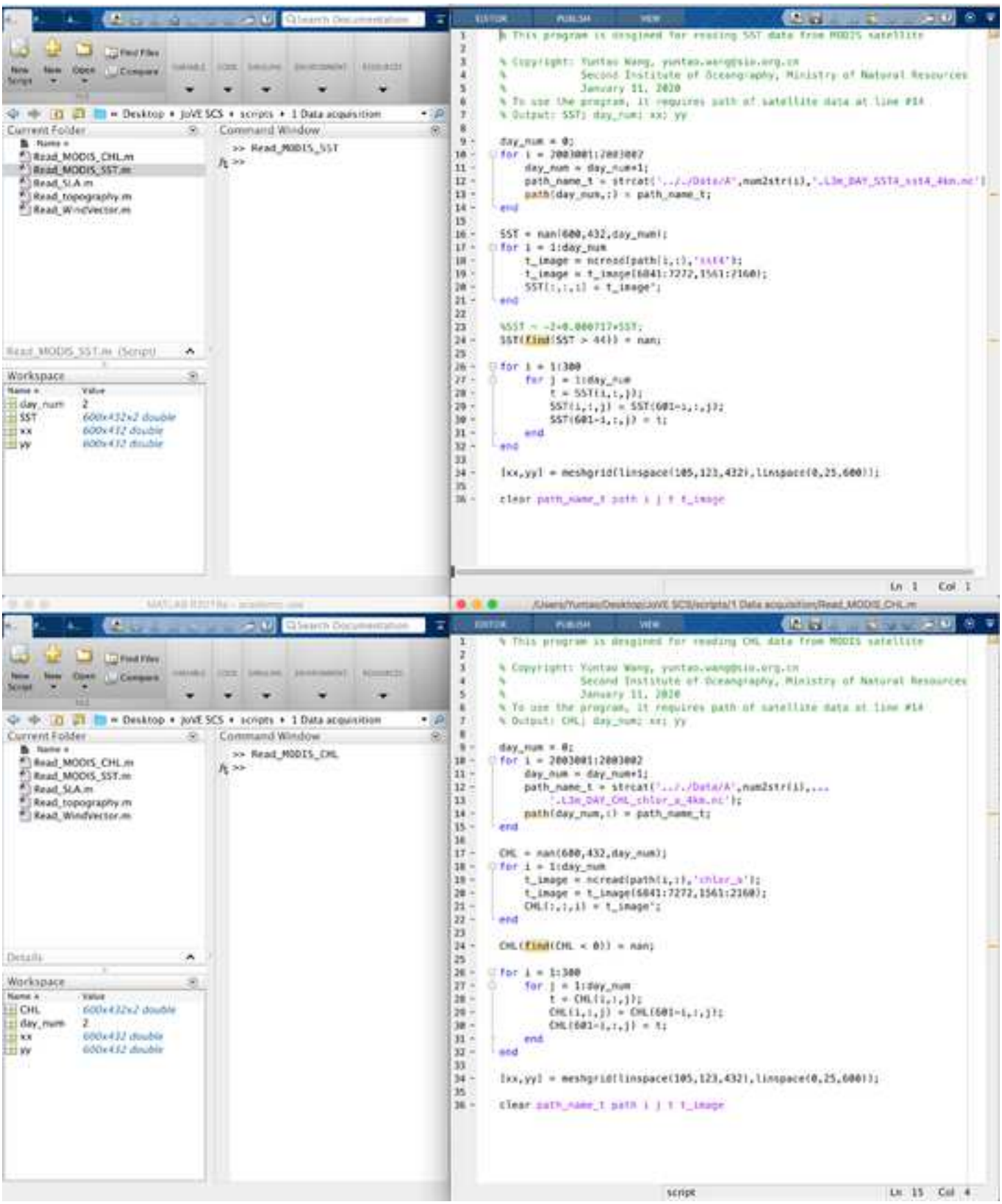

Screenfile4

Click here to access/download;Supplemental File (Figures, Permissions, etc.);Figure S4.psd

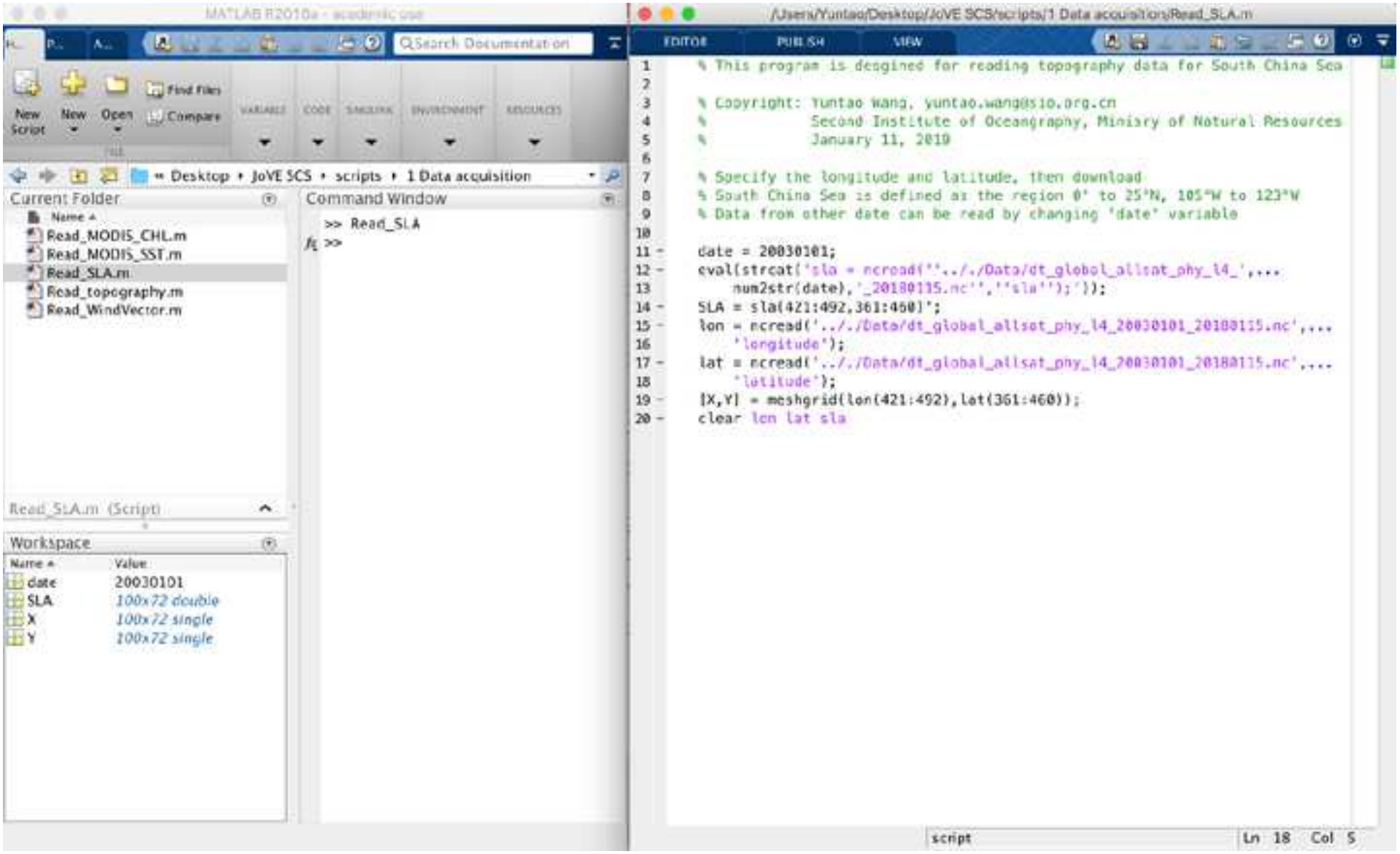

Screenfile5

Click here to access/download;Supplemental File (Figures, Permissions, etc.);Figure S5.psd

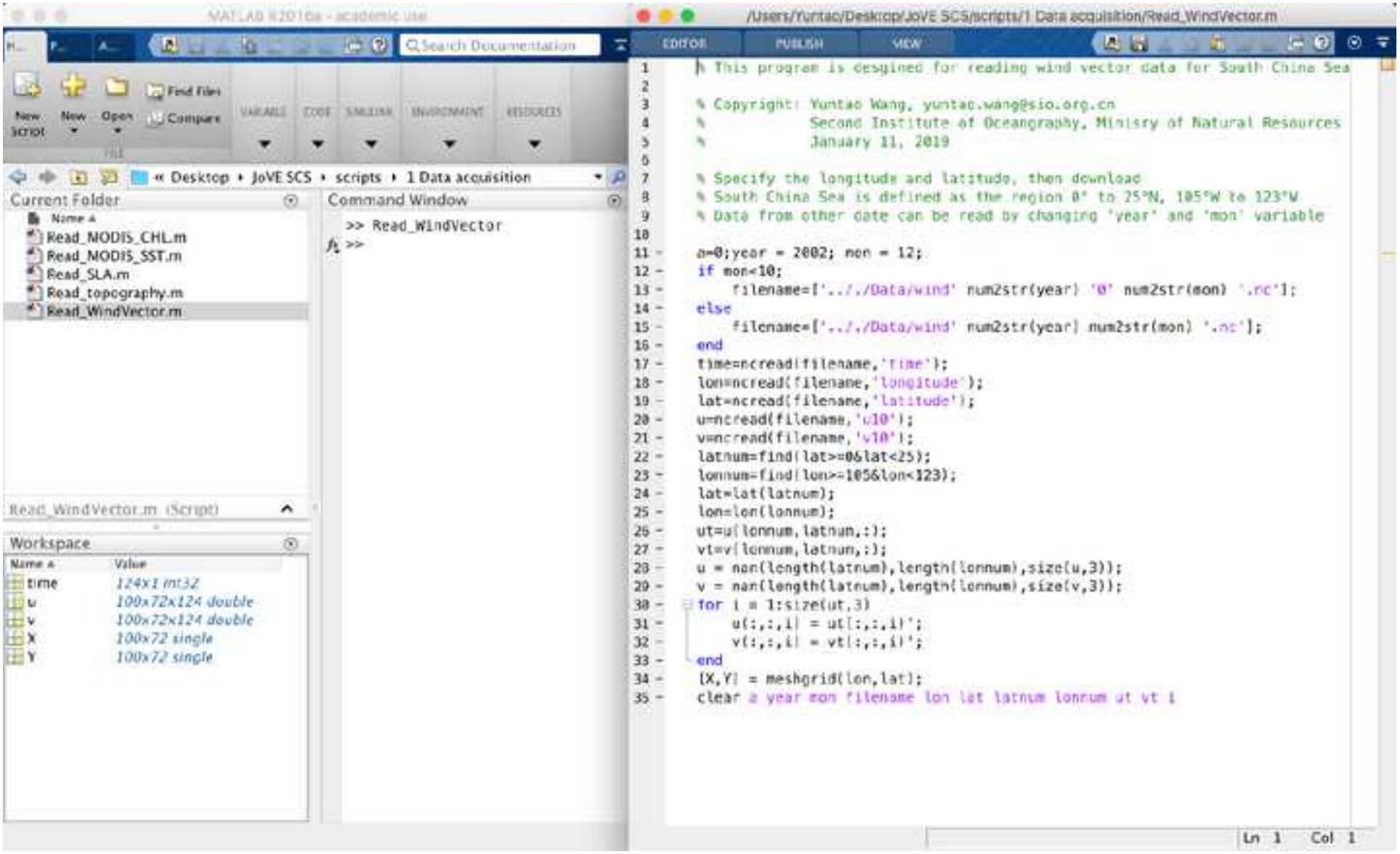

Screenfile6

Click here to access/download;Supplemental File (Figures, Permissions, etc.);Figure S6.psd

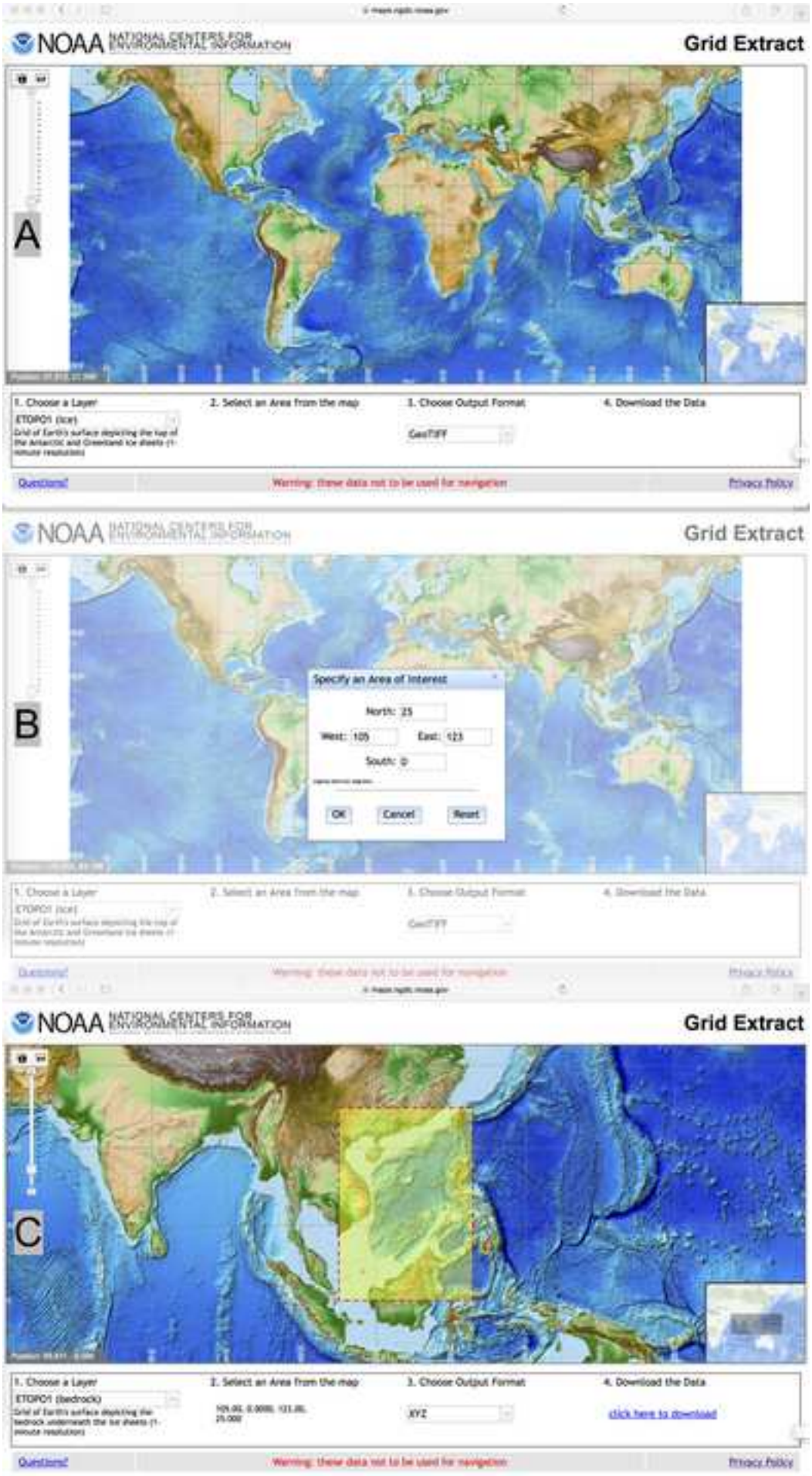

Screenfile7

Click here to access/download;Supplemental File (Figures, Permissions, etc.);Figure S7.psd

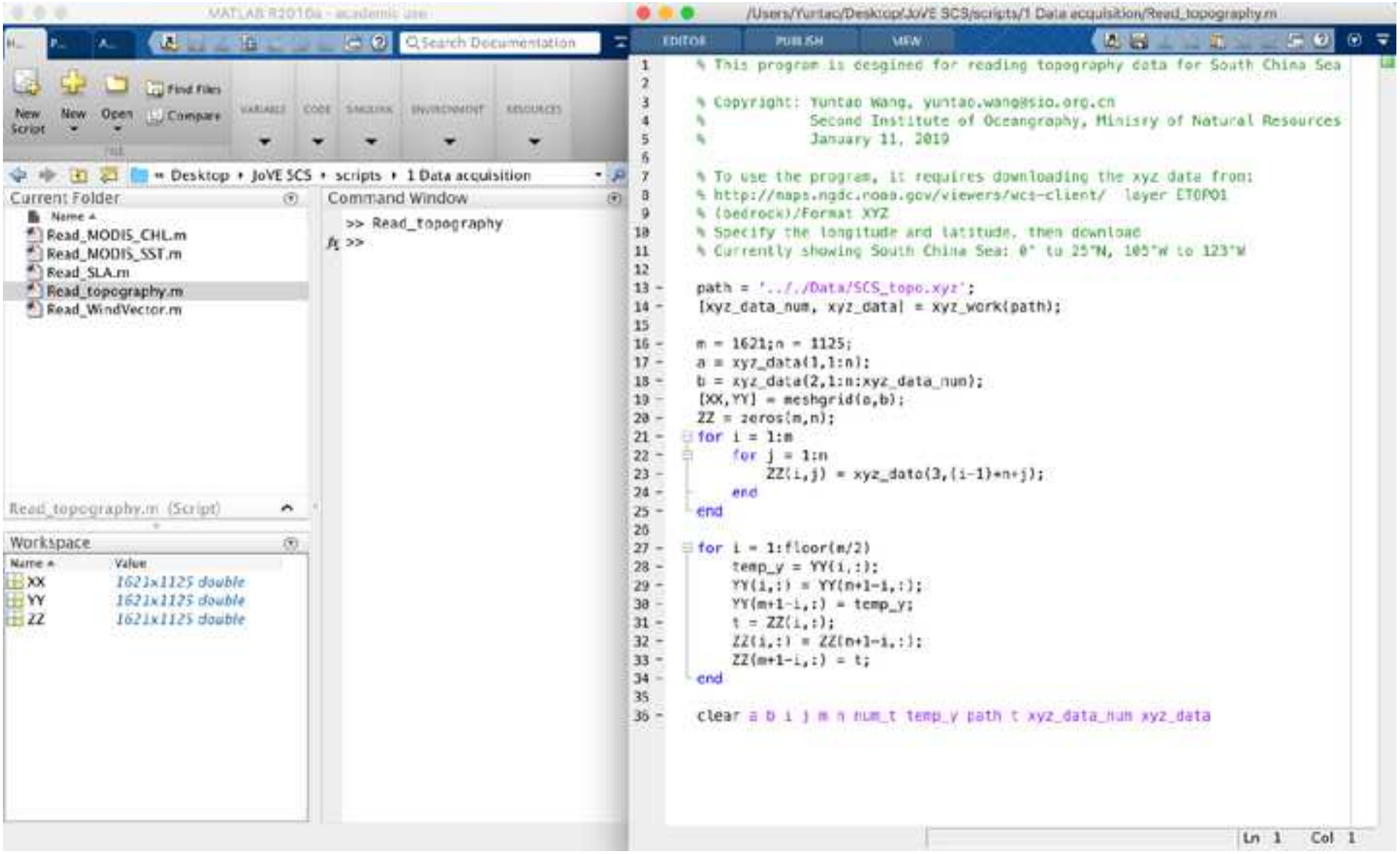

Screenfile8

Click here to access/download;Supplemental File (Figures, Permissions, etc.);Figure S8.psd

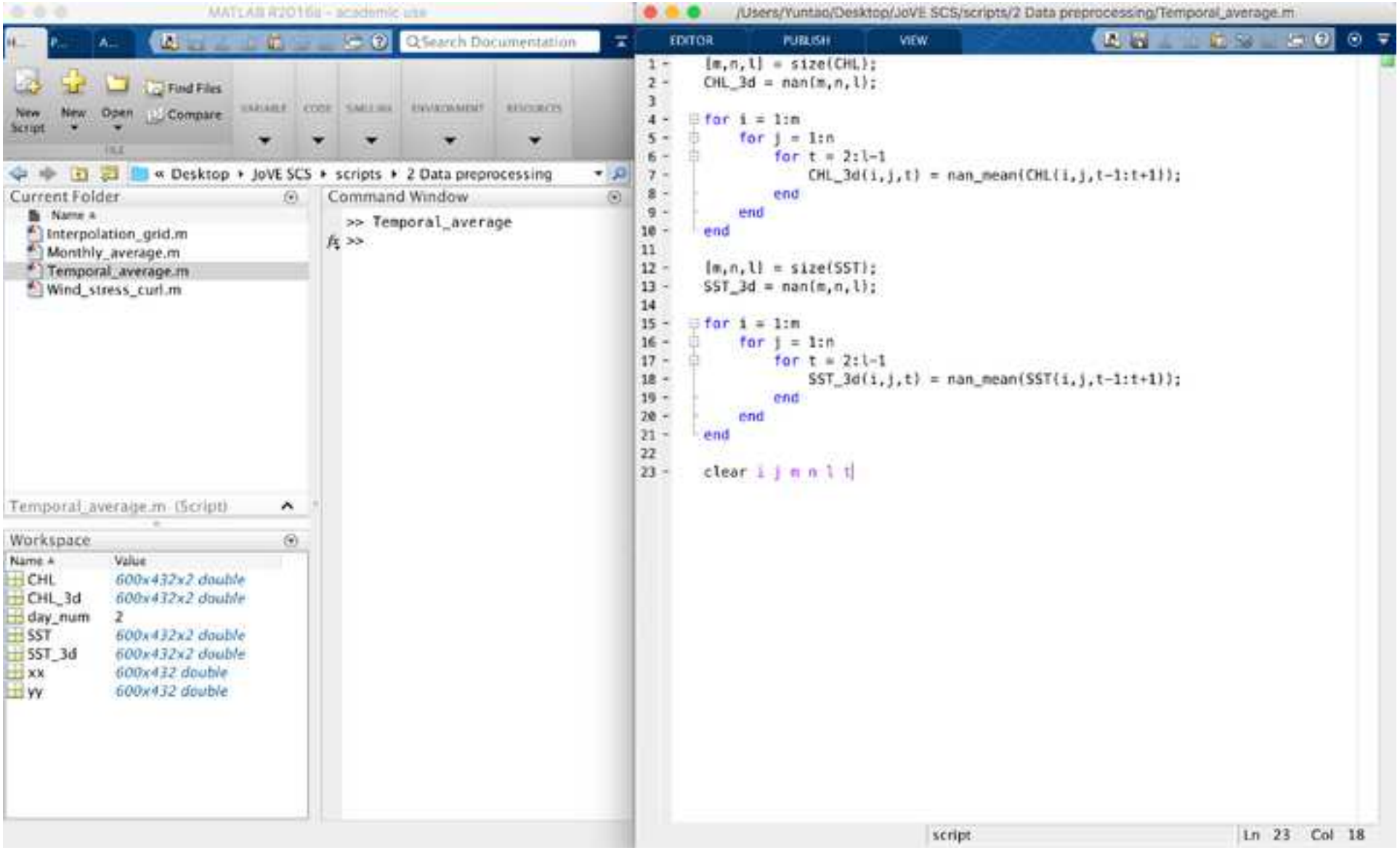

Screenfile9

Click here to access/download;Supplemental File (Figures, Permissions, etc.);Figure S9.psd

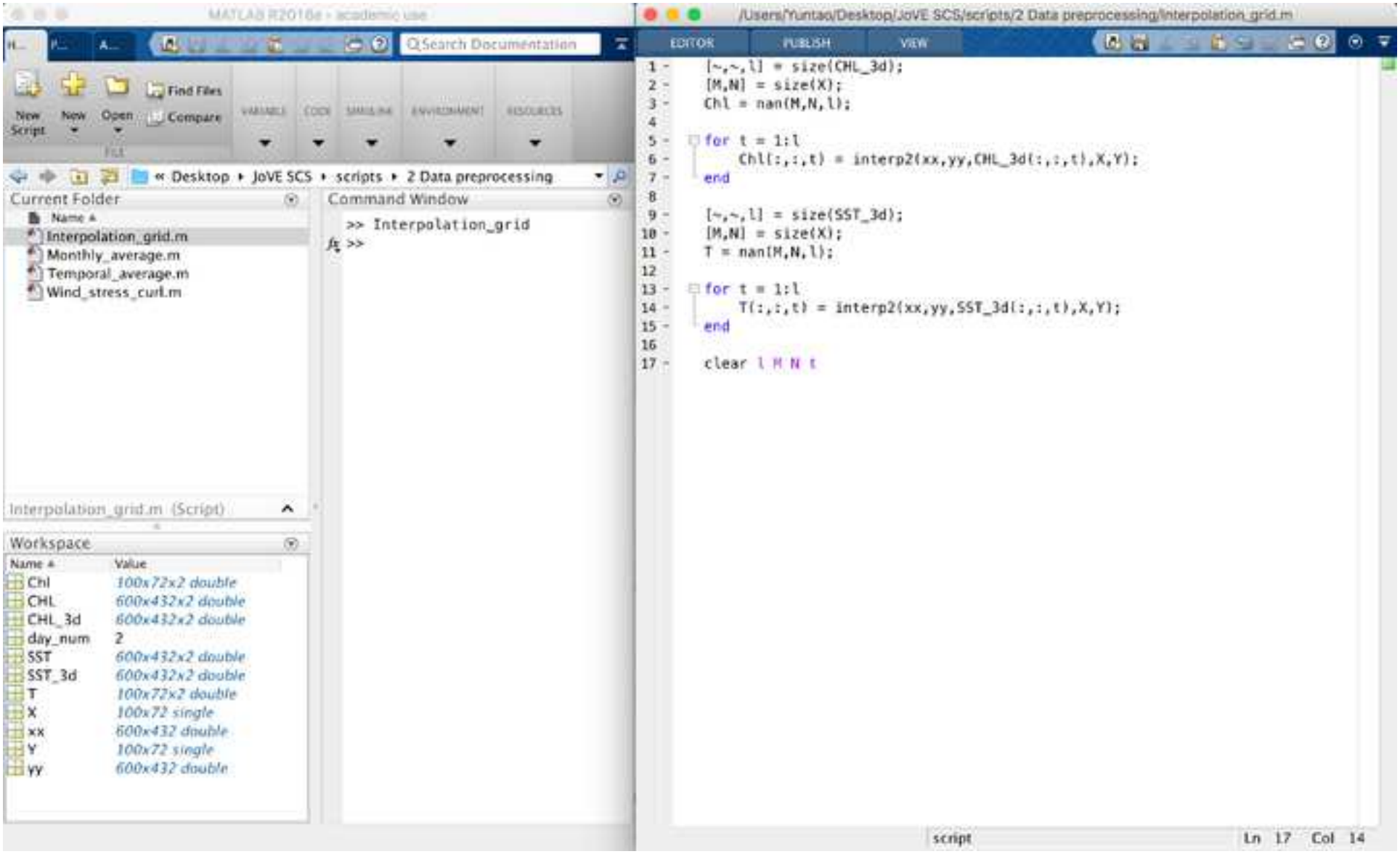

Screenfile10

Click here to access/download;Supplemental File (Figures, Permissions, etc.);Figure S10.psd

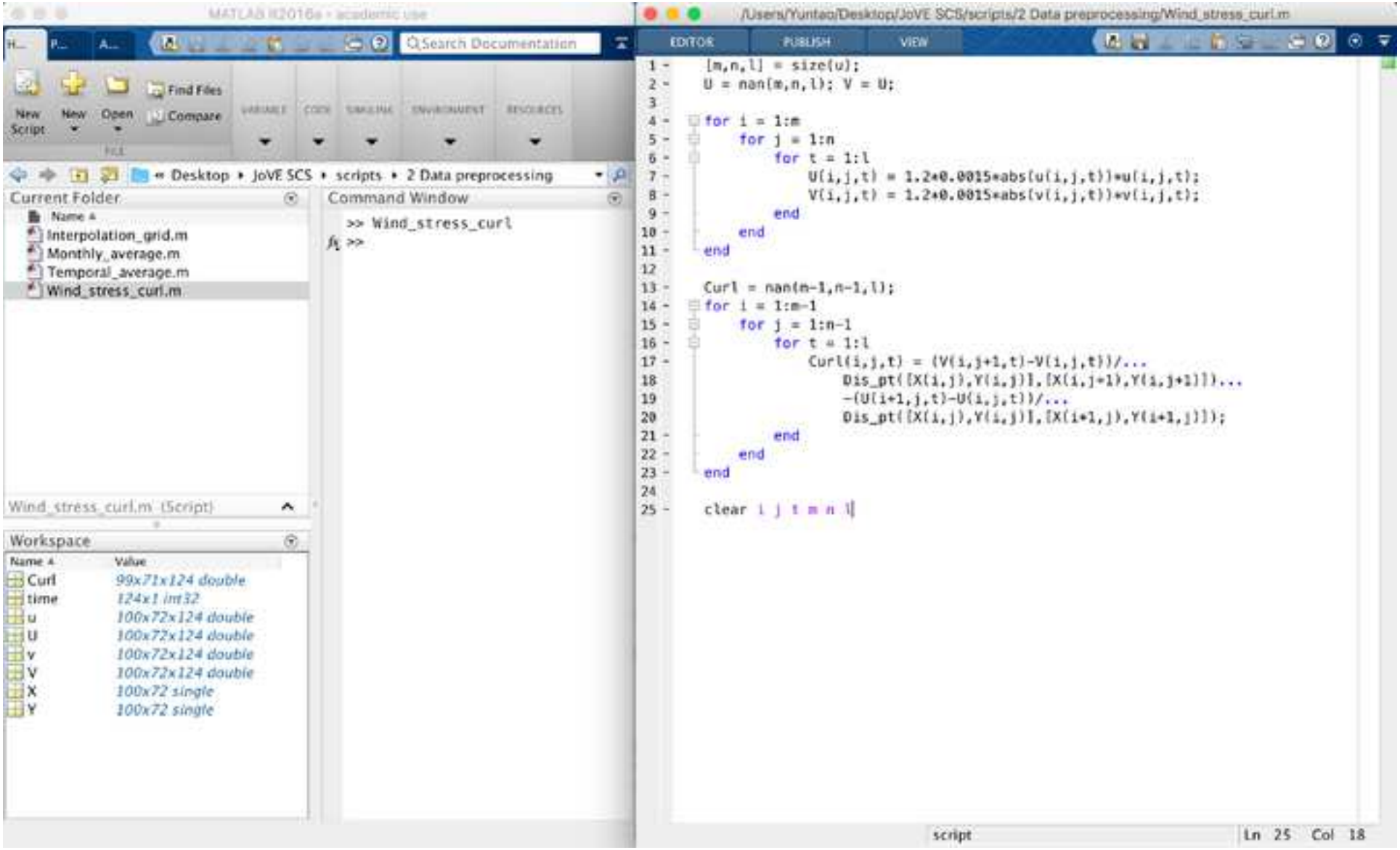

Screenfile11

Click here to access/download;Supplemental File (Figures, Permissions, etc.);Figure S11.psd

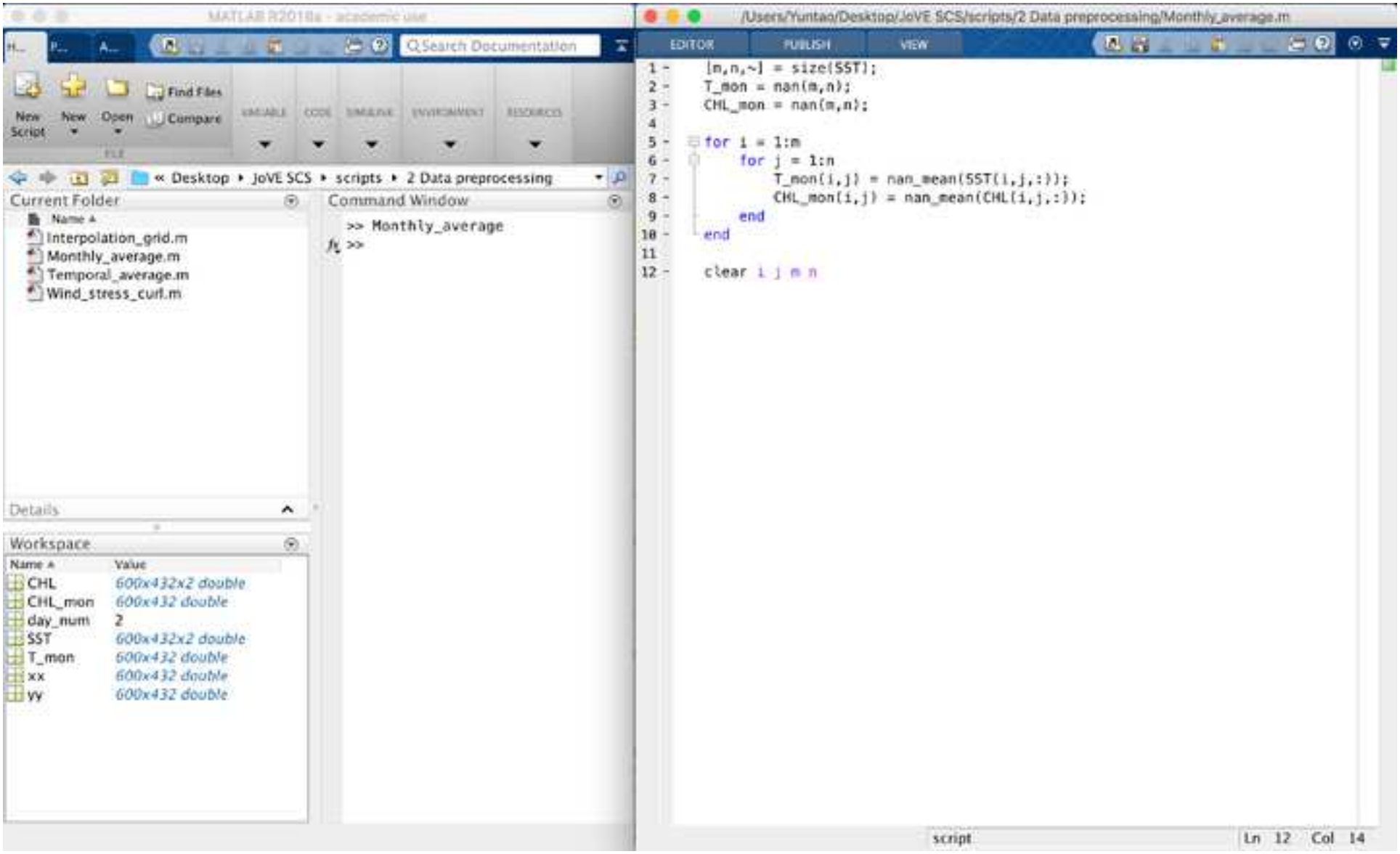

Screenfile12

Click here to access/download;Supplemental File (Figures, Permissions, etc.);Figure S12.psd

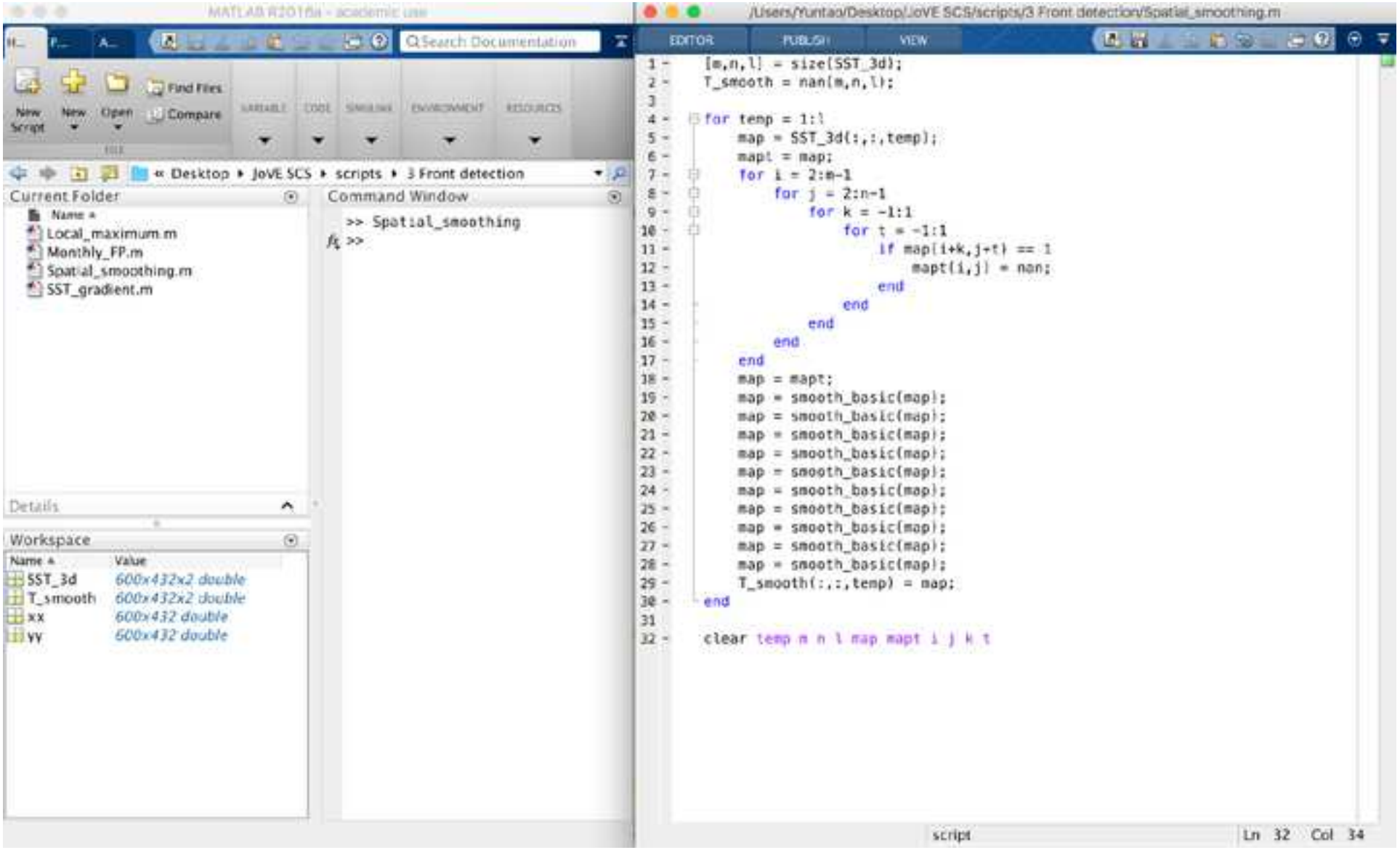

Screenfile13

Click here to access/download;Supplemental File (Figures, Permissions, etc.);Figure S13.psd

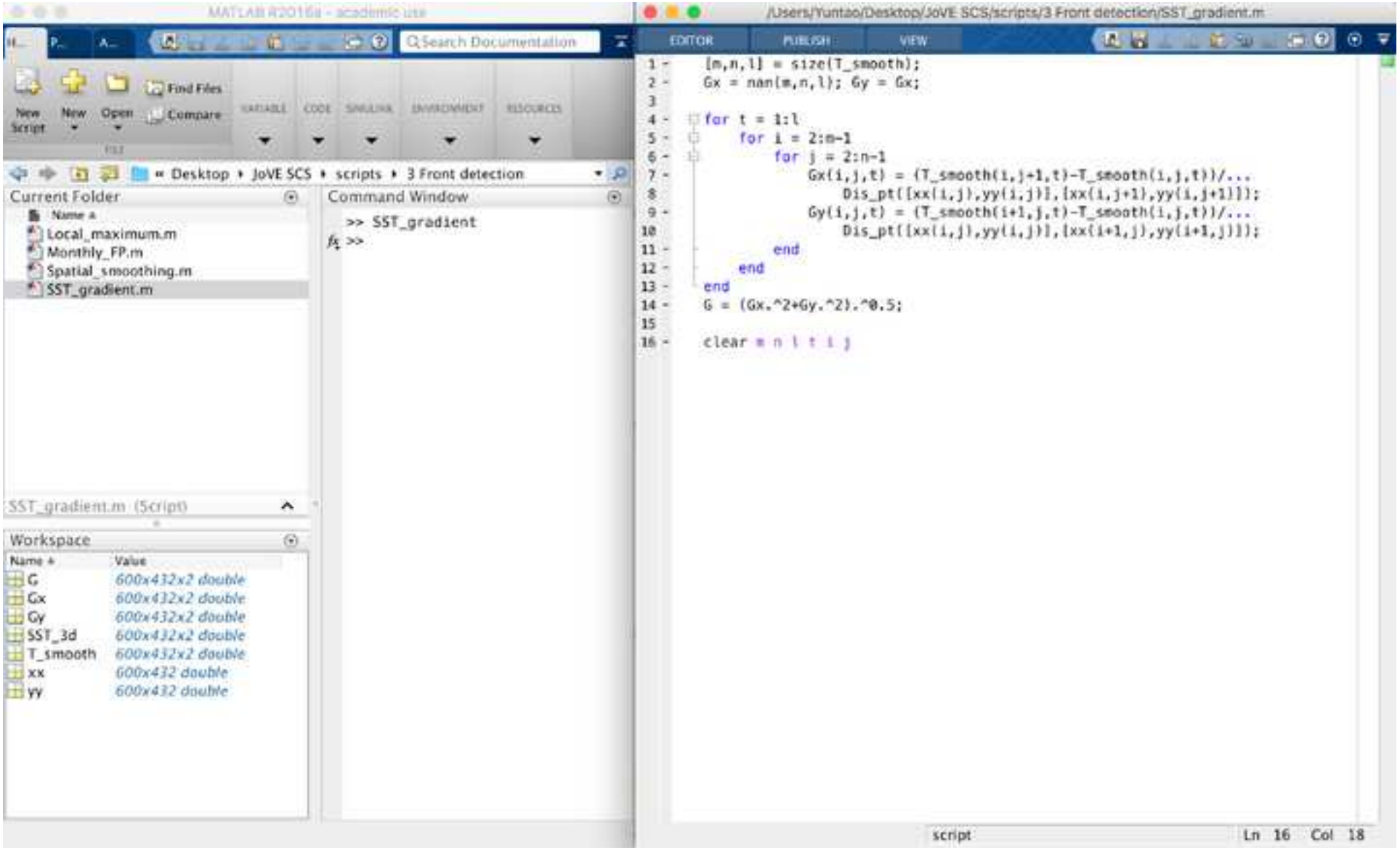

Screenfile14

Click here to access/download;Supplemental File (Figures, Permissions, etc.);Figure S14.psd

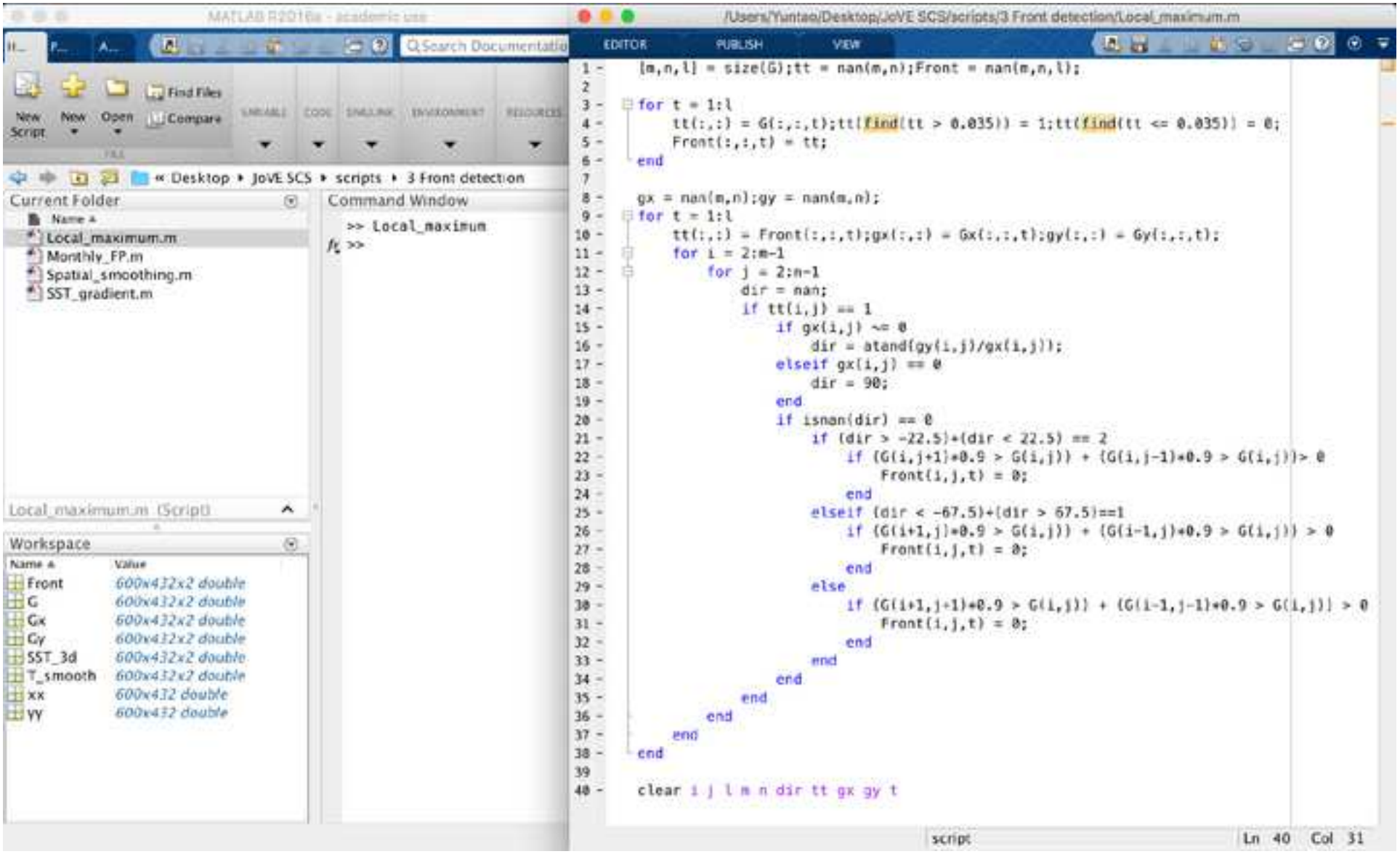

Screenfile15

Click here to access/download;Supplemental File (Figures, Permissions, etc.);Figure S15.psd

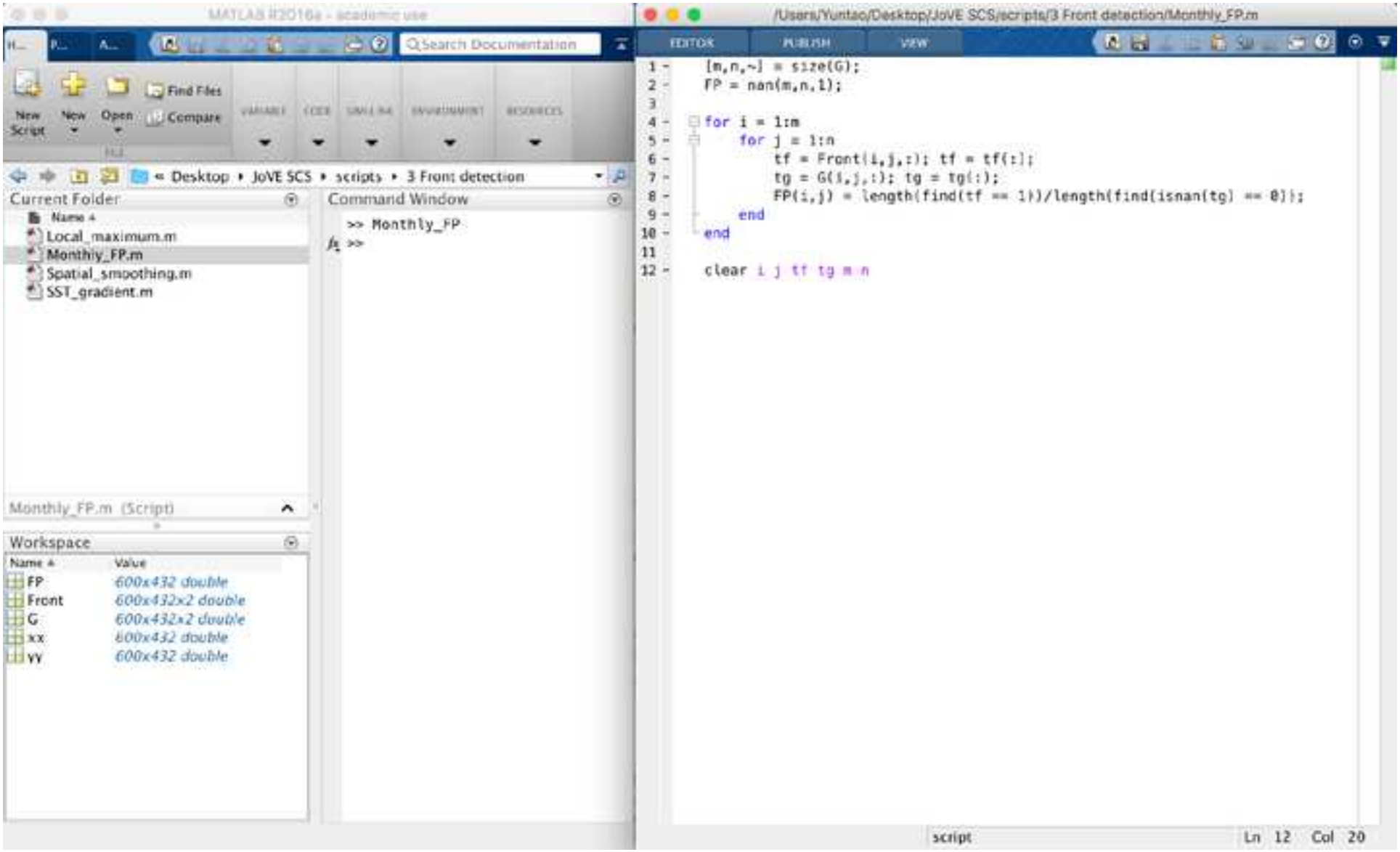

Screenfile16

Click here to access/download;Supplemental File (Figures, Permissions, etc.);Figure S16.psd

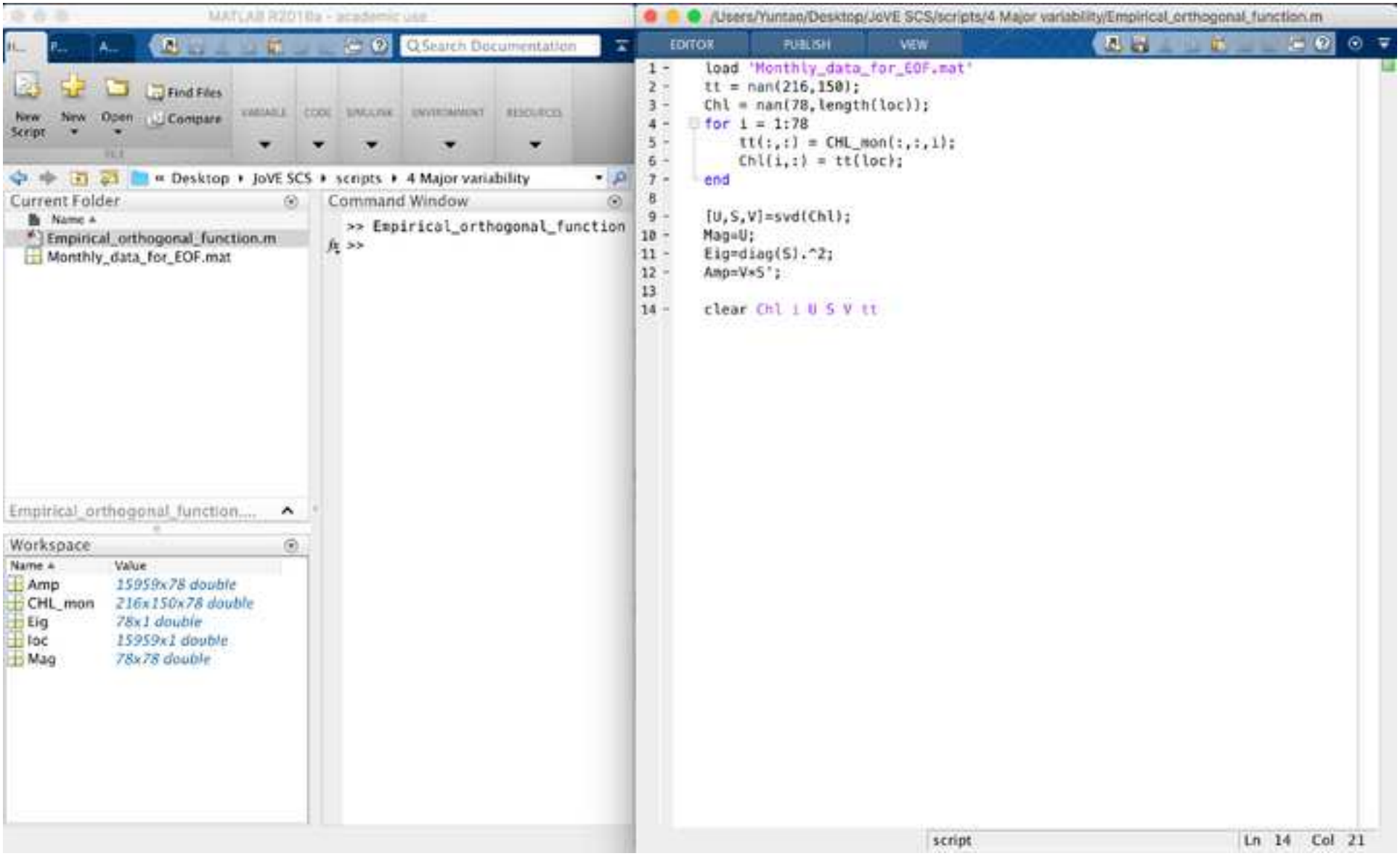

Screenfile17

Click here to access/download;Supplemental File (Figures, Permissions, etc.);Figure S17.psd

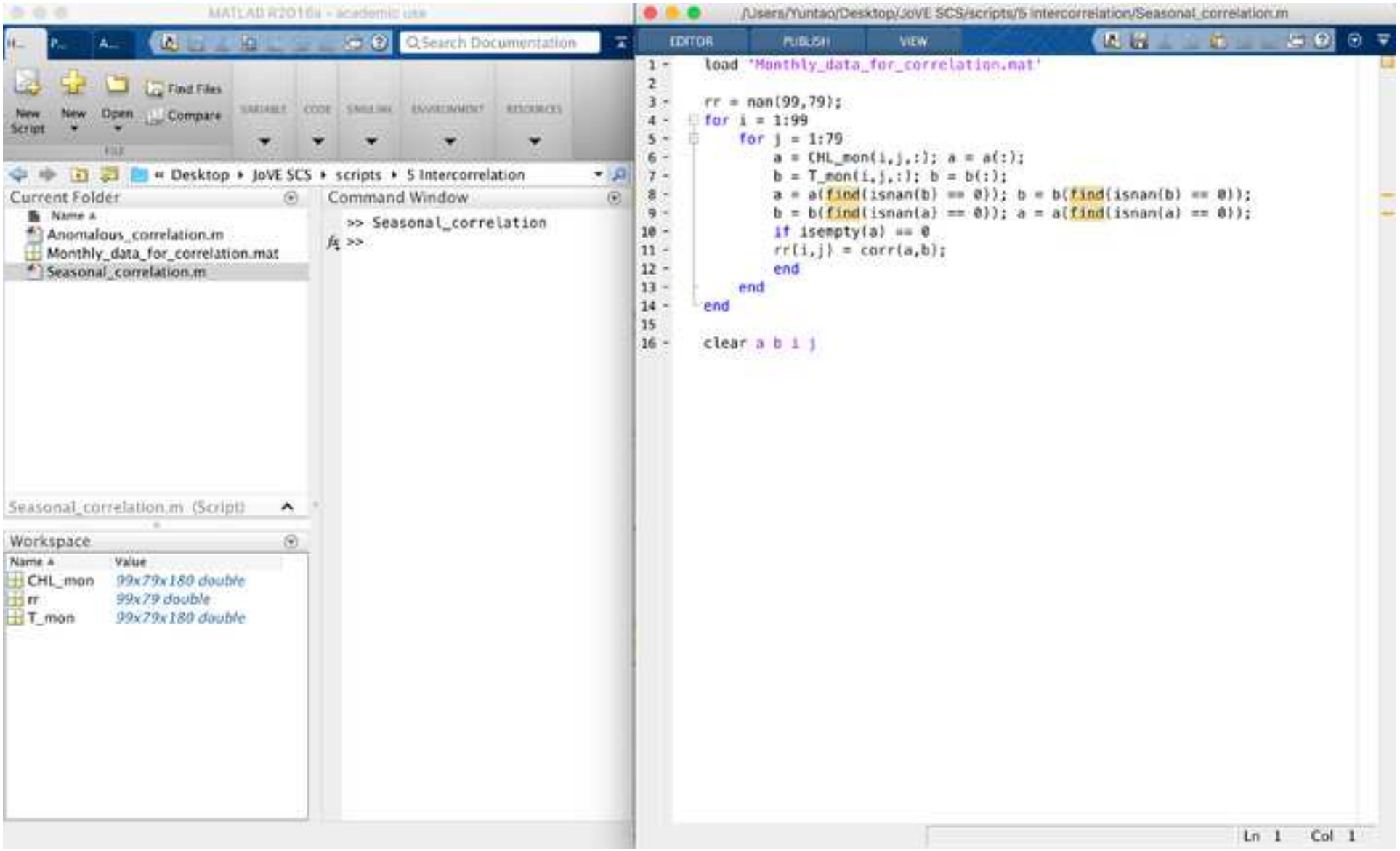

Screenfile18

Click here to access/download;Supplemental File (Figures, Permissions, etc.);Figure S18.psd

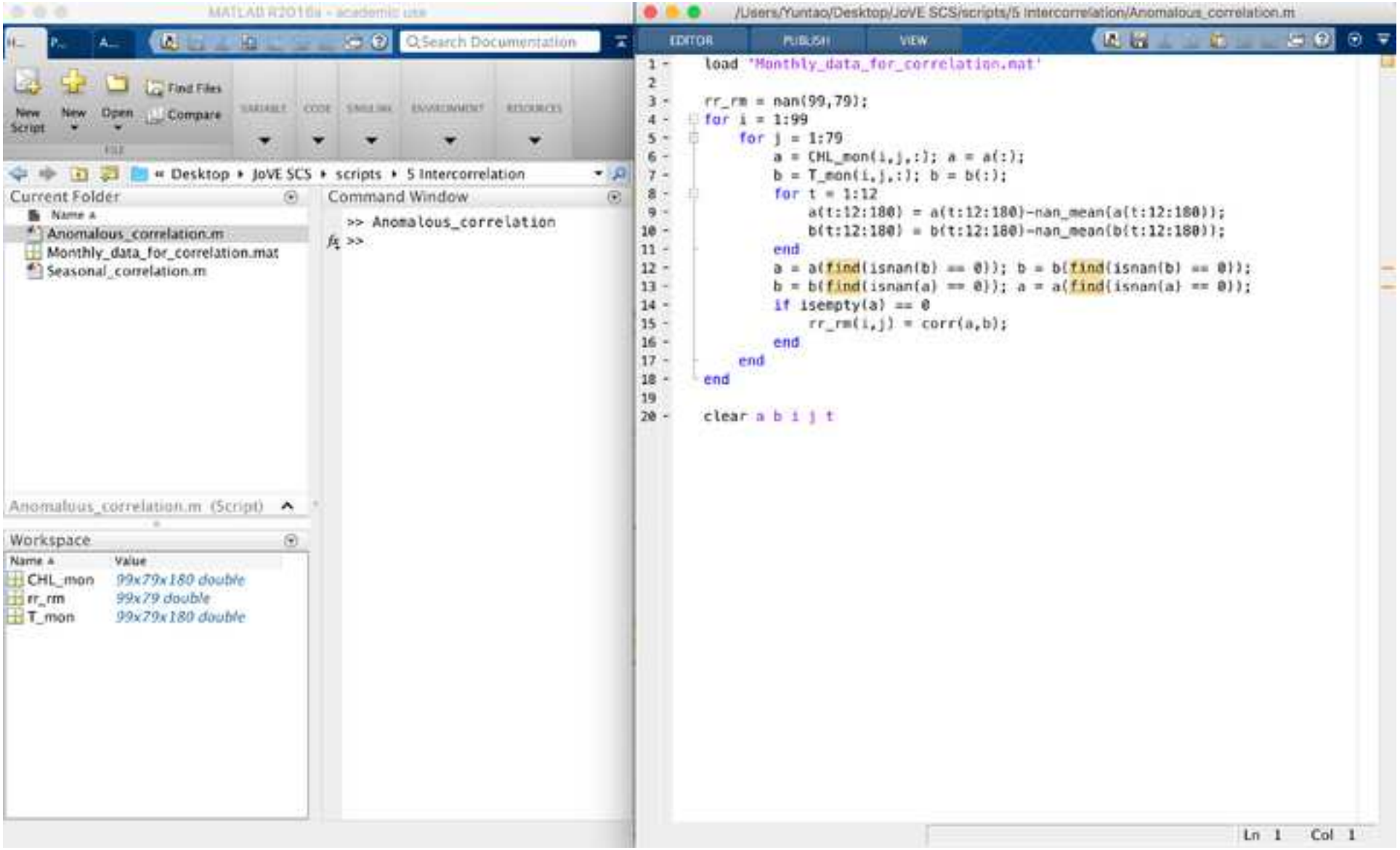

Screenfile19

Click here to access/download;Supplemental File (Figures, Permissions, etc.);Figure S19.psd

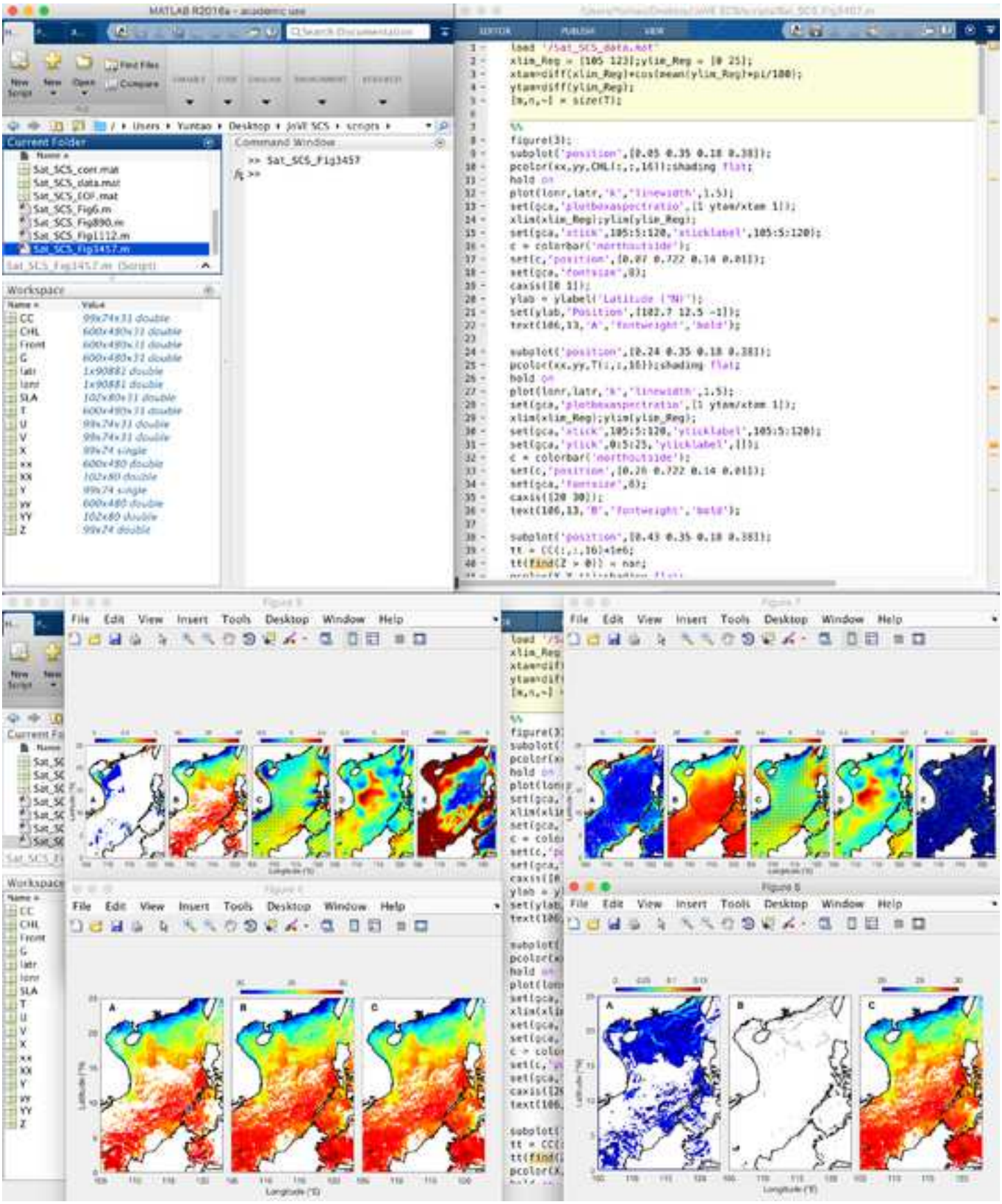

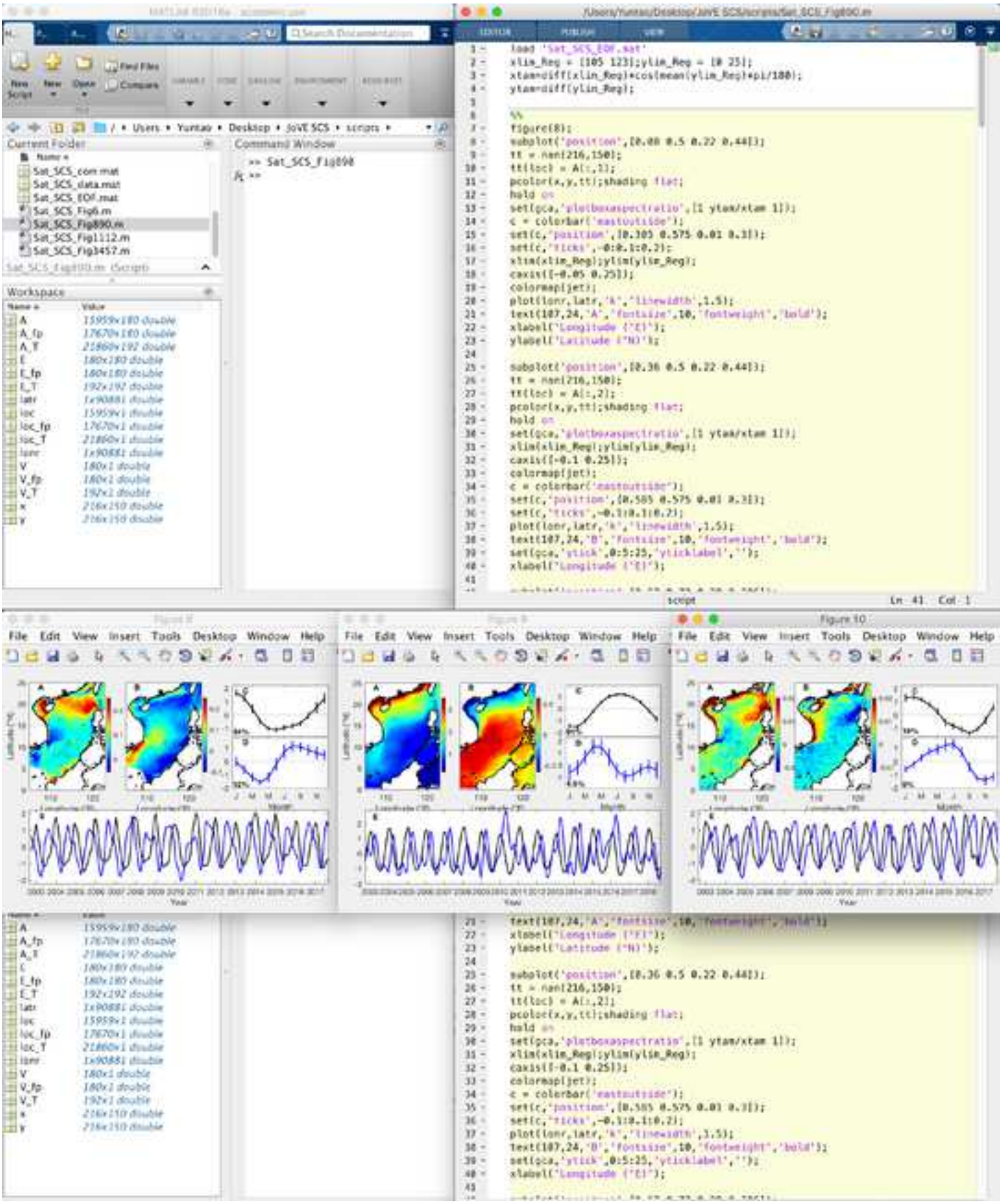

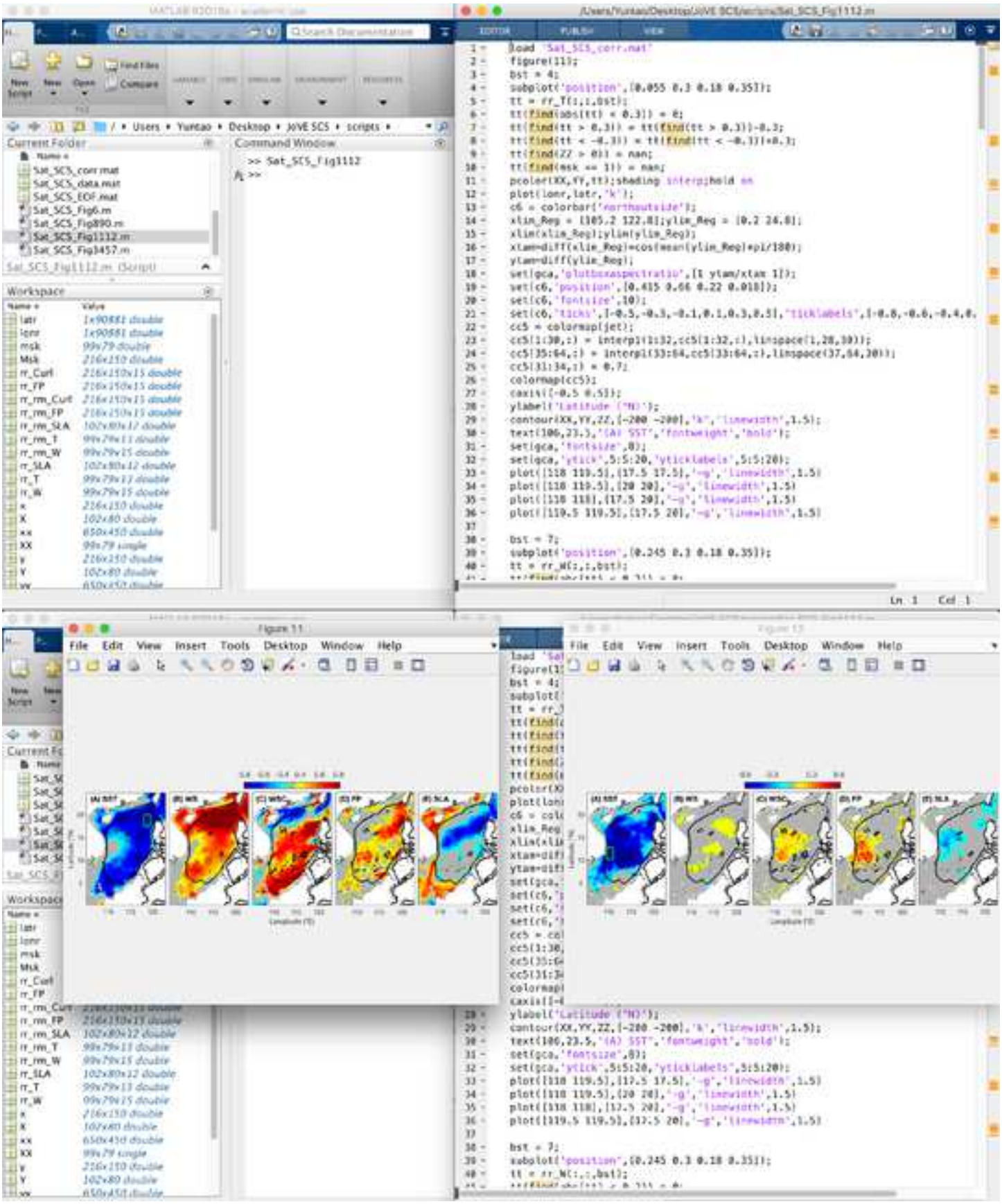

ELSEVIER LICENSE
TERMS AND CONDITIONS

Feb 24, 2020

This Agreement between Second Institute of Oceanography -- Yuntao Wang ("You") and Elsevier ("Elsevier") consists of your license details and the terms and conditions provided by Elsevier and Copyright Clearance Center.

License Number	4767981463063
License date	Feb 14, 2020
Licensed Content Publisher	Elsevier
Licensed Content Publication	Journal of Marine Systems
Licensed Content Title	The variability of chlorophyll-a and its relationship with dynamic factors in the basin of the South China Sea
Licensed Content Author	Yi Yu,Xiaogang Xing,Hailong Liu,Yeping Yuan,Yuntao Wang,Fei Chai
Licensed Content Date	Dec 1, 2019
Licensed Content Volume	200
Licensed Content Issue	n/a
Licensed Content Pages	1
Start Page	103230
End Page	0

Type of Use	reuse in a journal/magazine
Requestor type	academic/educational institute
Portion	figures/tables/illustrations
Number of figures/tables/illustrations	4
Format	both print and electronic
Are you the author of this Elsevier article?	Yes
Will you be translating?	No
Title of new article	Using satellite information to investigate sea surface chlorophyll and its relationship with major features
Lead author	Yuntao Wang
Title of targeted journal	JoVE Journal of Visualized Experiments
Publisher	JoVE Journal of Visualized Experiments
Expected publication date	May 2020
Portions	Figure 20, Figure 21, Table 1, Table 2
Requestor Location	Second Institute of Oceanography No 36 North Baochu Road Hangzhou, 310012 China Attn: Second Institute of Oceanography
Publisher Tax ID	GB 494 6272 12

Total 0.00 USD

Terms and Conditions

INTRODUCTION

1. The publisher for this copyrighted material is Elsevier. By clicking "accept" in connection with completing this licensing transaction, you agree that the following terms and conditions apply to this transaction (along with the Billing and Payment terms and conditions established by Copyright Clearance Center, Inc. ("CCC"), at the time that you opened your Rightslink account and that are available at any time at http://myaccount.copyright.com).

GENERAL TERMS

2. Elsevier hereby grants you permission to reproduce the aforementioned material subject to the terms and conditions indicated.

3. Acknowledgement: If any part of the material to be used (for example, figures) has appeared in our publication with credit or acknowledgement to another source, permission must also be sought from that source. If such permission is not obtained then that material may not be included in your publication/copies. Suitable acknowledgement to the source must be made, either as a footnote or in a reference list at the end of your publication, as follows:

"Reprinted from Publication title, Vol /edition number, Author(s), Title of article / title of chapter, Pages No., Copyright (Year), with permission from Elsevier [OR APPLICABLE SOCIETY COPYRIGHT OWNER]." Also Lancet special credit - "Reprinted from The Lancet, Vol. number, Author(s), Title of article, Pages No., Copyright (Year), with permission from Elsevier."

4. Reproduction of this material is confined to the purpose and/or media for which permission is hereby given.

5. Altering/Modifying Material: Not Permitted. However figures and illustrations may be altered/adapted minimally to serve your work. Any other abbreviations, additions, deletions and/or any other alterations shall be made only with prior written authorization of Elsevier Ltd. (Please contact Elsevier at permissions@elsevier.com). No modifications can be made to any Lancet figures/tables and they must be reproduced in full.

6. If the permission fee for the requested use of our material is waived in this instance, please be advised that your future requests for Elsevier materials may attract a fee.

7. Reservation of Rights: Publisher reserves all rights not specifically granted in the combination of (i) the license details provided by you and accepted in the course of this licensing transaction, (ii) these terms and conditions and (iii) CCC's Billing and Payment terms and conditions.

8. License Contingent Upon Payment: While you may exercise the rights licensed immediately upon issuance of the license at the end of the licensing process for the transaction, provided that you have disclosed complete and accurate details of your proposed use, no license is finally effective unless and until full payment is received from you (either by publisher or by CCC) as provided in CCC's Billing and Payment terms and conditions. If

full payment is not received on a timely basis, then any license preliminarily granted shall be deemed automatically revoked and shall be void as if never granted. Further, in the event that you breach any of these terms and conditions or any of CCC's Billing and Payment terms and conditions, the license is automatically revoked and shall be void as if never granted. Use of materials as described in a revoked license, as well as any use of the materials beyond the scope of an unrevoked license, may constitute copyright infringement and publisher reserves the right to take any and all action to protect its copyright in the materials.

9. Warranties: Publisher makes no representations or warranties with respect to the licensed material.

10. Indemnity: You hereby indemnify and agree to hold harmless publisher and CCC, and their respective officers, directors, employees and agents, from and against any and all claims arising out of your use of the licensed material other than as specifically authorized pursuant to this license.

11. No Transfer of License: This license is personal to you and may not be sublicensed, assigned, or transferred by you to any other person without publisher's written permission.

12. No Amendment Except in Writing: This license may not be amended except in a writing signed by both parties (or, in the case of publisher, by CCC on publisher's behalf).

13. Objection to Contrary Terms: Publisher hereby objects to any terms contained in any purchase order, acknowledgment, check endorsement or other writing prepared by you, which terms are inconsistent with these terms and conditions or CCC's Billing and Payment terms and conditions. These terms and conditions, together with CCC's Billing and Payment terms and conditions (which are incorporated herein), comprise the entire agreement between you and publisher (and CCC) concerning this licensing transaction. In the event of any conflict between your obligations established by these terms and conditions and those established by CCC's Billing and Payment terms and conditions, these terms and conditions shall control.

14. Revocation: Elsevier or Copyright Clearance Center may deny the permissions described in this License at their sole discretion, for any reason or no reason, with a full refund payable to you. Notice of such denial will be made using the contact information provided by you. Failure to receive such notice will not alter or invalidate the denial. In no event will Elsevier or Copyright Clearance Center be responsible or liable for any costs, expenses or damage incurred by you as a result of a denial of your permission request, other than a refund of the amount(s) paid by you to Elsevier and/or Copyright Clearance Center for denied permissions.

LIMITED LICENSE

The following terms and conditions apply only to specific license types:

15. **Translation**: This permission is granted for non-exclusive world **English** rights only unless your license was granted for translation rights. If you licensed translation rights you may only translate this content into the languages you requested. A professional translator must perform all translations and reproduce the content word for word preserving the integrity of the article.

16. **Posting licensed content on any Website**: The following terms and conditions apply as follows: Licensing material from an Elsevier journal: All content posted to the web site must maintain the copyright information line on the bottom of each image; A hyper-text must be

included to the Homepage of the journal from which you are licensing at http://www.sciencedirect.com/science/journal/xxxxx or the Elsevier homepage for books at http://www.elsevier.com; Central Storage: This license does not include permission for a scanned version of the material to be stored in a central repository such as that provided by Heron/XanEdu.

Licensing material from an Elsevier book: A hyper-text link must be included to the Elsevier homepage at http://www.elsevier.com . All content posted to the web site must maintain the copyright information line on the bottom of each image.

Posting licensed content on Electronic reserve: In addition to the above the following clauses are applicable: The web site must be password-protected and made available only to bona fide students registered on a relevant course. This permission is granted for 1 year only. You may obtain a new license for future website posting.

17. **For journal authors:** the following clauses are applicable in addition to the above:

Preprints:

A preprint is an author's own write-up of research results and analysis, it has not been peer-reviewed, nor has it had any other value added to it by a publisher (such as formatting, copyright, technical enhancement etc.).

Authors can share their preprints anywhere at any time. Preprints should not be added to or enhanced in any way in order to appear more like, or to substitute for, the final versions of articles however authors can update their preprints on arXiv or RePEc with their Accepted Author Manuscript (see below).

If accepted for publication, we encourage authors to link from the preprint to their formal publication via its DOI. Millions of researchers have access to the formal publications on ScienceDirect, and so links will help users to find, access, cite and use the best available version. Please note that Cell Press, The Lancet and some society-owned have different preprint policies. Information on these policies is available on the journal homepage.

Accepted Author Manuscripts: An accepted author manuscript is the manuscript of an article that has been accepted for publication and which typically includes author-incorporated changes suggested during submission, peer review and editor-author communications.

Authors can share their accepted author manuscript:

- immediately
  - via their non-commercial person homepage or blog
  - by updating a preprint in arXiv or RePEc with the accepted manuscript
  - via their research institute or institutional repository for internal institutional uses or as part of an invitation-only research collaboration work-group
  - directly by providing copies to their students or to research collaborators for their personal use
  - for private scholarly sharing as part of an invitation-only work group on commercial sites with which Elsevier has an agreement
- After the embargo period
  - via non-commercial hosting platforms such as their institutional repository
  - via commercial sites with which Elsevier has an agreement

In all cases accepted manuscripts should:

- link to the formal publication via its DOI
- bear a CC-BY-NC-ND license - this is easy to do
- if aggregated with other manuscripts, for example in a repository or other site, be shared in alignment with our hosting policy not be added to or enhanced in any way to appear more like, or to substitute for, the published journal article.

Published journal article (JPA): A published journal article (PJA) is the definitive final record of published research that appears or will appear in the journal and embodies all value-adding publishing activities including peer review co-ordination, copy-editing, formatting, (if relevant) pagination and online enrichment.

Policies for sharing publishing journal articles differ for subscription and gold open access articles:

Subscription Articles: If you are an author, please share a link to your article rather than the full-text. Millions of researchers have access to the formal publications on ScienceDirect, and so links will help your users to find, access, cite, and use the best available version.

Theses and dissertations which contain embedded PJAs as part of the formal submission can be posted publicly by the awarding institution with DOI links back to the formal publications on ScienceDirect.

If you are affiliated with a library that subscribes to ScienceDirect you have additional private sharing rights for others' research accessed under that agreement. This includes use for classroom teaching and internal training at the institution (including use in course packs and courseware programs), and inclusion of the article for grant funding purposes.

Gold Open Access Articles: May be shared according to the author-selected end-user license and should contain a CrossMark logo, the end user license, and a DOI link to the formal publication on ScienceDirect.

Please refer to Elsevier's posting policy for further information.

18. **For book authors** the following clauses are applicable in addition to the above: Authors are permitted to place a brief summary of their work online only. You are not allowed to download and post the published electronic version of your chapter, nor may you scan the printed edition to create an electronic version. **Posting to a repository:** Authors are permitted to post a summary of their chapter only in their institution's repository.

19. **Thesis/Dissertation**: If your license is for use in a thesis/dissertation your thesis may be submitted to your institution in either print or electronic form. Should your thesis be published commercially, please reapply for permission. These requirements include permission for the Library and Archives of Canada to supply single copies, on demand, of the complete thesis and include permission for Proquest/UMI to supply single copies, on demand, of the complete thesis. Should your thesis be published commercially, please reapply for permission. Theses and dissertations which contain embedded PJAs as part of the formal submission can be posted publicly by the awarding institution with DOI links back to the formal publications on ScienceDirect.

Elsevier Open Access Terms and Conditions

20. **Other Conditions**:

v1.9

Questions? customercare@copyright.com or +1-855-239-3415 (toll free in the US) or +1-978-646-2777.
